Nuclear Heat Transfer and Passive Cooling

Volume 6: **Molten Salt Thermal Hydraulics**

FRAZER-NASH CONSULTANCY

Introduction to the Technical Volumes and Case Studies

Convection, Radiation and Conjugate Heat Transfer

Natural Convection and Passive Cooling

Confidence and Uncertainty

Liquid Metal Thermal Hydraulics

Molten Salt Thermal Hydraulics

Liquid Metal CFD Modelling of the TALL-3D Test Facility

Fuel Assembly CFD and UQ for a Molten Salt Reactor

Reactor Scale CFD for Decay Heat Removal in a Lead-cooled Fast Reactor

System Code and CFD Analysis for a Light Water Small Modular Reactor

Authors:	Graham Macpherson	Frazer-Nash Consultancy
	Greg Cartland Glover	Science and Technology Facilities Council
Contributors:	Adam Owens	Moltex Energy
	Akash Dhandhukia	Terrestrial Energy
	Carolyn Howlett	Frazer-Nash Consultancy
	Milorad Dzodzo	Westinghouse Electric Company
Technical Volumes Lead:	Tim Houghton	Frazer-Nash Consultancy
Approver:	Richard Underhill	Frazer-Nash Consultancy

Document Number: FNC 60148/49313R

Issue and Date: Issue 1, December 2021

Legal Statement

Preface

Nuclear thermal hydraulics is the application of thermofluid mechanics within the nuclear industry. Thermal hydraulic analysis is an important tool in addressing the global challenge to reduce the cost of advanced nuclear technologies. An improved predictive capability and understanding supports the development, optimisation and safety substantiation of nuclear power plants.

This document is part of *Nuclear Heat Transfer and Passive Cooling: Technical Volumes and Case Studies*, a set of six technical volumes and four case studies providing information and guidance on aspects of nuclear thermal hydraulic analysis. This document set has been delivered by Frazer-Nash Consultancy, with support from a number of academic and industrial partners, as part of the UK Government *Nuclear Innovation Programme: Advanced Reactor Design*, funded by the Department for Business, Energy and Industrial Strategy (BEIS).

Each technical volume outlines the technical challenges, latest analysis methods and future direction for a specific area of nuclear thermal hydraulics. The case studies illustrate the use of a subset of these methods in representative nuclear industry examples. The document set is designed for technical users with some prior knowledge of thermofluid mechanics, who wish to know more about nuclear thermal hydraulics.

The work promotes a consistent methodology for thermal hydraulic analysis of single-phase heat transfer and passive cooling, to inform the link between academic research and end-user needs, and to provide a high-quality, peer-reviewed document set suitable for use across the nuclear industry.

The document set is not intended to be exhaustive or provide a set of standard engineering ‘guidelines’ and it is strongly recommended that nuclear thermal hydraulic analyses are undertaken by Suitably Qualified and Experienced Personnel.

The first edition of this document set has been authored by Frazer-Nash Consultancy, with the support of the individuals and organisations noted in each. Please acknowledge these documents in any work where they are used:

> Frazer-Nash Consultancy (2021) Nuclear Heat Transfer and Passive Cooling,
> Volume 6: Molten Salt Thermal Hydraulics.

Contents

1 Introduction

This technical volume describes the thermal hydraulic phenomena that are either unique to, or of particular relevance to Molten Salt Reactors (MSRs). It also provides an overview of the physics and chemistry of the salts typically used, and provides guidance on which modelling methods are best suited to make molten salt thermal hydraulic predictions, and how to use them.

It is recommended that Volumes 2 (Convection, Radiation and Conjugate Heat Transfer) and 3 (Natural Convection and Passive Cooling) are read before reading this volume, because it builds on and emphasises any areas of contrast with the descriptions of phenomena and methods applied in more conventional fluids. It is also relevant to consult Volume 4 (Confidence and Uncertainty) because of the comparatively large uncertainties that are found across a range of aspects in MSR analysis.

1.1 The Use of Molten Salt in Nuclear Reactors

The use of molten salts in a nuclear reactor has a number of advantages and features from a thermal hydraulic perspective: as a coolant, salts have high boiling points, so reactors do not need to be pressurised (unlike water cooled reactors); they can operate at high temperatures, giving high thermal efficiency and the possibility of cogeneration of hydrogen and process heat; they do not exhibit violent chemical reactivity with, for example, water (unlike sodium) and they have a high volumetric heat capacity, reducing plant size.

However, it is not principally for thermal hydraulic reasons that salts receive attention as part of reactor design. Certain salts containing dissolved fissile materials can be used as a liquid fuel, for example in a fast or thermal spectrum breeder configuration, providing efficiency in fissile resource utilisation and waste minimisation[1]. Some of the broader nuclear aspects and technical challenges of MSRs[2] are described by LeBlanc (2010) and Serp *et al.* (2014).

A wide variety of salt compositions have been proposed for use for a range of reactor purposes:

- Primary coolant for designs with solid fuels.
- Fissile and fertile material carriers for liquid fuelled designs, where salts of Uranium (U), Plutonium (Pu), Thorium (Th) or Minor Actinides (MAs) (for transmutation) are dissolved within the mixture.
- Secondary and tertiary heat transport loops.

[1] Including by reusing existing spent fuel and by transmutation of long lived fission products, substantially reducing the volume and half-life of waste.

[2] In some references, the term MSR is restricted to refer to reactors where the fuel is dissolved in the salt; in this technical volume it is used in its broadest sense, when a molten salt is used as a working fluid in any role.

Molten salts are also used in 'pyroprocessing' of spent fuel and there are cases where a molten salt is used or proposed as a secondary power transport or thermal energy storage fluid for other high temperature reactor types, or in non-nuclear applications, such as Concentrating Solar Power (CSP). Usually two or three component salt mixtures are used to reduce the melting point to a practical temperature.

1.2 Molten Salt Reactor Programmes

The main experience of MSRs was gained at Oak Ridge National Laboratory (ORNL) under the Aircraft Reactor Experiment (ARE) and Molten Salt Reactor Experiment (MSRE) programmes (Figure 1.1).

These first MSRs were thermal spectrum liquid fuelled reactors (ARE was moderated with BeO; MSRE with graphite). The MSRE in particular demonstrated the feasibility of many aspects of the technology, operating from 1965 to 1969. It is described in contemporary and retrospective overviews by Haubenreich and Engel (1970), Rosenthal *et al.* (1972) and MacPherson (1985). Reporting for the MSRE programme was extensive and detailed, and this documentation is freely available from the United States Department of Energy (US DOE) Office of Scientific and Technical Information (OSTI)[3] and also from third-party websites[4].

The US programme expected to build follow-on reactors from the MSRE (such as the Molten Salt Demonstration Reactor (MSDR), Bettis *et al.*, 1972 or Molten Salt Breeder Reactor (MSBR), Rosenthal *et al.*, 1972) and continued to create refined concept designs with improved safety and proliferation resistance (Gat, 1986, for example). There were also conceptual studies performed in a number of other countries, for example, in the UK at Winfrith (UKAEA, 1974), and at EIR (now PSI) in Switzerland (Taube, 1978, Taube and Heer, 1980).

More recently, there has been a resurgence in interest, in some cases drawing substantially on these previous designs. MSRs are one of the six Gen IV reactor concepts[5], and the subject of a number of development programmes (this list is not intended to be exhaustive – a selection of these reactors are characterised in more detail in Section 1.3):

USA: The Advanced High Temperature Reactor (AHTR) and Fluoride-Salt-Cooled High-Temperature Reactor (FHR) (Figure 1.2) have been developed as concept designs for the last two decades as fluoride salt cooled, solid fuel reactors (Andreades *et al.*, 2016, Qualls *et al.*, 2017). More recently Kairos Power have begun to develop a variant (KP-FHR) towards commercial deployment. There are other active commercial developers, for example Flibe Energy are developing the Liquid-Fluoride Thorium Reactor (LFTR); TerraPower are developing the Molten Chloride Fast Reactor (MCFR); ThorCon International are developing the Thorium Converter (ThorCon) reactor and Elysium Industries are developing the Molten Chloride Salt Fast Breeder Reactor (MCSFR).

Canada: Terrestrial Energy are currently developing the Integral Molten Salt Reactor (IMSR).

UK: Moltex Energy are developing the Stable Salt Reactor – Wasteburner (SSR–W).

[3] www.osti.gov
[4] moltensalt.org or energyfromthorium.com/pdf
[5] www.gen-4.org/gif

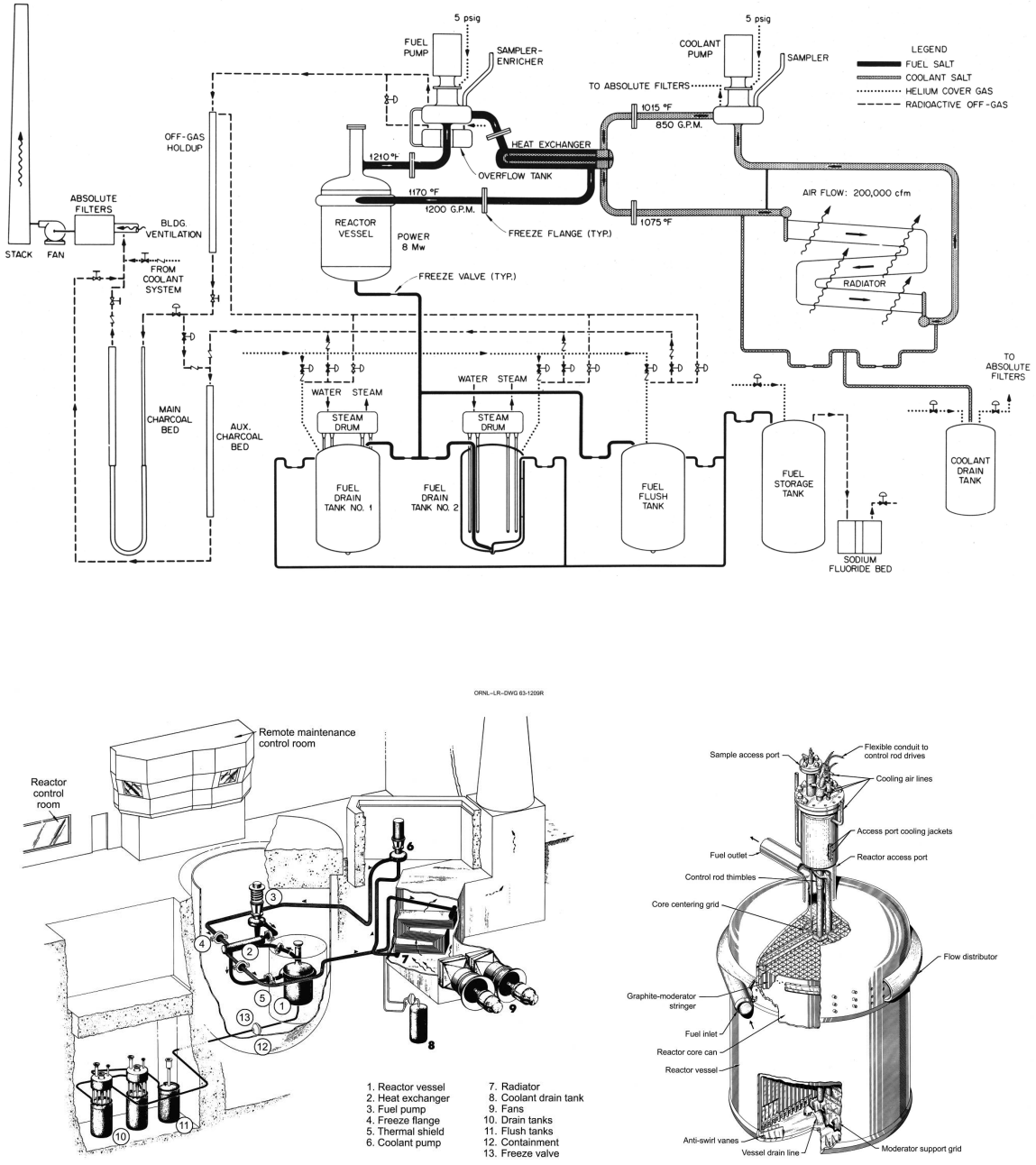

Figure 1.1: The MSRE layout and core (Rosenthal *et al.*, 1972 and Rosenthal, 2009).

Europe: The Molten Salt Fast Reactor (MSFR) (Figure 1.3) is under development, most recently supported by the EU SAMOFAR and SAMOSAFER[6] projects. Seaborg Technologies are developing the Compact Molten Salt Reactor (CMSR) and the Copenhagen Atomics Waste Burner is a small heavy water moderated design.

China: Parallel development programmes are ongoing for Thorium Molten Salt Reactors (TMSRs) with solid and liquid fuels (Pioro, 2016, Chapter 14). There are plans for a small scale solid fuelled demonstrator to be developed soon (TMSR-SF1) with a larger power reactor to follow (TMSR-SF2), and a similar staged approach to a liquid fuelled variant (TMSR-LF1/2).

Japan: Thorium Tech Solutions are developing the Thorium Molten-Salt Reactor (Th-MSR/FUJI).

Russia: The MOlten Salt Actinide Recycler and Transforming (MOSART) reactor is being developed by the Kurchatov Institute (Ignatiev *et al.*, 2014), and by collaboration with the SAMOFAR project.

High level (although not necessarily current) information on these reactors can be found in the IAEA Advanced Reactor Information System (ARIS) database[7] or on the World Nuclear Association website[8].

In addition, a commonality in technology is starting to emerge with some designs of high power-density fusion reactor, which intend to use the same salt as some MSRs as a liquid cooling and tritium breeding blanket (Forsberg *et al.*, 2019).

1.3 Design Features of Molten Salt Cooled Reactors

The candidate MSR designs exhibit a wide range of reactor sizes, shapes and flowpaths. The primary circuit flowpath is mostly a consequence of the choice of fuel and the neutron spectrum. The flow paths from the active core to the primary heat exchangers is via pipework in some designs. In others, the heat exchangers are immersed in the primary coolant (in a pool type reactor) or otherwise closely integrated (such as the MSFR, Figure 1.3).

The choice of static or mobile fuel, neutron spectrum, salt type and emergency or Decay Heat Removal (DHR) approach distinguish the types of reactor under development – each is discussed below. The choice of these design features is closely interdependent, and will determine the reactor physics, thermal hydraulics, and material/structural performance assessments that are required for design and licensing. The features of some of the example reactors noted above (and the MSRE for comparison) are shown in Tables 1.1 and 1.2.

Static or mobile fuel: Some reactor designs use solid fuels, mostly TRISO fuel, where encapsulated fissile particles are embedded in graphite prismatic blocks, or in spheres forming a pebble bed. This is a very similar fuel design to that proposed for High Temperature Gas-cooled Reactors (HTGRs). The notable exception is the Moltex SSR–W design, which uses a conventional fuel assembly, similar to that used in Light Water Reactors (LWRs) or Liquid Metal-cooled Fast Reactors (LMFRs), except that the fuel is a molten salt within the (vented) tube of each fuel pin.

[6] samosafer.eu
[7] aris.iaea.org
[8] www.world-nuclear.org/information-library/current-and-future-generation/molten-salt-reactors.aspx

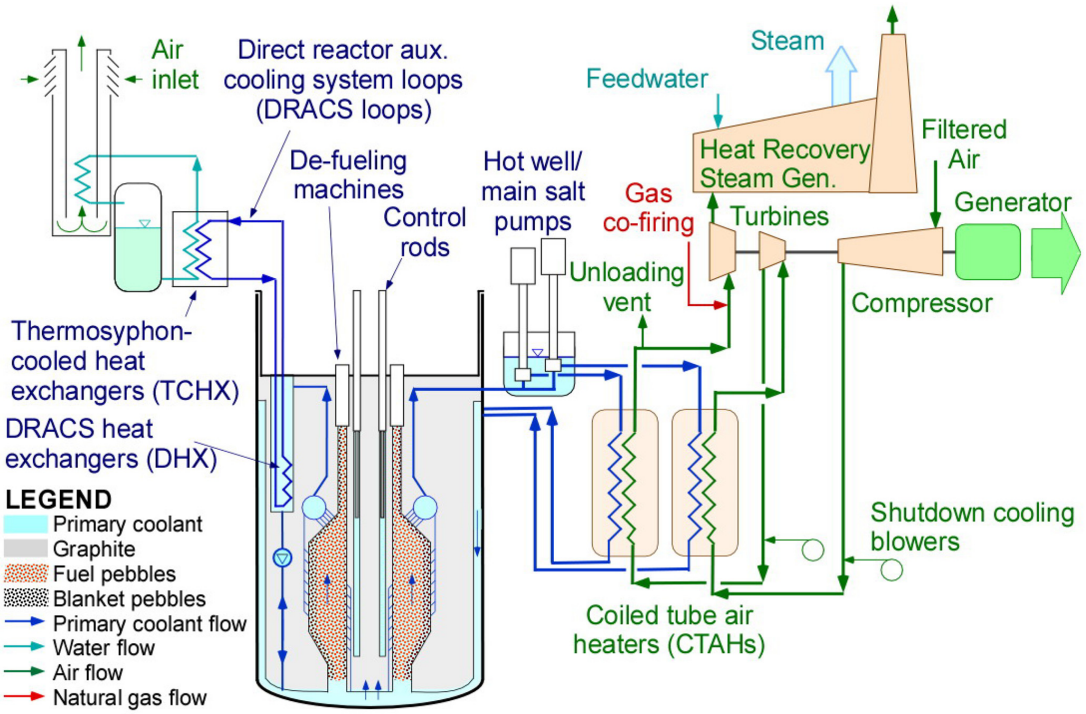

Figure 1.2: Layout of pebble bed FHR flow and heat transfer paths, showing the DRACS DHR system (Forsberg *et al.*, 2015).

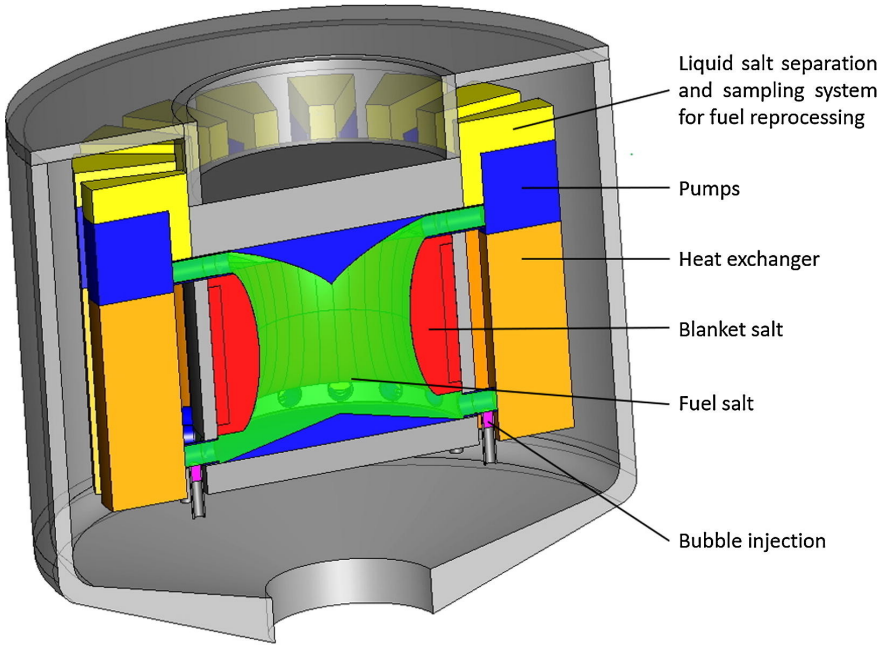

Figure 1.3: Core of the MSFR (Cervi *et al.*, 2019).

Reactor	Type	Power (MWt)	Shutdown/cooling
MSRE	Thermal, liquid fuel	8	Drain tank
SSR–W	Fast, static molten fuel	750	Reactor vessel cooling
TMSR-SF1/2	Thermal, pebble bed TRISO	10/384	Reactor vessel cooling/DRACS
TMSR-LF1/2	Thermal breeder	2/373	Drain tank
AHTR	Thermal, prismatic TRISO	3400	DRACS
KP-FHR	Thermal, pebble bed TRISO	320	Reactor vessel cooling
LFTR	Thermal breeder, liquid fuel	600	Drain tank
IMSR	Thermal, liquid fuel	400	Reactor vessel cooling
MSFR	Fast breeder, liquid fuel	3000	Drain tank

Table 1.1: Features of a selection of MSRs under development, and the MSRE for comparison. The information source for each reactor is given in the corresponding row of Table 1.2.

Reactor	Primary salt(s)	Secondary salts(s)	Reference
MSRE	$^{7}LiF-BeF_2-ZrF_4-UF_4$ (65.0-29.1-5.0-0.9 mole %)	$^{7}LiF-BeF_2$ (66-34 mole %)	Haubenreich and Engel (1970)
SSR–W	$(Na-U-Pu-MA)Cl_3$ (fuel) $NaF-KF-ZrF_4$ (coolant)	$NaNO_3-KNO_3$ ('Solar salt', tertiary)	Moltex (2018)
TMSR-SF	$LiF-BeF_2$ (FLiBe, coolant)	$LiF-NaF-KF$ (FLiNaK)	Zhimin *et al.* (2016)
TMSR-LF	$LiF-BeF_2-UF_4-ThF_4$ (fuel)	$NaF-BeF_2$	Xu (2017)
AHTR	$LiF-BeF_2$ (FLiBe, coolant)	$KF-ZrF_4$ (secondary and DRACS)	Lin *et al.* (2019)
KP-FHR	$LiF-BeF_2$ (FLiBe, coolant)	$NaNO_3-KNO_3$ (intermediate)	Blandford *et al.* (2020)
LFTR	$LiF_2-BeF_2-^{233}UF_4$ (fuel) $LiF_2-BeF_2-^{232}ThF_4$ (blanket)	$LiF-BeF_2$ (FLiBe)	EPRI (2015)
IMSR	UF_4 + fluorides	Fluoride salt	ARIS
MSFR	$LiF-ThF_4-^{235}UF_4-(Pu-MA)F_3$ or $LiF-ThF_4-^{233}UF_4$ (fuel) $LiF-ThF_4$ (blanket)	$LiF-NaF-KF$ (FLiNaK) or $LiF-BeF_2$ (FLiBe)	Di Ronco *et al.* (2019)

Table 1.2: Salts used in a selection of MSRs under development, and the MSRE for comparison.

Other designs use molten/liquid fuels, where the fissile material is dissolved in the primary coolant and flows around the reactor primary circuit[9]. The heat source from fission is released directly in the coolant (e.g. it is a heat-generating fluid). This has the advantage that no fuel assembly fabrication is necessary and fuel assemblies cannot 'melt' in an accident. In an emergency, the fuel salt can be drained into tanks of a sub-critical configuration by passive equipment. The fuel salt can be continuously reprocessed while the reactor is operating, removing fission products and minimising excess reactivity in the core. More details on the fuel cycle and broader features of liquid fuelled MSRs can be found in Křepel *et al.* (2014) and with an emphasis on the MSFR in Pioro (2016, Chapter 7).

Neutron spectrum and fuel cycle: Both thermal and fast spectrum reactor designs exist, both of which can operate as breeders, including with a thorium fuel cycle or for the transmutation ('burning') of MAs from existing spent-fuel stockpiles. Thermal designs are typically moderated by graphite that is immersed in coolant or fuel salt. For a TRISO fuelled thermal reactor, the graphite is present in the fuel pebbles or prisms, as well as in reflectors at the edge of the core.

Salt type: The choice of what salt composition to use depends on a range of considerations:

- Melting point and vapour pressure.
- Thermophysical properties (density, coefficient of thermal expansion, viscosity, thermal conductivity, heat capacity, infrared absorptivity).
- Material compatibility, corrosion potential and susceptibility or resistance to contamination by trace environmental species (such as oxygen, nitrogen or water).
- Cost.
- Solubility of fissile and fertile materials as well as fission products (including metals and gases).
- Stability under irradiation and at high temperature.
- Neutronic characteristics: moderating ability and absorption.
- Neutron activation[10] and tritium production[11].

The coolant or carrier salts used in MSRs are generally chlorides and fluorides of alkali (Li, Na, K) or alkaline earth metals (Be). This position was arrived at during the initial reactor developments described in Section 1.2. The precise composition of the salts used in a reactor design will, in some cases, be a proprietary and protected piece of information of a commercial technology developer. The composition is also not necessarily fixed during operation, because of the evolution of the presence of fission products, contamination by corrosion products, or material addition and removal through on-line reprocessing and fissile inventory control.

[9] The distinction of mobile vs. static fuel is made instead of liquid vs. solid because the ability of the fuel to move is the key feature, e.g. in the SSR–W, the fuel is liquid, but does not move except by circulation confined within its fuel pin.

[10] For example, in chloride salts ^{35}Cl (which has a natural abundance of 76%, with ^{37}Cl comprising the remaining 24%) can be activated to ^{36}Cl a beta emitting isotope with a long half-life. This may require isotopic separation of ^{37}Cl for fuels (Holcomb *et al.*, 2011).

[11] For example, lithium based salts are a common choice, but the ^{6}Li + n reaction produces tritium, which in a high temperature reactor migrates through structural components, this can be minimised by enriching the salt to contain high purity of the ^{7}Li isotope (>99.99% compared to the natural abundance of 92% ^{7}Li and 8% ^{6}Li) – this increases the salt cost. The converse situation applies to lithium based salts used in fusion reactor blankets, which are trying to maximise tritium breeding, and so require ^{6}Li enriched salts (Forsberg *et al.*, 2019).

Minimum operating temperatures are likely to be above the melting point of a salt mixture (by 50 to 100 K) for example) to avoid solidification in the primary circuit. Therefore, the selection of the composition of a salt mixture and the resulting operating temperature affects the selection of vessel materials according to their safe operating temperature, which is in-turn affected by corrosion, neutron embrittlement and creep.

Emergency shutdown and cooling: During a postulated station blackout or loss of forced cooling flow event, there is a need to both shutdown the fission chain reaction and remove decay heat from the fission products in the reactor core. It is expected that if primary heat exchangers are operating when there is a loss of forced primary circuit flow, then natural circulation will be able to be established. However, where this is not possible, there are a range of options to assure shutdown and provide heat rejection to an ultimate heat-sink:

Reactor vessel cooling: In common with other Gen IV reactors (such as several LMFR designs), some MSRs have an 'always-on' natural circulation flow path created by an annulus around the reactor vessel, either in an open-loop to atmosphere (such as an air-chimney), or in a closed loop via a heat exchanger to the environment[12]. There is a constant heat-loss during normal operation, but when the vessel temperature increases in the event of an accident, the convective and radiative heat transfer are designed to increase to the point where it dissipates the decay heat load. In Sodium-cooled Fast Reactor (SFR) designs dating back to the 1980s, this type of system is referred to as a Reactor Vessel Auxiliary Cooling System (RVACS); similar designs applied to HTGRs are referred to as Reactor Cavity Cooling Systems (RCCSs).

Drain tank: The fissile salt is drained under gravity into tanks with a subcritical geometry with an adequate reactivity margin – the draining can be initiated without operator intervention when elevated temperatures occur, via the melting of a 'freeze valve'. The drain tanks may need to have a large thermal mass (e.g. be surrounded by water) and/or will be either actively or passively cooled, including by systems similar to those described for reactor vessels above.

Direct Reactor Auxiliary Cooling System (DRACS): A heat exchanger is immersed in the primary coolant in the reactor vessel, and connected by one or more natural circulation loops to an air-cooled heat exchanger in an air-chimney (Figure 1.2).

The reactor vessel cooling and DRACS approaches still require shutdown to be ensured by neutron absorbing control rods or similar. Predicting the performance of these DHR systems with a suitably high-level of confidence for design and licensing will be one of the primary thermal hydraulic analysis tasks required.

[12] Neutron activation of Ar in the reactor vessel cooling air to ^{41}Ar may make discharging it continuously an unacceptable radiological release. This is also a potential release route for tritium (Section 2.4.4).

2 Technical Context

2.1 Molten Salt Reactor Phenomena

It is not uncommon for thermal hydraulics engineers to regard the prospect of performing analysis with molten salts with some trepidation; the unfamiliarity of them as materials creates an element of mystery around how they should be considered. Given the number of interlinked phenomena that an MSR exhibits, this is a reasonable initial view. However, for thermal hydraulic modelling aspects specifically, there is nothing particularly different about modelling molten salts compared to other working fluids, but how they are employed does require that any analysis is considered from the perspective of a fundamental understanding of the heat transfer processes. The main challenges and considerations in an analysis arise because of flows with low Reynolds number, the presence of participating thermal radiation (made more important by high operating temperatures), heat generation in the fluid, possible solidification, and the need to have salt-specific and temperature varying material properties, that are not necessarily known with high certainty.

When considering the available guidance on the physical phenomena and their analysis for MSRs it is notable that there is significantly less detailed and consolidated documentation available from, for example, the IAEA and OECD NEA, compared to the scale of that available for LWRs and LMFRs, as described in Volume 3 (Natural Convection and Passive Cooling) and Volume 5 (Liquid Metal Thermal Hydraulics). Other than the documentation from the MSRE programme, the most comprehensive general-purpose references are related to salt properties (Section 2.3). For mechanical engineering analysis aspects, the state of the available literature reflects the diversity of configurations, and the lack of programmes that have progressed to detailed design, as well as the limited operating experience with demonstration reactors. This, along with more uncertainty and variability in fuel and coolant salt properties, leads to greater uncertainty in thermal hydraulic assessments compared to other advanced reactor types. This potentially requires additional efforts to establish the necessary confidence in any analysis performed, depending on the stage of design development and the margin available.

The following reports and papers are a suggested primer giving a wide-ranging overview of the phenomena relevant to MSRs, their thermal hydraulic analysis, and the context into which that analysis will provide information:

Williams and Clarno (2008): An ORNL review of salts and the reasons to choose between them. This is a summary paper of detailed assessments of several different aspects of salt choice: thermochemical and thermophysical properties; neutronic performance (capture and moderation) and activation; material compatibility and corrosion, and material cost.

Holcomb and Cetiner (2010): An ORNL overview of salt heat transport systems, with applications not restricted to nuclear reactors, although it draws on the MSRE background knowl-

edge. This is a useful 'signposting' document to historical ORNL reports on aspects such as materials, pumps, valves, instrumentation, preheating, tritium handling and degassing, salt vapour pressure, chemistry and corrosion control, freezing, salt preparation and purification. The salt properties and heat transfer sections of this report have been largely superceded by more recent reports (Sections 2.2, 2.3 and 3.1).

Lin *et al.* (2019): A group of experts from US National Laboratories, Universities and the US NRC produced a Phenomena Identification and Ranking Table (PIRT) for the AHTR, which can usefully serve as a basis for understanding the important aspects of solid fuelled MSRs.

Diamond *et al.* (2018): Similarly to the above, a pre-PIRT was carried out for liquid fuelled MSRs[1], considering a range of potential design concepts, including fast and thermal spectrum variants.

Betzler *et al.* (2019): A description of the modelling and simulation functional needs, their interrelation and prioritisation for the purposes of demonstrating the safety of MSRs for licensing.

The last three references in particular provide descriptions of a wide range of phenomena that need to be considered in MSR analysis. The most relevant and important of these from the perspective of thermal hydraulic modelling (as opposed to neutronics and reactor physics, materials, fuel and moderator performance, structural integrity or instrumentation and control) are described in the remainder of this section. Methods for modelling the relevant phenomena are discussed in Section 3.

There are a number of features and phenomena that are related to the flow and heat transfer of molten salts:

- Flow in the core, primary circuit, and DHR circuits could be laminar, or in the laminar-turbulent transition region in some designs, because of small flow paths and the moderately high viscosity of the salts. This could be in narrow fuel channels or gaps, pebble beds or heat exchangers. This contrasts with flows in most reactor designs with non-salt coolants which are usually fully turbulent for processes of interest. Modelling this will require pressure drop and heat transfer correlations that are specific to this flow regime.
- Uncertainty and temperature dependence in the value of the viscosity of salts will lead to uncertainty in the primary circuit pressure drop and in natural circulation flow rates, both of which are important characteristics.
- Compared to LWRs, low pressure operation means that energetic vessel or pipe break flows, depressurisation, and the associated two-phase flow phenomena are not possible, simplifying some aspects of the thermal hydraulic analysis of an MSR.
- There are expected to be geometrical features (such as open plena) and reactor conditions where asymmetric or 3D flows occur.
- Reactor designs with DRACS DHR systems include a 'fluid diode' in the core flowpath that includes the DRACS heat exchanger, which has a high flow resistance under normal operation to limit thermal losses, but a low resistance when the flow direction is reversed under loss-of-flow conditions.

[1] Considered 'pre-' because the state of knowledge of candidate MSR designs and the selection of licensing basis events was not considered to be sufficiently mature.

- Thermal spectrum MSRs contain graphite, either as part of the fuel or as a moderator. The dimensions and properties (including heat capacity, thermal conductivity and coefficient of thermal expansion) of graphite change under irradiation, as is well studied in Advanced Gas-cooled Reactors (AGRs), and recently measured under high temperature conditions by Heijna *et al.* (2017). Changes in fuel prism or moderator channel geometry with core life will affect heat transfer, pressure drop and flow distribution in the core. Changes in graphite temperature will also affect the reactivity of a liquid fuelled core, because, by expanding, it can reduce the quantity of fissile material in the core.

Aspects relevant to understanding and modelling these phenomena are described in Section 2.2. Further features and phenomena that relate to MSR design and operation are:

- Temperature effects on reactivity are particularly important in MSRs, because there is a strong negative reactivity feedback from Doppler broadening with increasing fuel temperature. For liquid fuelled reactors this coupling is stronger, because an increase in temperature also reduces the fluid density, including reducing the quantity of fissile material in the core in some designs. The effect of any reactivity increase changes the primary fluid temperature directly (it is a heat generating fluid), so the feedback is immediate.
- Temperature feedback can be coupled to laminar-turbulent transition flows – where a transition occurs, the salt mean temperature (and the shape of its profile in a channel) will change, and potentially induce a reactivity change. This change in reactivity may lead to a change in buoyancy forces, that could interact with the generation or suppression of turbulence, and so this may be a coupled effect.
- For liquid fuelled reactors, the transport of Delayed Neutron Precursors (DNPs) is a unique feature, because the source of an important proportion of the neutrons required for criticality and reactivity control moves through the reactor in the interval between absorbing a neutron and fissioning. This alters the reactivity and kinetics of the core by affecting k_{eff} (effective neutron multiplication factor) and β_{eff} (effective delayed neutron fraction):
  - The movement changes the location of reactivity in the core.
  - DNPs that flow out of the core emit their neutrons elsewhere in the primary circuit (exposing pumps, piping and heat exchangers to a neutron flux).
  - DNPs that travel around the whole primary circuit before decaying will then flow to the core entrance, creating a reactivity source. The complexity of this increases during transients, such as a reactor start-up. This will require particular attention when assessing the dynamic stability of the reactor.
- Similarly, for liquid fuelled reactors it is necessary to quantify the salt composition/inventory and mass transport throughout the primary circuit through time to account for fuel depletion (requiring the neutron flux distribution) and material addition, removal and deposition. This will be used to evaluate reactivity as well as corrosion (redox) potential, thermophysical properties of the salt and radiological source terms.
- The level of uncertainty in aspects of MSR material properties and operation, and the interdependency of the reactor phenomena, mean that coupled multiphysics methods and Sensitivity Analysis (SA) and Uncertainty Quantification (UQ) will be necessary, particularly for neutronic feedback, chemistry and species tracking.

- Freezing and melting of coolant or fuel salts may play a role in normal operation (via 'freeze valves') or in fault conditions. 'Freeze plugs' are intended to melt at temperatures that occur during accidents, draining the salt from the core. Conversely, overcooling faults could freeze salt in pipework and heat exchangers, preventing flow. This is also a concern where salt vapour may condense on surfaces in cover gas systems and pools.
- Dissolved gases can be present in molten salts, and their transport and removal needs to be understood. They can be generated in the form of tritium or fission products produced by the reactor, or they may be inert gases injected to remove these species, that are themselves entrained in the salt. Transport of soluble gases can create localised reactivity feedbacks due to the evolution of bubbles or high neutron absorption cross-section species such as ^{135}Xe.

The aspects of these phenomena that pertain to developing the thermophysical properties necessary for thermal hydraulic modelling and analysis are discussed in Section 2.3. Additional phenomena relating to salt chemistry, nuclear effects and multiphase behaviour are described in Section 2.4. It is important to be aware of these, but, because they are not directly part of single-phase thermal hydraulics analysis, they are not covered further in Section 3.

Many molten salts are not fully opaque or fully transparent to thermal radiation (unlike, for example, water or helium respectively). Therefore, the coolant will transmit thermal radiation over distances relevant to heat transfer in the core, and also absorb and emit it, depending on the salt composition and state of contamination. The underlying theory and optical properties of relevant salts are described in Section 2.5.

2.2 Flow, Convection and Conjugate Heat Transfer

The behaviour of molten salts in terms of flow, pressure drop and convection is not particularly different to that of other more common Newtonian fluids. Salts do not exhibit complex rheological effects and do not have properties that are outside the range of others that are routinely analysed in engineering systems. Salts have relatively high Prandtl numbers (Pr), but other liquids (for example, oils and glycols) have substantially higher values, and water at room temperature is also a moderate Pr fluid.

The behaviour in high Pr boundary layers is well understood, and well described by Kader (1981) and Kays (1994). The high Pr means that the thermal boundary layer will be smaller (or gradients higher) than the momentum boundary layer in laminar flows and steeper in the near-wall (sublayer) region of turbulent boundary layers (Figure 2.1). This is the opposite to the effect in fluids with low Pr, where the thermal boundary layer is much larger – this is discussed in detail in Volume 5 (Liquid Metal Thermal Hydraulics). The small thermal conductivity means that within the sublayer of the momentum boundary layer, turbulent energy transport plays a proportionally bigger role because of the smaller molecular transport. The effect of the high Pr needs to be taken into account in heat transfer correlations and in the near-wall treatment in Computational Fluid Dynamics (CFD), but the implications for modelling are not as systemic and important as they are for low Pr thermal hydraulics (especially for turbulent flows, because the effect is mainly confined to the near-wall region).

The moderately high viscosity of salts and narrow flow paths in some core geometries means that

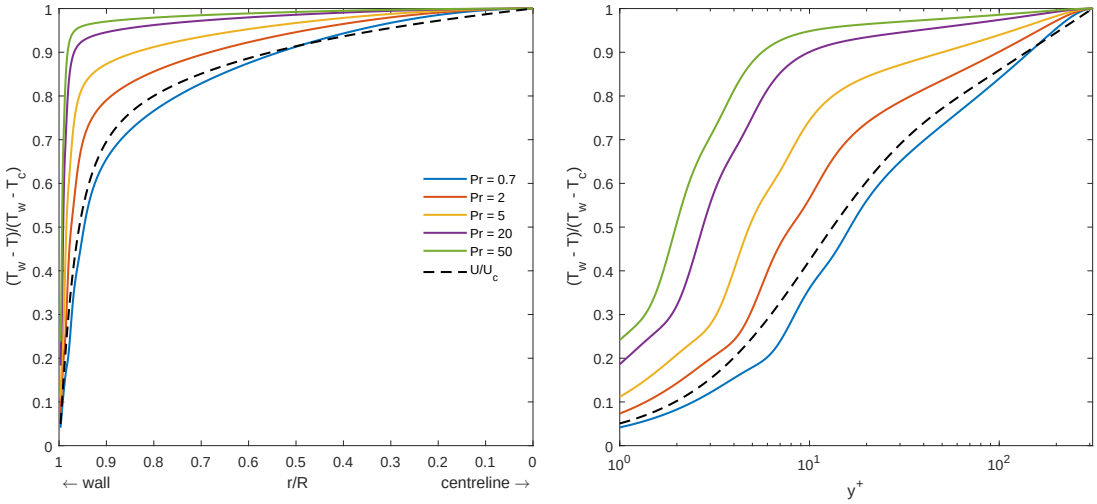

Figure 2.1: Temperature profiles for fully developed turbulent flow in a pipe (normalised by the difference between the wall, T_w and centreline, T_c) at $Re = 10^4$ for a range of values of Pr, using the expression given by Kader (1981). The corresponding normalised velocity profile (U/U_c) is shown for comparison, indicating close agreement in shape for $Pr = 0.7$, but steeper near-wall temperature gradients (smaller thermal boundary layers) with higher Pr. Left: normalised radial position, right: comparing the same profiles, plotted logarithmically against y^+.

there will be more need to model low Re flows than for other reactor designs. For example, in channel flow, there could be laminar-to-turbulent transition then re-laminarisation of flow downstream of an entrance or spacer. Alternatively, in a rod (or tube) bundle, the flow in the more open part of the cross-section could be weakly turbulent but the flow between the narrow rod-to-rod gaps could be laminar, resulting in complex and unstable interactions.

Laminar-to-turbulent transition leads to a significant local increase in pressure drop and heat transfer, and this may manifest itself during a relatively minor transient or change in operating condition. More extensive transients could include reversal of the flow direction, for example in DRACS flow loops during a loss of forced flow event, and a transition to natural circulation. In these cases the effects of buoyancy on turbulence and velocity profiles in a channel, and the resulting impact on pressure drop and heat transfer, will need to be carefully accounted for. The guidance on these topics in Volume 3 (Natural Convection and Passive Cooling) is applicable to the flow of salts. In addition, there are flow paths in buoyancy driven reactor vessel cooling DHR systems that are external, so do not use salt as a working fluid, and for these the guidance in Volume 3 is also applicable. High Pr values, coupled with low Re flows and a substantial temperature dependence of viscosity, will mean that in some conditions there is a strong temperature and hence viscosity variation near to the wall of a channel where the temperature gradient is steep. This will need to be accounted for when applying heat transfer correlations.

There are core designs, such as the MSFR (Figure 1.3), that have large open flow areas where power is generated, rather than more confined channel layouts. In these cases, there is an increased chance of complex effects caused by buoyant plumes or transiently occurring large turbulent structures, resulting in localised or rapidly changing variations in the temperature of the salt that impinges on a surface. This can have implications for structural integrity.

Some designs use pebble bed cores. While these have been studied in the context of HTGRs, the fluid properties of salts are likely to mean that the flow in the bed is in a different *Re* range for pressure drop and heat transfer predictions. An additional feature is that in FHRs, the pebbles are buoyant in the salt coolant (Andreades *et al.*, 2016); this is a feature that may require prediction in itself, and will also tend to dynamically redistribute the arrangement of pebbles in some regions of the core. This variability in possible geometric arrangements[2] will lead to localised uncertainty in flow and heat transfer performance in regions of the reactor. In addition, the localised variability in flow paths between pebbles will create hotter and cooler locations on individual pebble surfaces, and the fuel will need to be resilient to this.

Liquid fuelled reactors feature a moving heat generating fluid and mobile heat generating species (fission products and DNPs). In the context of convective heat transfer, this is not an extensively studied flow configuration compared to the detailed assessment available in textbooks that has been carried out for convection in channels without internal heat generation. This is relevant to the applicability of convection correlations, because they implicitly contain information about the shape of the temperature distribution over the fluid cross-section; internal heat generation changes this shape.

2.2.1 Conjugate Heat Transfer

In common with other reactor types, MSRs require and will benefit from modelling Conjugate Heat Transfer (CHT). Including solid structures in an analysis provides the ability to move away from unrealistic, idealised boundary conditions and allows the stored energy in fuel and reactor structures to be incorporated. The guidance available in Volume 2 (Convection, Radiation and Conjugate Heat Transfer) is relevant and applicable to MSRs.

A related phenomenon is the solidification of salt that could occur under either adverse conditions (such as an overcooling fault) or deliberately in long-term storage and material handling in filling or drain tanks. Incorporating realistic wall solids, potentially including nuclear heating, should be considered as the default option in these cases. For example, it was noted by Cartland Glover *et al.* (2019) that when CHT reactor walls were included in a MSFR reactor vessel simulation, compared to idealised boundary conditions, less freezing of the salt at a solid surface was predicted.

Freezing is possible in primary circuit pipework and in heat exchangers, potentially preventing salt from flowing at all in some regions of a heat exchanger, or reducing the available cross-section for flow in channels[3] and creating a low conductivity solid wall layer. Another possibility for the modification of the heat transfer at the interface between a molten salt and a structural solid is the formation of high thermal resistance surface layers, especially where redox control is poor (Section 2.4).

Considering solidification may also be necessary for pebbles or other solid fuel elements where the salt ‘wets’ the surface (depending on surface properties and the salt surface tension). Any adhering

[2] Aleatory uncertainty, see Volume 4.

[3] A range of more complex behaviours could also occur, such as freezing being inhibited in the centre of channels by the accelerated flow caused by narrowing of the cross-section (this may present issues for freeze plugs, where they cannot be fully frozen while the salt is flowing), or the formation of an oscillating flow where the salt repeatedly freezes due to localised cooling, but melts as a result of hotter temperatures that the flow reduction causes.

salt may freeze if removed to a lower temperature region (depending on the decay heat in the fuel), which will need to be considered in the design of refuelling processes and equipment.

2.3 Thermophysical Properties

There are two interpretations of the 'variation' of the thermophysical properties of a salt mixture:

1. Variation of the properties of a salt of a given composition with temperature.
2. The variation of the properties with the salt composition.

This section describes the available data with respect to 1, and 2 is discussed in Section 2.4.

There are a number of review papers and reports that collate and assess the available thermophysical properties for relevant salts. The incomplete and nuanced state of the available data means that obtaining and evaluating the applicable data in the following (and their references where necessary) is suggested:

Cantor (1968) and Cantor (1973): Much of the data related to fluoride coolant and fuel salts originates from these MSRE era reports. They contain important details on the experimental or estimation methods and uncertainties, qualifications and caveats that are not necessarily repeated or noted in more recent references that cite them.

Janz *et al.* (1979) and Janz (1988): The first reference presents correlations for all thermophysical properties for 49 salt systems. The latter provides density, surface tension, electrical conductance and viscosity correlations (vs temperature) for hundreds of one and two component molten salt systems. While these are extensive resources, only a very small fraction of the salts are directly relevant to reactors, and this information (and that of many other references by Janz) is generally extracted and discussed in review articles below. However, the broader data relates to salt systems with constituents relevant to MSR coolants, and is used to help with property estimation methods for other salt compositions.

Williams (2006a) and Williams (2006b): A wide ranging review of the characteristics and properties of alkali fluorides, ZrF_4 salts, fluoroborate salts and chloride coolant salts, including the reasons to select them for a particular application.

Romatoski and Hu (2017): A recent review of widely cited references which produces a set of recommended properties for $LiF{-}BeF_2$ (FLiBe), $NaF{-}ZrF_4$ (NaFZrF), $LiF{-}NaF{-}KF$ (FLiNaK), with representative uncertainties. No thermal radiation (optical) properties for these salts are presented and it is acknowledged that the dataset is incomplete, and that additional experiments to improve the confidence in the data and better quantify the uncertainties are necessary. For fluoride salts, this reference compares most of the others listed here.

Khokhlov *et al.* (2009) and Beneš and Konings (2012): A wide range of thermophysical, chemical and thermodynamic properties for a range of fluoride coolant and fuel salts. Data from various experimental and estimation sources are combined and discussed, with recommended values or correlations provided.

Sohal *et al.* (2013) and Serrano-López *et al.* (2013): Two reviews of a similar scope of the available data for density, viscosity, specific heat capacity, and thermal conductivity properties for FLiBe, FLiNaK, $LiF{-}NaF{-}BeF_2$, $NaF{-}NaBF_4$, $KF{-}ZrF_4$, $KCl{-}MgCl_2$, $NaNO_3{-}KNO_3$ (So-

lar Salt) and $NaNO_3-NaNO_2-KNO_3$ (HITEC); the latter two are common in CSP systems. The need for more complete, high accuracy correlations with wider applicable temperature ranges (especially at higher temperatures) is noted.

While the references above are able to provide property values or correlations for common salts, there would be considerable benefit in a consolidated database of improved properties (with more accuracy and over a wider range of temperatures) to support modelling and simulation. Jerden (2019) provides an interim report from a programme that is in the process of building a thermophysical properties database. This report reviews availability of a range of salts and concludes:

> *. . . some key properties for MSR-relevant salts exist in the open literature. However, the existing literature data sets are sparse and incomplete for the actinide-bearing salts relevant to modern MSR applications. It is concluded that there remains a need for an experimental program focused on collecting data needed to address the design and licensing needs of current MSR concept developers.*
> *. . . There is also a need to continue to strengthen the technical link between the MSR modeling and simulation work and the experimental thermophysical properties measurement work. For example, MSR models could provide sensitivity runs to rank the relative importance of particular salt systems and thermophysical properties so that the experimental work can be prioritized and more directly linked to the modeling and simulation work needs.*

2.3.1 Example Salt Properties

Salts that are likely to be used in reactor applications can be characterised, in comparison to water, as having similarly high volumetric heat capacities (ρc_p, one of the few coolants where this is the case), similar thermal conductivity, and substantially higher viscosity, giving higher Prandtl numbers ($Pr \approx 10$ to 30). These properties are compared to water (and helium where suitable) for a number of coolant and fuel salts in Figure 2.2 over the approximate temperature range in which they would be employed[4]. The melting points, T_M, of the salts are also shown in the legend.

In addition to the basic thermophysical properties (ρ, μ, c_p, k, ρc_p and Pr), the temperature dependence (at constant pressure) of density (volumetric thermal expansion, β) is plotted:

$$\beta = -\frac{1}{\rho}\left(\frac{\partial \rho}{\partial T}\right)_p$$

This is β that appears in the Grashof and Rayleigh numbers, and so is relevant to buoyancy driven flow and buoyancy effects in heat transfer. The values for β in the salts shown are similar to each other, and are substantially lower than for water or helium.

The normalised viscosity gradient

$$\frac{1}{\mu}\frac{\partial \mu}{\partial T}$$

is also shown, which for salts is similar to that of water (at reactor temperature). This is relevant because, in channels where there is a substantial temperature variation over the cross-section (due to internal heat generation and/or convection transfer to the channel walls and as a result of the

[4] For water this is from 25°C to close to saturation temperature at 155 bar (typical PWR primary circuit pressure).

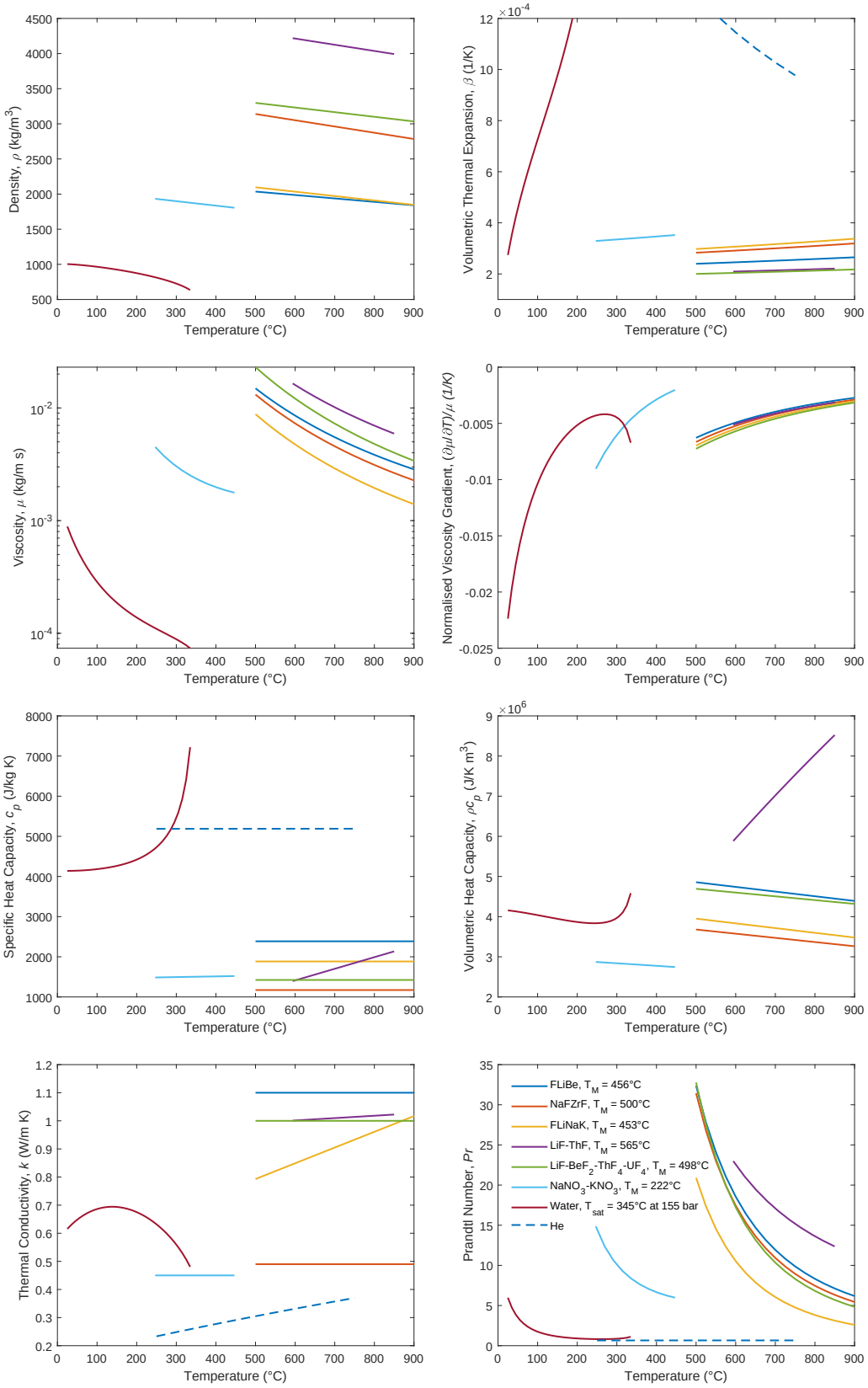

Figure 2.2: Thermophysical properties of example salts, water and helium.
Data sources: FLiBe, NaFZrF, FLiNaK: Romatoski and Hu (2017) and Beneš and Konings (2012);
LiF—ThF: Rouch *et al.* (2014); LiF—BeF_2—ThF_4—UF_4: Cantor (1968);
$NaNO_3$—KNO_3: Serrano-López *et al.* (2013) and Jin *et al.* (2016);
Water: IAPWS (Wagner *et al.*, 2000); He: NIST Chemistry WebBook (webbook.nist.gov).

high Pr), then there will be a corresponding variation in viscosity, which may need to be accounted for in a convection heat transfer correlation (Section 3.1).

A similar set of figures and more detailed comparison to a wider range of coolants, including supercritical water, CO_2, and liquid metals (but only one salt, FLiNaK) can be found in Appendix A.2 of Pioro (2016).

There are similarities in the responses to temperature of the example salt properties which are described below. The behaviour and functional forms indicate the variation of a property that should be expected with temperature. These descriptions are intended to assist in interpreting Figure 2.2 as well as the property estimation methods described in Section 2.3.2. They are also the forms of the equations that are typically found in the evolving databases and literature regarding salt properties described above.

Melting point: Fluoride salts have melting points in the region of 500°C; the nitrate solar salt is significantly lower at 222°C.

Density: The density of each salt has a linear decrease with temperature:

$$\rho = A - BT$$

Viscosity: Molten salts exhibit Newtonian viscosity behaviour (Holcomb and Cetiner, 2010), and the typical exponential decrease with reciprocal temperature (which can be referred to as the Andrade equation):

$$\mu = Ae^{B/T}$$

Specific heat capacity: Thermochemistry data in the NIST Chemistry WebBook[5] is provided as functions for enthalpy and entropy at standard pressure as a function of temperature. These can also be formulated to give c_p:

$$c_p = A + BT + CT^2 + DT^3 + E/T^2$$

Coefficients for this equation are available for pure substances, including salt constituents of interest, but not for mixtures. Because the measured accuracy of this property will be limited, it is unlikely that more than the linear terms (A and B) will be used, although the database under construction at Argonne National Laboratory (ANL) (Jerden, 2019) does also have provision for the terms in T^2 (A, B, C and E).

Thermal Conductivity: The hardest property to measure for molten salts (Cooke, 1973), which led to some confusion and errors in heat transfer calculations in the MSRE programme. Where the temperature dependence is presented, it is linear with temperature:

$$k = A + BT$$

[5] webbook.nist.gov, originating from Chase (1998)

2.3.2 Property Estimation Methods

The uncertainties in the salt properties shown in Figure 2.2 are large compared to those for water, despite these being salt mixtures (in terms of their species and concentration ratios) that are amongst the most well-studied. In some cases, the values of c_p and k are plotted as being constant with temperature; only single values are presented in the references, largely because the uncertainty in the value is of a comparable magnitude to the expected variation with temperature.

In reactor component development and testing, it is likely that alternative/simulant salts will be used, especially where fissile materials are to be dissolved in the final salt. The composition of a salt may also vary with irradiation or operational adjustments. Therefore, it is not expected that experimental data for the properties of all compositions of a salt that may be encountered will be available.

For salts without reliably measured data, the issue becomes how accurately it can be determined, either by derivation from first principles, or by estimation from correlations derived from measured data for similar salts (or the same salt constituents at a different concentration ratio). Directly measuring the properties is relatively difficult because the measurements need to be made at high temperatures and there are challenges in purifying and handling materials correctly to obtain accurate measurements. Without measures to control contamination and corrosion, the data is easily corruptible. This requirement for purity does, however, indicate that in reactor conditions, where ideal laboratory conditions are not likely to be achievable (nor necessary), then there will be a level of uncertainty or variation compared to results for pure substances.

The methods available for estimating values for the five thermophysical properties discussed above (Section 2.3.1) are described below. Guidance is available on the evaluation of density, viscosity, heat capacity, and thermal conductivity for various molten salt mixtures Na, Be, K and Li fluorides with Zr, Th, U, and Pu fluoride components. Less information is available for chloride salts, although in many cases the methods described should be equally applicable, and can be compared to the data that does exist (such as Bystrai *et al.*, 1974 and Katyshev *et al.*, 1982). The details of the methods are not reproduced here because of the level of complexity and nature of the qualifications, caveats and notes on accuracy and applicability. The noted references should be used directly.

Melting point: According to Holcomb and Cetiner (2010), an extensive database of phase diagrams exists for salt systems of all types, and there is no need to pursue estimation techniques. The majority of the binary phase diagrams of interest have been measured, as well as many of the ternary systems. Sources for this data are described in Section 2.4.3.

Density: According to Williams (2006a), density is among the most straightforward of properties to measure and is one of the most readily estimated for new compositions. The estimation method is a mole fraction weighted sum of the molar volume of the constituent salts in a mixture, which themselves are known from experiments. Given that the variation of density with temperature is linear, if molar volumes of the constituents are known at two temperatures, then the temperature variation of the mixture can also be calculated. This method is also applied by Khokhlov *et al.* (2009) and Beneš and Konings (2012), where examples are given and the accuracy discussed.

Viscosity: Viscosity is the property that varies most with temperature and salt composition. There are no simple methods for estimating it from first principles, although many systems have been studied experimentally. Determining the viscosity (and other properties) of an arbitrary salt mixture by molecular simulations is, however, a developing method, and will be discussed in Section 4.1. Khokhlov *et al.* (2009) describes a method for combining experimental data for the molar viscosity of salt components and (preferably) binary mixtures based on their molar proportions to estimate the properties of a ternary mixture. For example in Khokhlov *et al.* (2009), the viscosity of two compositions of $LiF{-}BeF_2{-}ThF_4$ are estimated from the viscosity of the $LiF{-}BeF_2$ and $LiF{-}ThF_4$ binary mixtures. Again, Beneš and Konings (2012) give examples and comments on accuracy.

Specific heat capacity: The molar mixing methods that are suitable for density and viscosity can also be applied for c_p where the data of the constituents is known. Because there is a lack of suitable experimental data, it cannot be applied for the heat capacity of mixtures containing Zr, Th, U, and Pu fluoride. However, an empirical linear correlation between experimental values for c_p ($\mathrm{J/kg\,K}$) for 30 molten fluoride salts (including those containing actindes) and inverse molar mass (M, $\mathrm{kg/kmol}$) was found by Khokhlov *et al.* (2009):

$$c_p = 291.6 + 8.02 \times 10^4 / M$$

Beneš and Konings (2012) note the following about this method:

> *Data on experimental heat capacity of molten fluoride systems containing actinide fluorides are generally lacking.* [Khokhlov *et al.* (2009)] *derived an estimation equation that is based only on the reverse molar mass of the salt mixture. However, this method must be considered only as an approximation as it sometimes gives relatively large deviations to the experimentally determined heat capacity (e.g., pure LiF or NaF). Thus, more measurements are required in order to describe the heat capacity behavior of the liquid fluoride solutions more precisely.*

An alternative is the Dulong and Petit method, which assumes a constant contribution to c_p per mole of each atom in the mixture. It is described and compared to experiment and the above expression of Khokhlov *et al.* (2009) by Williams (2006a) and Romatoski and Hu (2017). Computational thermodynamics methods (Section 2.4.5) are also able to provide c_p assessments.

Thermal Conductivity: The lack of reliable sources of experimental data for k in salts with relevant compositions makes the estimation of more complex mixtures by molar mixing not possible. However, Khokhlov *et al.* (2009) does provide an empirical expression for k ($\mathrm{W/m\,K}$) based only on temperature (K) and molecular mass ($\mathrm{kg/kmol}$):

$$k = -0.34 + 0.5 \times 10^{-3} T + 32/M$$

Beneš and Konings (2012) also provide a discussion of this method:

> *Experimental data for the thermal conductivity of molten fluoride systems are generally lacking. Although* [Khokhlov *et al.* (2009)] *recently derived an estimation method for this quantity on the basis of the available data for the molten chlorides, bromides, and iodides, more measurements are needed in order to justify*

his approach.

An alternative is the Rao-Turnbull correlation that depends on molecular weight, salt density and melting temperature, and again is discussed and compared by Williams (2006a) and Romatoski and Hu (2017).

2.4 Salt Chemistry, Thermodynamics, Dissolved Gases and Nuclear Effects

The scope of guidance on methodology described in Section 3 is limited to predictions of flow and heat transfer under single-phase (liquid) conditions, and does not provide details on the methods described in this section. However, many of the phenomena of interest in analysing MSRs are not thermal hydraulic *per se* (if that is defined as pertaining to the temperature, pressure and velocity fields of a fluid), but they either:

- depend on temperature, and so require accurate heat transfer assessment, or
- are a function of salt composition, which will define (or introduce uncertainty into) the thermophysical properties that a thermal hydraulic calculation or simulation will use, or
- involve species transport and potentially reactions within the primary, secondary or DHR circuits.

Therefore, it is necessary to be aware of how any thermal hydraulic analysis fits within or interfaces to this broader context. In many cases, these broader issues could be implemented as a sub-model within the structure of a thermal hydraulic tool, or in another tool that is closely coupled to it.

2.4.1 Salt Chemistry

For liquid fuelled reactors, the composition and chemistry of the salt is the issue around which most other considerations revolve:

> *Fuel chemistry is an area of vital importance to a fluid-fuel reactor comparable to fuel structure, cladding integrity, and coolant stability in a solid-fuel reactor.*
>
> Haubenreich and Engel, 1970

Chemical considerations are key to the selection of a salt to use as a fuel or coolant, and monitoring and controlling its chemical state will comprise a large portion of the instrumentation, operation and maintenance challenge of any MSR. One of the principal considerations is material compatibility; graphite is generally not reactive with the salts chosen when it is used as a fuel component or moderator structure, so the reactivity of the salt with structural metals (corrosion) is of greatest concern.

The alloy Hastelloy N was developed by the MSRE programme. Using this material, it was possible to control corrosion sufficiently well to have confidence that it would not be a significant technological barrier to reactor development (Grimes, 1970, Haubenreich and Engel, 1970). These materials and the understanding of their corrosion behaviour have been the subject of substantial ongoing research (Delpech *et al.*, 2010, Zheng and Sridharan, 2018). It is accepted that it is necessary to exclude oxygen and moisture from a salt and that active ‘redox control’ should be applied to

minimise corrosion (Zhang *et al.*, 2018). The redox potential of a salt measures its tendency to acquire electrons from or lose electrons to structural metals and be reduced or oxidised respectively. Holcomb and Cetiner (2010) discuss the reasons why corrosion control is very important, and an overview of corrosion in the context of broader chemical considerations can be found in Ottewitte (1992) and Fredrickson *et al.* (2018).

A corollary to corrosion and dissolution of structural materials is the deposition process, where noble-metal fission products can 'plate out' on surfaces (Haubenreich and Engel, 1970). This effect and the solubility and oxidation state of other salt constituents depends on the redox conditions (which are affected by the presence of fission products). Fission products can detrimentally alter the neutronic performance of a core, and so the design and operation of reactor chemistry may want to enable the extraction of certain elements from the salt during operation. Rigorous prediction of these processes requires transport modelling of their production rates (or thermodynamic equilibrium concentrations) and of surface deposition reaction rates, all of which can have a dependence on temperature. This could be achieved in coupled, multiphysics simulations underpinned by thermal hydraulics, although bounding and exclusion of the effects by simpler methods may be preferable (at least during reactor concept design).

For statically fuelled reactors, a subset of the salt chemistry issues are equally important, but other aspects are less severe because of the comparative stability of the composition of the fluid and its significantly reduced radioactivity and heat generation.

From a thermal hydraulic perspective, the most directly relevant phenomena are:

- The development of high thermal resistance layers on salt-metal interfaces where redox control has not been implemented and deposition occurs, which will alter convective heat transfer performance.
- Dissolution of constituents of structural alloys (such as chromium) or the presence of fission products can significantly alter the optical properties of a salt, changing the radiative heat transfer behaviour.

2.4.2 Nuclear Effects

Nuclear effects mainly impact on thermal hydraulics modelling in the form of heat sources in solid or liquid fuel regions, and nuclear heating from neutron moderation and absorption as well as gamma absorption in the salt, moderator and structure. A PIRT assessment of the neutronic modelling phenomena and needs can be found in Rahnema *et al.* (2019) (solid fuel) and in Diamond *et al.* (2018) (liquid fuel).

In all types of MSR there is an important nuclear reactivity feedback from increases in fuel temperature as a result of Doppler broadening. For liquid fuelled reactors, as described by Křepel *et al.* (2014), there is a further strong negative feedback from fuel density reduction, and in a thermal spectrum reactor, also potentially from moderator expansion (reducing the liquid space available in the core). This strong interdependency requires the physics of neutronics and thermal hydraulics to be coupled for operational and safety analysis in liquid fuelled reactors. This needs to account for the motion of DNPs, and the heat generation within the fluid from the decay of fission products, which will produce heat outside the core region (for example, in heat exchangers).

The presence of fission products and transmuted elements in the salt modifies its composition, which itself modifies the neutronics behaviour. The new species, and changes in valence state caused by their production, impacts on the salt chemistry, and the solubility and retention of gaseous fission products or the deposition of other solids, including fissile constituents. The implications for transport, retention and behaviour of these radiotoxic elements therefore is linked to Sections 2.4.1 above and 2.4.3 below.

2.4.3 Melting and Solidification: Salt Mixture Phase Equilibria

It is unlikely that a single composition salt would be used in a reactor application; a mixture of salts is used to reduce the melting point. An example of the variation in melting point with composition is shown in Figure 2.3, the phase diagram of the binary mixture $LiF-BeF_2$ (a common choice of salt, Table 1.2). Starting at the left, with pure LiF, the decrease in the liquidus[6] temperature (melting point) with increasing BeF_2 concentration can be seen. It reaches a peritectic equilibrium point at a 33.5 mole % BeF_2, 454°C, then a eutectic equilibrium point at a 52 mole % BeF_2, 355°C, before increasing with increasing BeF_2. Note that more recent evaluations of this salt have produced slightly different equilibrium points for this salt system compared to the 1950s ORNL data shown in Figure 2.3, hence the melting point of 456°C shown in Figure 2.2.

To have the minimum melting point, the eutectic composition would be chosen, but this salt is a good example of why this is not always the case. For example, one of the constituents may be significantly more expansive than the others, or there are implications for properties such as vapour pressure or viscosity. Williams and Clarno (2008) notes (citing data in Williams, 2006a) that having BeF_2 as a constituent in salt mixture can cause a large increase in viscosity:

> *In general, the other salt properties do not place severe limitations on the choice of coolant composition, and they are usually considered in combination with respect to their influence on heat transfer. The one exception to this concerns the viscosity of BeF_2-containing salts. Salts rich in BeF_2 form extremely viscous mixtures that completely restrict their use to compositions of $BeF_2 < 45\%$. Most other salts do not possess this property of forming highly viscous mixtures.*

Similarly, because of substantial increases in vapour pressure:

> *. . . the range of useful compositions is usually restricted to 40 to 45% of BeF_2 or ZrF_4 , depending upon coolant*

hence the 66.5–33.5 mole % $LiF-BeF_2$ peritectic composition is favoured, despite the higher melting point compared to the eutectic composition. One implication of this is that, in low temperature conditions, at the onset of solidification (dropping to the liquidus), one salt component will preferentially crystallise and the remaining liquid salt composition will be altered. For simple closed systems under equilibrium conditions (the type of system used to generate phase diagrams) this process will be reversible and the total composition is not altered. However, in a complex flow process in, for example, a heat exchanger, this may lead to preferential deposition on surfaces of one species and localised composition, and hence property and potentially reactivity changes.

[6] The liquidus is the line separating the area of the phase diagram that is all liquid from that where there is a mixture of liquid of one component as well crystals of another. The solidus is the line separating the area of the phase diagram that is all solid from that which is a mixture of liquid and crystals. For a more detailed introduction to the terminology, see www.tulane.edu/~sanelson/eens211/2compphasdiag.html.

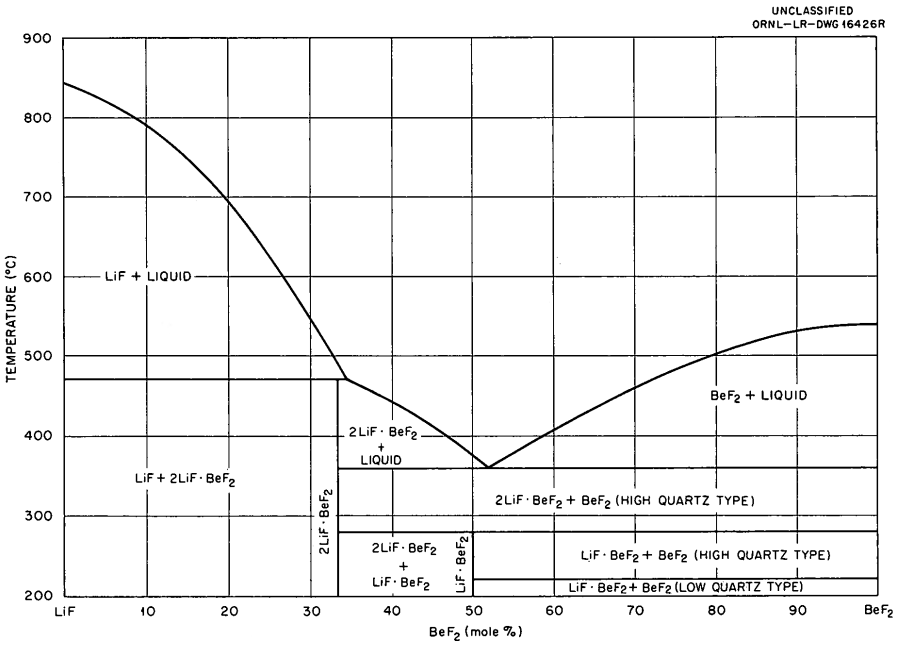

Figure 2.3: Phase diagram for LiF−BeF_2 (FLiBe) (Weaver *et al.*, 1961).

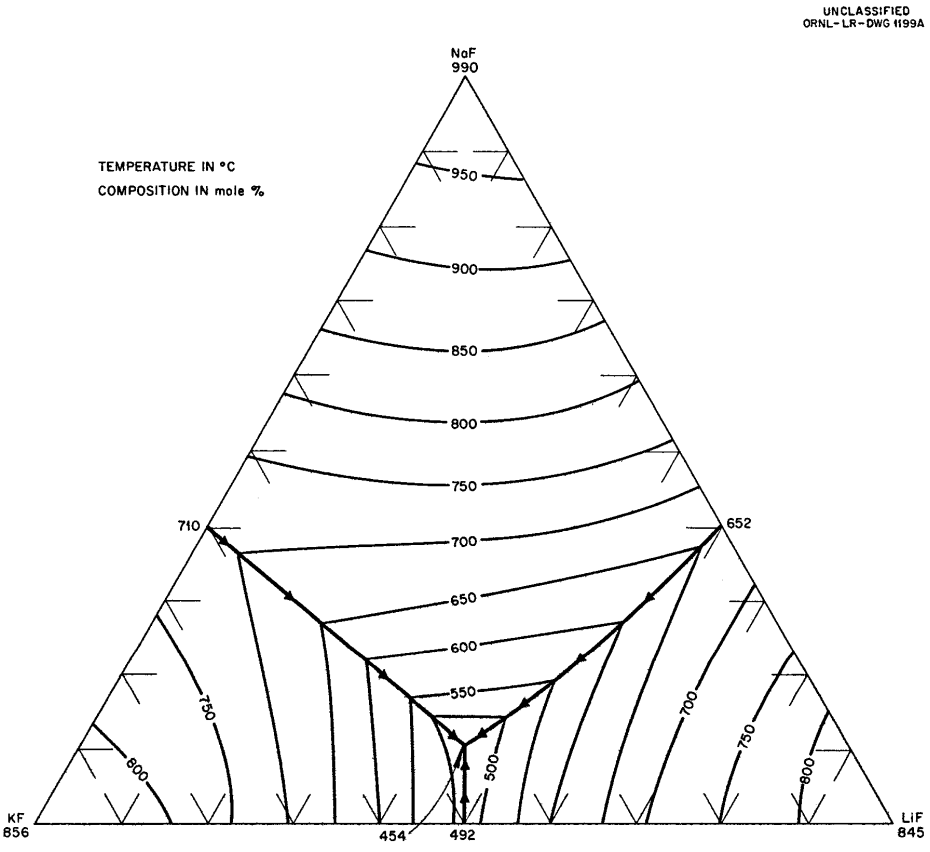

Figure 2.4: Phase diagram for LiF−NaF−KF (FLiNaK) (Thoma, 1959).

Phase diagrams can become very complex with more than two components and multiple equilibrium points; a simple ternary system is shown in Figure 2.4, which is a projection of the liquidus surface against the concentration of the three components. It has a single eutectic point at 46.5–11.5–42 mole % LiF−NaF−KF, 454°C.

Phase diagrams can be found for a range of salts considered for reactor application in Thoma (1959), Weaver *et al.* (1961), Sangster and Pelton (1987) and Beneš and Konings (2012). Ricci (1958) provides guidance on their interpretation. Data on the eutectic composition and melting point of more than 6000 salt mixtures is given by Janz *et al.* (1978).

2.4.4 Dissolved Gases, Boiling and Vapour Pressure

One of the reasons to choose a molten salt as a reactor coolant is their high boiling point[7]. In the candidate salts for reactors, the boiling points are very high (>1400°C, Williams, 2006a, Beneš and Konings, 2012) and there is therefore expected to be large thermal margins to boiling, even for onerous postulated accidents.

While boiling is not a significant concern, the vapour pressure of salts is of interest in designing reactors that are likely to have pool-like layouts (with a free surface) in either their core or other system components. This will require an inert cover gas, and gaseous fission products and tritium are expected to require removal, as described by Williams (2006a):

> *Even in a low-pressure system, the magnitude and nature of vapor produced from the salt needs to be evaluated. Experience with the ARE and the MSRE shows that very low salt vapor pressures (<1 mm Hg) simplify the off-gas system design and that certain vapor species can present problems.*
> *In any high-temperature salt system, a purged cover gas will be necessary. The transport of significant amounts of salt vapor in this cover gas system can cause problems. In the operation of the ARE, it was found that the vapor over the ARE salt (53%NaF–41%ZrF_4–6%UF_4) was nearly pure ZrF_4. Because ZrF_4 sublimes rather than boils, ZrF_4 'snow' was found in the exhaust piping.*

The composition of the salt mixture affects the vapour pressure considerably. Not all components of a mixture will have the same vapour pressure, and the fact that they are in mixtures alters their vapour pressures (their 'native' volatility is suppressed). It may also be the case that some dissolved species that arise as fission products will be volatile at normal operating conditions, while the underlying carrier salt is not.

Correlations for the variation of vapour pressure with temperature for some common MSR mixtures are given by Beneš and Konings (2012); for example, for LiF−BeF_2 (66-34 mole %) in the range of 823 to 1473 K the vapour pressure, P_{vap} (in $\mathrm{N/m^2}$) as a function of temperature, T (in K) is

$$P_{vap} = 10^{(11.914 - 13003/T)}$$

giving, $P_{vap} = 6.7\,\mathrm{N/m^2}$ at $T = 1173\,\mathrm{K}$ (900°C).

[7] The temperature at which the partial pressure of vapour salt species above a liquid surface is 1 atm.

The retention and/or controlled release of gaseous fission products (such as xenon and krypton) will need to be addressed in any design, and will depend on temperature. Some data exists for solubility (e.g. IUPAC, 1991). It was shown in the MSRE that xenon could be effectively 'stripped' (removed) from a fuel salt into an off-gas system during operation by sparging (bubbling) an inert gas into it, although this did have the effect of introducing a 'mist' of fine salt droplets into the gas space and allowing gas bubbles to circulate in the core, introducing perturbations in reactivity due to voids (Haubenreich and Engel, 1970, Engel *et al.*, 1970). In a system where entrained gases are encountered, knowledge of the surface tension of the salt will be required, and is available for a number of salts (Desyatnik *et al.*, 1975, Janz, 1988).

Another dissolved gas that requires consideration is tritium, which is produced from several neutronic reactions with Li, Be, F, in the fuel and coolant salt, and by ternary fission. At high temperatures, hydrogen and (hence tritium) can diffuse through structural metals. It can therefore escape from the primary circuit, principally through heat exchangers because they have a deliberately large surface area and thin walls as part of their design. This means that tritium will migrate to secondary or DHR circuits. There are methods available to control the concentration and migration of tritium, and they can interact with the redox control of the salt. Gas sparging is able to remove tritium from molten salts in the same way as with Xe and Kr, and tritium can be captured onto materials such as carbon. A review on the current state of knowledge and development is given by Forsberg *et al.* (2017).

2.4.5 Computational Thermodynamics

Experimentally determining the properties of mixtures of salts is not always practical or economic. To address this, computational thermodynamic modelling of phase diagrams for multi-component mixtures (a semi-empirical calculation method referred to as CALculation of PHAse Diagrams (CALPHAD), Saunders and Miodownik, 1998, Pelton, 2019) is used. This takes information that is known about the pure constituents of the mixture[8] to predict the phase diagram of complex mixtures. This allows the assessment of melting behaviour as well as the possibility for the precipitation of solid phases (including noble-metals or fission products). The solubility of dissolved gases, vapour pressure of the salt, redox potentials, density and specific heat capacity are also able to be predicted as a function of salt composition and temperature (Besmann and Schorne-Pinto, 2021).

This prediction is made by using a numerical Gibbs Energy Minimisation (GEM) algorithm to determine the interfaces between phases; Gibbs energy is related to enthalpy, temperature and entropy by

$$G = H - TS \quad \text{(or } g = h - Ts \text{ as 'specific' quantities)}$$

For a condensed (liquid or solid) phase of a pure constituent (Smith *et al.*, 2020)

$$\tilde{g}^{\circ}(T) = \Delta_f \tilde{h}^{\ominus} + \int_{T_0}^{T} \tilde{c}_p(T)dT - T\tilde{s}^{\ominus} - T\int_{T_0}^{T} \frac{\tilde{c}_p}{T}dT$$

where $\tilde{g}^{\circ}(T)$ is the molar Gibbs free energy of the material in the form of a potential, with units of $\mathrm{J/mol}$. The enthalpy of formation, $\Delta_f \tilde{h}^{\ominus}$, is the change in the sum of the internal energy and flow

[8] Pure constituents are known as 'end-members' – they are the ends/corners of phase diagrams, so LiF and BeF_2 are the end members on Figure 2.3.

work ($P\tilde{v}$) resulting from the formation of 1 mol of the substance from its constituent elements at the standard state, which is a pressure of 1 bar and a temperature of $T_0 = 298.15$ K (25°C, for more detail see Rogers and Mayhew, 1992). The absolute entropy at the standard state is represented by $\tilde{s}^{\ominus}$ (units $\mathrm{J\,K^{-1}\,mol^{-1}}$), which is the change in the entropy that results from increasing the temperature of a substance from 0 K to 298.15 K. Here $\tilde{c}_p$ is the molar specific heat capacity at constant pressure (also units $\mathrm{J\,K^{-1}\,mol^{-1}}$). This description only accounts for dependence on temperature (because it is typically dominant), but it is possible to include the effect of pressure dependence on the Gibbs energy. Data for $\Delta_f \tilde{h}^{\ominus}$, $\tilde{s}^{\ominus}$ and $\tilde{c}_p$ are available from the NIST-JANAF Thermochemical Tables (Chase, 1998)[9] for a very large range of substances.

The Gibbs energy function that results from a specific mixture of such components and the thermodyanmics of their interactions determines its response as a function of temperature, and the equilibrium state is found by minimising it (maximising entropy). Commercial GEM tools such as FactSage, Thermo-Calc or open source tools such as OpenCalphad or Thermochimica are available to perform this modelling, and the availability of databases for the necessary inputs are a key consideration. The application of CALPHAD methods is common in the assessment of metal alloys (Kattner, 1997), where there have been extensive studies, and the necessary models and data exist. The nature of salts as ionic liquids, that display local structure (short range order) mean that the models and data are less extensive and mature.

Computational thermodynamics is one part of a set of tools and specialist scientific disciplines needed to understand the detail and reasons underlying the behaviour and properties of salts. It is necessary to combine available data and comparisons from all sources and aggregate them to construct the best model possible. To provide support to modelling and simulation, ORNL are creating a Molten Salt Thermodynamic Database (McMurray *et al.*, 2019), and it is acknowledged that more measured data is needed to be able to reliably make assessments (McMurray *et al.*, 2021). A similar project is underway at the European Commission Joint Research Centre (JRC) (for example, Schacherl *et al.*, 2021 and Beneš *et al.*, 2021). While some data sources are experimental, there is also an increasing use of molecular modelling to supply inputs, and to complement CALPHAD type calculations (Smith *et al.*, 2020); this is discussed in more detail in Section 4.1.

2.5 Radiative Heat Transfer

Radiative heat transfer is a complex and nuanced discipline of physics in its own right, and it is generally only applied in a simplified and approximate manner in mechanical engineering analysis. In systems containing water or liquid metal, it is not considered because thermal radiation does not penetrate any appreciable distance before it is absorbed (although radiative heat transfer is highly relevant in the inert gas space above, for example, a liquid metal pool). In systems containing non-participating media (one that neither absorbs, emits or scatters radiation at the Infrared (IR) wavelengths of interest, such as air at moderate temperatures), there are established methods for predicting radiative heat transfer between surfaces, where simplifications to ignore the variation of surface properties with temperature and wavelength are usually applied. Radiation plays an important role in heat transfer in combustion systems, where water vapour, CO_2 and soot are present at high temperatures and in significant concentrations, and emit, absorb and scatter

[9] and from webbook.nist.gov

radiation significantly. In a nuclear thermal hydraulics context, for heat transfer over moderate distances, pressurised CO_2 (as present in AGRs), steam or gas mixtures with significant water vapour concentrations may need to be considered as a participating medium.

From this starting point, the following questions are relevant to identify what is different about thermal radiation in molten salts, and how well it is understood:

1. Are salts transparent? Do they participate in radiation? Do they scatter radiation, or just emit and absorb?
2. What components, flows, length scales and temperatures require radiation to be considered?
3. How does the emission and absorption of a salt vary with temperature and wavelength?
4. How do specific salts compare to each other and to other materials in terms of absorption and refractive index?
5. How complete and accurate is the available material property data for relevant salts?
6. What effect does the surface have (emissivity, changes with ageing, corrosion, contamination)?
7. What is the effect of additives like fissile materials or fission products (such as actinides, lanthanides or transition metals) or contaminants from impurities from the corrosion of structural materials?
8. What additional considerations are necessary beyond (or approximations necessary to use) conventional heat transfer based on the familiar $q = \epsilon\sigma T^4$ relation (as in Volume 2, Section 2.1.3; ϵ is the surface emissivity[10] and σ is the Stefan Boltzmann constant).

In general, simplified (and where possible bounding) models for accounting for radiation will be preferred. When these are implemented in a CFD code, the solution of the Radiative Transfer Equation (RTE) will already be implemented by the software, but the question will be, 'what are the appropriate models, settings and properties to apply?' For simpler calculations and system code models, similar choices will need to be applied, but in a form appropriate for the model. The approaches to implementing these calculations will be described in Section 3; the underlying theory and methods for developing the appropriate material properties are discussed below.

2.5.1 Spectral Variation and Absorption

To understand how to interpret the optical properties of a salt to calculate effective coefficients to be used in radiative heat transfer predictions, it is necessary to understand both:

- how the spectrum of emitted and absorbed wavelengths varies with temperature, and
- how this is combined with the optical properties of a salt that themselves vary with wavelength.

The blackbody emissive power from a (black) surface surrounded by a transparent medium of

[10] Modest (2013) states that strictly the term 'emittance' should be used for real surfaces with 'emissivity' reserved for pure, perfectly smooth surfaces. The same applies to absorptance vs absorptivity, reflectance(-ivity), transmittance(-ivity). However, there is not a consistent application of terminology, and the -ivity convention familiar from engineering references such as Incropera *et al.* (2011) will be applied.

constant refractive index, n, is a function of temperature and wavelength, as given by Planck's law

$$E_{b\lambda} = \frac{2\pi h c_0^2}{n^2 \lambda^5 (e^{hc_0/n\lambda k_b T} - 1)}$$

where k_b is Boltzmann's constant, h is Planck's constant and c_0 is the speed of light in a vacuum (Modest, 2013). It has the units of $\mathrm{W/m^2\,\mu m}$, so is a spectrally resolved energy flux emitted from a surface (subscript λ denotes a wavelength varying (spectral) quantity). The total emissive power of a blackbody is

$$E_b = \int_0^\infty E_{b\lambda} d\lambda = n^2 \sigma T^4$$

where it can be seen how the Stefan-Boltzmann constant arises from a combination of the fundamental physical constants found in Planck's law:

$$\sigma = \frac{2\pi^5 k_b^4}{15 h^3 c_0^2}$$

A related quantity that will be important in the RTE, because it accounts for the directionality of a radiation field, is the radiative intensity, I, which is the energy emitted from a surface in a particular direction (so the units are $\mathrm{W/m^2\,sr\,\mu m}$, where sr is steradian, solid angle). Integrating the blackbody radiative intensity leaving a blackbody, $I_{b\lambda}$ over the solid angles in a hemisphere gives

$$I_{b\lambda} = E_{b\lambda}/\pi$$

and the total intensity is the integral of the spectral intensity over all wavelengths:

$$I_b = \int_0^\infty I_{b\lambda} d\lambda$$

For real surfaces, their emissivity, absorptivity and reflectivity depend on surface temperature, and the direction and wavelength of the radiation as well as the surface finish or condition. It is common and preferable to average over all directions and wavelengths to obtain a single value for the hemispherical emissivity. Another common approximation, that leads to a single value for a surface property, is that surfaces are diffuse (there is no preferred direction) and 'gray', where there is no variation with wavelength over the region of spectrum where $E_{b\lambda}$ is large, and that the property does not depend on temperature. A consequence of applying the assumption of local thermodynamic equilibrium, stated by Kirchoff's law, is that the emissivity and absorptivity of a surface (either as single values, or resolved by temperature, directional and spectral dependence) are the same, so $\epsilon = \alpha$ can be applied. This also applies in the volume of any participating medium. From this, if scattering is ignored, the quasi-steady form of the RTE for the radiative intensity in an absorbing and emitting medium[11], along a given direction for distance s, at a given wavelength is

$$\frac{dI_\lambda}{ds} = \kappa_\lambda (I_{b\lambda} - I_\lambda)$$

where κ is the absorption coefficient (with units $1/\mathrm{m}$). Integrating with respect to the direction ds

[11] It is not possible for a medium to absorb radiation but not emit.

from 0 to s for a isothermal layer gives

$$I_\lambda(s) = I_\lambda(0)e^{-\tau_\lambda} + I_{b\lambda}(1 - e^{-\tau_\lambda})$$

where

$$\tau_\lambda = \int_0^s \kappa_\lambda ds$$

and is known as the optical thickness (for a spatially uniform value of κ_λ then $\tau_\lambda = \kappa_\lambda s$). κ is related to k, the imaginary part of the complex index of refraction, m

$$m = n - ik$$

by (Modest, 2013, Equation 2.43)

$$\kappa = 4\pi\eta_0 k$$

where η_0 is the wavenumber in a vacuum ($\eta_0 = 1/\lambda_0$).

Considering only absorption, and assuming no variation with wavelength, the more familiar quantity of absorptivity, α, from Beer's law is found (omitting λ for simplicity, but this equally applies spectrally):

$$\alpha = \frac{I(0) - I(s)}{I(0)} = 1 - e^{-\tau}$$

Similarly, considering only emission ($I(0) = 0$), emissivity is defined as the ratio of the energy emitted to emission by a blackbody at the same temperature

$$\epsilon = \frac{I(s)}{I_b} = 1 - e^{-\tau}$$

which, as for surfaces, is the same as the expression for absorptivity.

Solving the RTE in general is difficult, partly because it needs to be integrated over all angular directions, in three dimensions of space, and over all wavelengths (or alternatively be framed as gray – without wavelength dependence in properties). It requires the temperature of the medium at all points to evaluate the blackbody function, I_b, which requires the thermal radiation to be coupled to and solved with the overall energy equation for the medium. Solving the RTE can be achieved in one dimensional geometries with the gray assumption, or included in combination with conduction and convection, by approximations requiring a domain to be an optically thick ($\tau \gg 1$) or thin ($\tau \ll 1$) geometry. It can be solved numerically in realistic 3D geometries by a number of methods included in CFD codes (Section 3.3).

2.5.2 Thermal Radiation Material Properties

The IR absorption spectrum of liquid water is shown in Figure 2.5, and is compared to the blackbody emission spectra (Planck's law) at two high-temperature reactor relevant temperatures (500°C, 1000°C), and the solar spectrum. The absorption coefficient of water increases quickly after the end of the visible spectrum, and is large over the reactor temperature wavelength ranges (the temperatures relevant to water cooled reactors are even lower, hence further into the highly absorbing range).

For molten salts, the question is *'how does the absorption spectrum compare, how much does this depend on salt composition and temperature, and how much data is known?'* Significant research has been carried out into a range of single composition crystals that are constituents of reactor relevant salts because they are used as optical components for high-powered laser systems with wavelengths in the near-IR[12].

The Lorentz model is the relevant theory for the interaction between electromagnetic waves and ionic crystals. It predicts absorption in the Ultraviolet (UV) region caused by electronic excitations by short wavelength photons (referred to as the 'Urbach tail') and strong absorption at long wavelengths due to photon excitations of lattice vibrations (phonons) which begins in the mid-infrared (also called 'Reststrahlen bands'). In between these regions, the material is transparent, with the remaining absorption attributable to many factors, notably crystal vacancies and dislocations (in solid crystals), impurities and surface contamination.

Li (1980) produced a correlation and coefficients for the phonon absorption region of alkali halide salts, including LiF and NaF and NaCl[13]. A schematic representation of the absorption spectrum of an alkali halide crystal based on the Lorentz model is shown in Figure 2.6. The wavelengths where the UV and IR bands (steep increases) occur depend on the material, and the absorption level in the impurity dominated 'floor' will depend on the type and concentration of impurities. The correlation of Li (1980) was used, along with other experimental data sources by Derdeyn *et al.* (2018) and Chaleff *et al.* (2016), who produced estimates of the absorption spectrum of FLiBe and FLiNaK respectively. These estimates are shown in Figure 2.7, along with a comparison to water and to LiF and NaCl for reference. It can be seen that the wavelengths where absorption starts to increase significantly includes a substantial portion of the wavelength spectra at the reactor relevant temperatures (particularly for FLiBe).

To add complexity, as the salt or surface temperatures increase, the emitted wavelengths move towards the low absorption region, and so a salt will become more transparent to thermal radiation with increasing temperature. This may have an effect on the progress of a reactor event, where increased temperature will cause less of the emitted radiation to deposit within the coolant and will increase the exchange between solid surfaces. Because a large proportion of the heat transfer is in the impurity dominated 'transparent' wavelength region, the effect of impurities (such as chromium from structural materials) may significantly increase the absorption in this region, affecting the overall absorption (Chaleff *et al.*, 2016, Chaleff *et al.*, 2018). For salts that are used in CSP applications (including solar nitrate salts and (K−Na)Cl), their absorption spectrum is such that they absorb more strongly in the visible wavelength region (Tetreault-Friend *et al.*, 2017) and can have their absorption deliberately and substantially modified, for example by the inclusion of small concentrations of other metal chlorides (Myers *et al.*, 2015).

As a thermal hydraulics example of the processes that are occurring, consider a salt at an intermediate temperature bounded between a hotter and colder wall (assumed to be 'gray'). The emission spectrum of the hot wall, at temperature T_W, will be in the shorter wavelength region (the black

[12] There are several definitions of the spectral banding of IR. ISO 20473:2007, *Optics and photonics – Spectral bands* defines the visible spectrum to be 0.38 µm to 0.78 µm, near-IR to be 0.78 µm to 3 µm, and mid-IR to be 3 µm to 50 µm. Other disciplines such as astronomy or lighting define the banding differently.

[13] A correlation and coefficients for the UV absorption (the Urbach tail region) for the same alkali halides considered by Li (1980) (and more) can be found, if necessary, in Senatore *et al.* (1984).

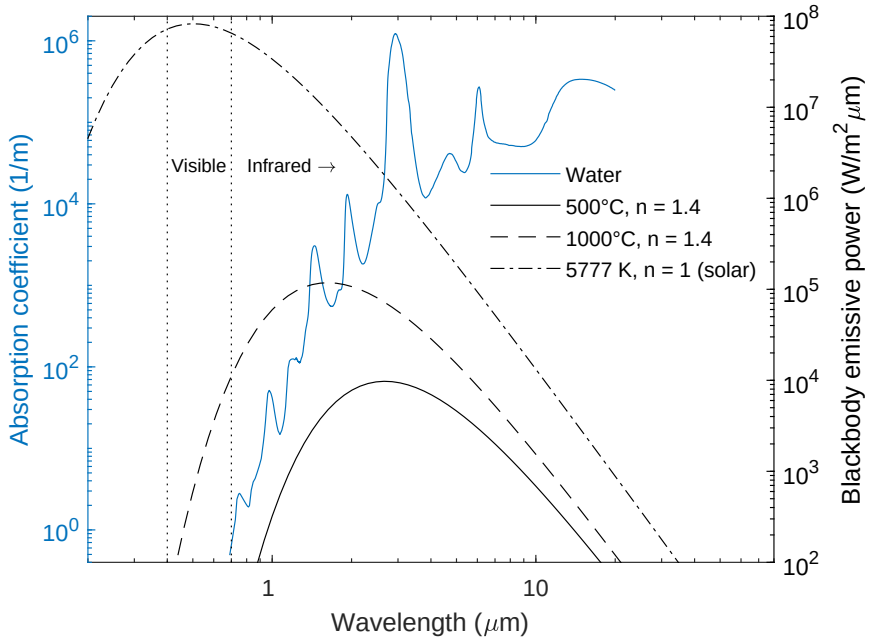

Figure 2.5: Thermal radiation emission spectrum at reactor relevant temperatures, compared to the solar spectrum, and the IR absorption spectrum of water (Palmer and Williams, 1974 and Wieliczka *et al.*, 1989).

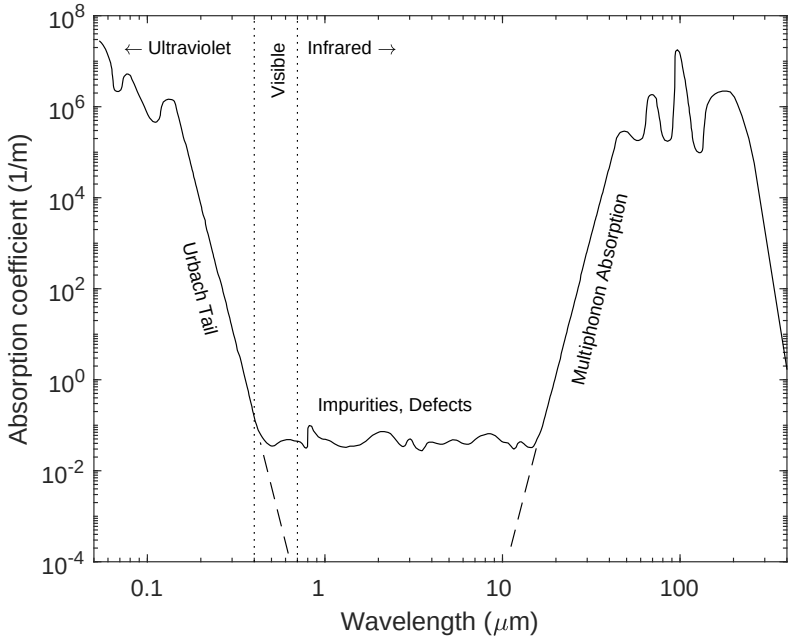

Figure 2.6: Representative absorption spectrum of an alkali halide crystal. Adapted from Li (1980).

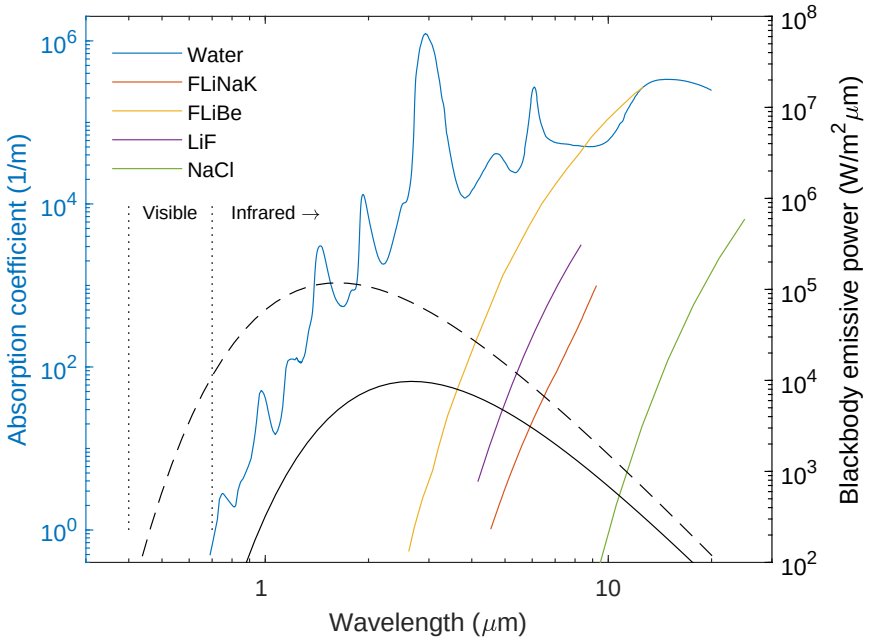

Figure 2.7: Representative IR absorption spectra of some salts compared to water. The 500°C and 1000°C emission spectra from Figure 2.5 are included for comparison.
Data sources: Water: Palmer and Williams (1974) and Wieliczka *et al.* (1989); FLiBe: Derdeyn *et al.* (2018); FLiNaK: Chaleff *et al.* (2016); LiF and NaCl (at 600°C, crystalline solid) Li (1980).

curves being further to the left on Figure 2.7) than that of the salt at T_S. The salt will absorb the different wavelengths emitted from the T_W spectrum to different degrees according to its absorption spectrum as the IR passes through it, and it will also emit according to the combination of this absorption spectrum (recalling that $\alpha_\lambda = \epsilon_\lambda$) and the blackbody spectrum at T_S ($\kappa_\lambda I_{b\lambda}$). The cold wall will receive a combination of the radiation that has been emitted from the hot wall, plus that which has been emitted from the salt, minus that from both sources which has been absorbed in the fluid.

In general the IR absorption spectrum of a salt itself, κ_λ, can vary with temperature, but not substantially. It is not even thought to be significantly different between its solid and molten phases:

- Li (1980) notes that, except for LiF, where a change in absorption was noted when molten, compared to when solid, there was no notable variation in molten samples compared to crystals (although the molten data was obtained for temperatures that were not substantially higher than the melting points).
- Tetreault-Friend *et al.* (2017) notes that the general behaviour of their molten solar salt absorption spectra agree with the Lorentz model, and that the model is considered valid for both solids and liquids.
- There is some dependence of absorption spectrum on temperature, but this is less in amorphous material (molten salts or non-crystalline solids) than for crystal lattices (Modest, 2013, Section 3.5). The IR absorption edge moves towards shorter wavelengths with increasing temperature. However, with increasing temperature the wavelength spectrum of radiation

also moves to shorter wavelengths.

The presence of fissile actinides and a range of fission products from across the periodic table is possible in a liquid fuelled reactor. There is significant information available in the chemistry literature regarding the IR absorption of relevant compounds containing many of these elements (Mamiya, 1965 for example). This is because IR absorption and Raman spectroscopy are tools used in inorganic chemistry to study the structure and composition of these materials. It would, however, require some degree of chemistry or spectroscopy domain knowledge to be able to assemble this literature into data to be used in a participating medium heat transfer prediction. No readily applicable methods have been found to robustly approximate and combine the absorption data for molten salt mixtures, let alone add arbitrary concentrations of other elements. There is, however, sufficient evidence that actinides, lanthanides and transition metals can contribute significantly to absorption in the near-IR and visible region, such that the effect cannot be ignored. There is a link to redox control in this area, because IR spectroscopy could be used as a method for determining the composition and contaminants in a salt (Zhang *et al.*, 2018).

The conclusion from this high-level assessment of the emission and absorption spectra is that thermal radiation is important for surface-to-fluid heat transfer, but, because there also is substantial potential transparency, it will also be important for surface-to-surface heat transfer. The importance will depend on the dimensions of the heat transfer channels and temperatures involved. It is likely to be the case that, in many heat transfer analyses, justifying the omission of the modelling of radiation may require more effort than including it in some form. Given the requirement for salt specific optical properties, the lack of comprehensive data, and their variation with composition and contamination, judging how much effort to put into the thermal radiation component of an analysis will benefit from an assessment of its significance to the figures of merit (via SA and UQ).

2.5.2.1 Scattering

The available literature generally does not consider salts to be scattering media to a great extent, at least in the absence of significant impurities and contaminants. Highly contaminated salts may need to be considered as scattering media, and methods exist to model this, but the increase in absorption that may arise from the necessary level of impurity may dominate any scattering that arises.

2.5.2.2 Refractive Index

The refractive index of a medium, n, plays a role in thermal radiation heat transfer in semi-transparent media. A number of sources of values for relevant salts are available, for example:

- From Modest (2013, Figure 3.16), $n = 1.3$ for NaF and $n = 1.55$ for NaCl or KBr as room temperature solids at near-IR wavelengths.
- Li (1980, Table 1) has values for optical dielectric constant $\epsilon_\infty \approx n^2$ for LiF ($n = 1.38$), NaF ($n = 1.08$) and NaCl ($n = 1.53$).

For comparison, $n \approx 1.3$ for water at IR wavelengths (Wieliczka *et al.*, 1989), which is similar to the example values for salts above. This reinforces the point that the reason that thermal radiation is not considered in thermal hydraulic analyses related to water, but is considered in salts, is related to the higher absorption coefficient in water at relevant IR wavelengths. The absorption coefficient

is related to the imaginary part, k, of the complex refractive index $m = n + ik$, and not to the real part, n, which determines the speed of propagation (or equally the wavelength) of the photons. It should be noted that n is present in Planck's law, and so influences the blackbody emission; the example spectra plotted at 500°C and 1000°C on Figure 2.5 are shown with $n = 1.4$ as a representative value.

2.6 Neutronics

Energy in fission reactors is generated by the splitting of atoms of plutonium and uranium. As the atoms split, energy and neutrons are released along with fission products. The neutrons released promote more fission events to occur, which in-turn generate more neutrons, energy and fission products. The resultant power generated by the neutron reactions is directly proportion to the quantity of fissile material in the core region and the flux of neutrons.

While neutronics calculations are necessary for all reactor types, the topic is described in this volume because there are some features specific to MSRs, and also there are similarities in the concepts and modelling approaches between participating medium radiation and neutronics.

With a sufficient mass of fuel and the correct positioning of devices, such as control rods or moderators, the reactor reaches criticality, where there is a balance between the neutrons generated, absorbed, scattered and lost. This balance is quantified by the effective neutron multiplication factor, generally known as the k effective or k_{eff}. The balanced (critical) state is achieved when the value of k_{eff} is around 1. With values below 1 the reactor is subcritical, while with values well in excess of 1, the reactor is supercritical, resulting in an exponential increase in the number of neutrons and loss of control of the reactor if no action is taken, or physical feedback mechanisms do not sufficiently reduce multiplication.

The aim for safe operation of nuclear reactors is to maintain a value of k_{eff} as close to 1 as possible, to ensure that the nuclear chain reaction is self-sustaining, and the aim of neutronics calculations is to predict how to achieve this. From the beginning of the use of nuclear reactors, numerical solvers for neutronics were developed with the aim of determining the distribution of the flux of neutrons in the reactor core. This allows the prediction of the quantities of fuel required to reach and maintain criticality, the rate of fuel use, and the effectiveness of active or passive control measures to maintain safe operation or shutdown the reactors.

Accurate predictions of the neutronic state of a reactor also enables accurate predictions of the burn-up of the fuel, which in turn allows operators to account for the material inventories of the reactor:

> *Two important analyses involved in licensing any reactor design are those of mass accountancy and radiological source terms. Mass accountancy calculations are typically done from a nuclear safeguards and non-proliferation perspective. The goal of these calculations is to confirm that from fuel production to disposal, the exact amount and location of all nuclear material is both knowable and known. While these calculations require accounting for a broad scope of possible factors, one of these factors is the evolution of the nuclear material while in the reactor. Radiological source term analysis, on the other hand, focuses on the safety implications of a particular design. This*

analysis asks what the total radiological source is in terms of possible dose rates to the surrounding areas in the event of an accident scenario.

Graham *et al.*, 2021

These issues are particularly important in liquid fuelled reactors, where the nuclear material is not held stationary and confined in solid fuel elements, and are discussed further in Section 4.2.

2.6.1 Cross Sections and Energies

The nuclear reactions that are expected in a reactor are quantitatively described in databases of neutron 'cross sections', which represent the probability of a neutron with specific incident energy interacting with a given isotope.

The neutron cross sections used in reactor calculations are held in data libraries, such as the ENDF/B-VII.1, ENDF/B-VIII.0 or JEFF 3.x libraries that are available from Brookhaven National Laboratory[14] or the NEA[15].

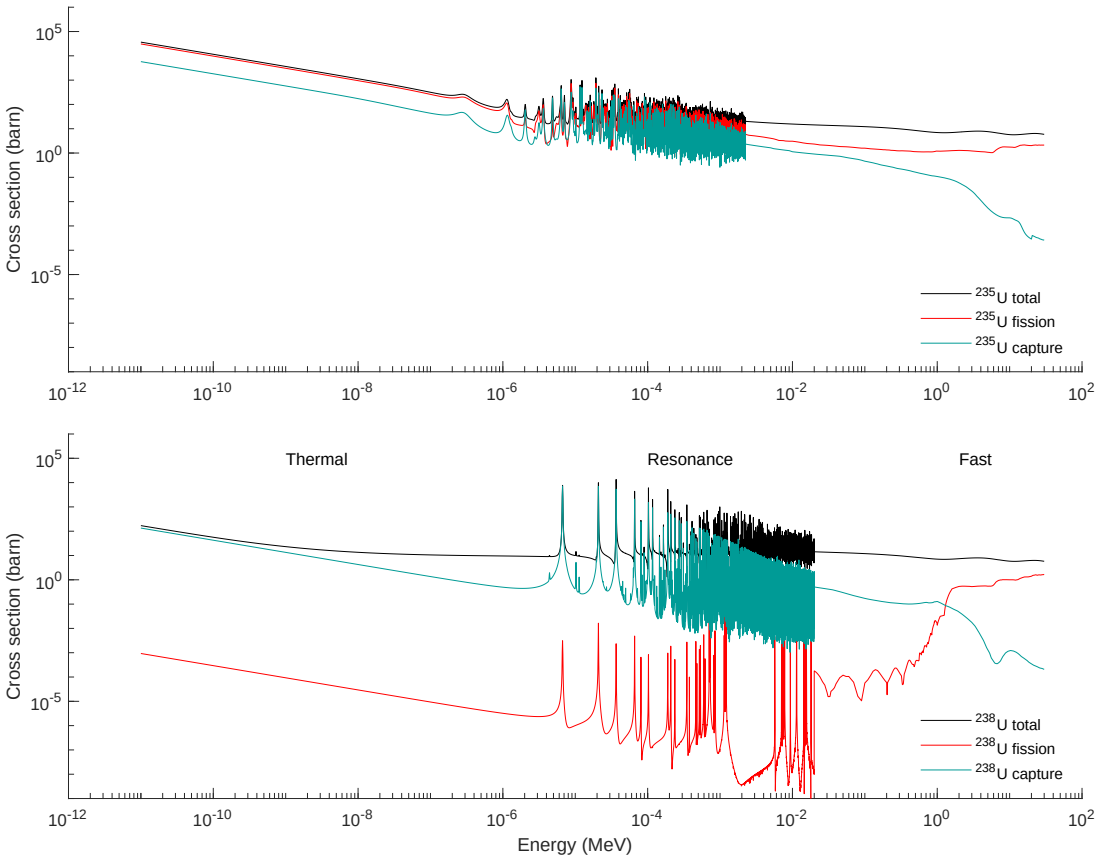

Figure 2.8: Comparisons of the microscopic neutron cross sections of the fissile (^{235}U) and fertile (^{238}U) isotopes of uranium at 21°C. NEA JEFF-3.3 library data. The cross section unit is 1 barn = 10^{-28} m^2.

The microscopic neutron cross sections for the fissile (^{235}U) and fertile (^{238}U) isotopes of uranium used in nuclear fuels are plotted in Figure 2.8 as an example. The reactions with available cross

[14] Brown *et al.* (2018), www.nndc.bnl.gov/exfor/endf00.jsp
[15] Plompen *et al.*, 2020, www.oecd-nea.org/dbdata/jeff/jeff33/index.html

section data are the fission of nuclei, the capture of neutrons by nuclei and the scattering (elastic and inelastic, contributing to moderation) of neutrons by nuclei they encounter. Three categories of neutron energy are indicated on the figure: thermal neutrons, with energies of approximately 1 eV or less[16], resonance neutrons associated with the region of many peaks and fast neutrons with energies of 1 MeV to 20 MeV.

The microscopic cross section, denoted by σ, characterises the probability of an interaction of a neutron with an individual nucleus, and has the units of area. Multiplying this by N, the number density of a given type of atom (units $1/\mathrm{m}^3$), gives the macroscopic cross section $\Sigma = N\sigma$ (units $1/\mathrm{m}$). This represents the probability per unit path length that neutrons will interact with a nucleus in a region of material of a given composition.

Figure 2.8 also demonstrates the different fission and capture behaviour between ^{235}U and ^{238}U. Fission reactions dominate over capture reactions for ^{235}U, while ^{238}U has the opposite behaviour. A large range of factors influence the cross sections. For example, the 'spin'[17] of the nuclide involved in the scattering interactions plays a significant role in the degree of scattering the neutrons undergo. The collision trajectory of a neutron's motion relative to the nuclei will influence the probability of whether it 'bounces off' a nucleus and scatters, or is captured. The nuclide temperature influences the cross sections through 'Doppler broadening,' where the resonance absorption peaks broaden due to the increase in the thermal motion of nuclei at higher temperatures. An introduction to these effects can be found in Duderstadt and Hamilton (1976).

For calculations, the neutron cross sections can be applied either in a continuous way (every datapoint is considered for each nuclide) or they are divided into a number of groups of differing energies. The distribution of the groups depends on where on the energy spectrum of incident neutrons the reactor is considered to operate. For example, LWRs are thermal spectrum reactors whose neutron cross section can be adequately approximated by two energy groups, while fast spectrum reactors will require more energy groups to approximate the distribution of absorbance peaks in the resonance region of the spectrum. The discretisation of the neutron cross sections considered for fast reactors is dependent on the numerical method used and the geometry considered.

2.6.2 Neutron Transport

The different equations that are solved by the variety of methods applied in modelling the neutronics are derived from the Boltzmann equation for the transport of neutrons (also called the neutron transport equation).

The neutron density, depending on the location in space, angle (direction) of travel, energy[18] of the neutron, and varying in time is denoted by

$$n(\mathbf{r}, \hat{\mathbf{\Omega}}, E, t)$$

This means that, at time t, the number of neutrons in an infinitesimal volume $d^3\mathbf{r}$ around the

[16] 0.025 eV at room temperature, corresponding to a mean speed of approximately 2200 m/s
[17] Here spin refers to the intrinsic angular momentum carried by elementary particles (quarks, leptons and bosons), hadrons (neutrons and protons) and atomic nuclei. Neutrons and protons have a spin of 1/2, so the addition of a neutron, forming a different isotope, could change the spin state of a nucleus and therefore it could affect the scattering behaviour of the isotope.
[18] In the form of kinetic energy, hence related to speed, $E = \frac{1}{2} m_n v^2$

position $\mathbf{r}$, travelling a direction $\hat{\mathbf{\Omega}}$[19] contained in the infinitesimal solid angle $d^2\hat{\mathbf{\Omega}}$ and an energy, E, contained in the infinitesimal energy dE is

$$n(\mathbf{r}, \hat{\mathbf{\Omega}}, E, t) d^3\mathbf{r} d^2\hat{\mathbf{\Omega}} dE$$

The *angular*[20] *neutron flux*, used in the neutron transport equation, is obtained by multiplying the *angular neutron density* by velocity

$$\psi(\mathbf{r}, \hat{\mathbf{\Omega}}, E, t) = v(E) n(\mathbf{r}, \hat{\mathbf{\Omega}}, E, t)$$

and integrating this over all possible angles of neutron travel gives the *scalar neutron flux*

$$\phi(\mathbf{r}, E, t) = \int_{4\pi} \psi(\mathbf{r}, \hat{\mathbf{\Omega}}, E, t) d^2\hat{\mathbf{\Omega}}$$

The flux of neutrons of all energies is given by

$$\phi(\mathbf{r}, t) = \int_0^\infty \phi(\mathbf{r}, E, t) dE$$

Terms using ψ and ϕ are combined to give the neutron transport equation. The description of the quantities and the terms above and the equation introduced below are a summary of the step-by-step derivation that is presented by Duderstadt and Hamilton (1976) or Demazière (2020), and it is recommended that these references are consulted for more detail, and further guidance on approaches to numerical solution.

$$\frac{1}{v(E)} \frac{\partial}{\partial t} \psi(\mathbf{r}, \hat{\mathbf{\Omega}}, E, t) + \hat{\mathbf{\Omega}} \cdot \nabla \psi(\mathbf{r}, \hat{\mathbf{\Omega}}, E, t) + \Sigma_t(\mathbf{r}, E, t) \psi(\mathbf{r}, \hat{\mathbf{\Omega}}, E, t)$$

$$= \int_{4\pi} \int_0^\infty \Sigma_s(\mathbf{r}, E' \to E, \hat{\mathbf{\Omega}}' \to \hat{\mathbf{\Omega}}, t) \psi(\mathbf{r}, E', \hat{\mathbf{\Omega}}', t) d^2\hat{\mathbf{\Omega}}' dE'$$

$$+ \frac{\chi_p(E)}{4\pi} \int_0^\infty (1 - \beta(\mathbf{r}, E')) \nu(E') \Sigma_f(\mathbf{r}, E', t) \phi(\mathbf{r}, E', t) dE' + \sum_{i=1}^{N_d} \frac{\chi_{d,i}(E)}{4\pi} \lambda_i C_i(\mathbf{r}, t)$$

The macroscopic neutron cross sections are introduced to the neutron transport equation by Σ_t, Σ_f and Σ_s, for all possible collision reactions/interactions (total, t), all fission interactions (f) and double-differential[21] scattering (s).

The average number of neutrons produced per fission is represented by ν. A fraction of $(1 - \beta)$ of these are released as 'prompt' neutrons by a fissioning nucleus, and the rest are 'delayed' neutrons, originating from fission products that have a relatively short half-life (seconds to a minute), and emit a neutron when they decay.

The probability density function for the energy of neutrons resulting from fission events is χ_p. The

[19] Where $\hat{\mathbf{\Omega}}$ is the direction unit vector, usually expressed in spherical coordintates, related to the neutron velocity vector by $\hat{\mathbf{\Omega}} = \mathbf{v}/|\mathbf{v}|$.
[20] Meaning simply that it depends on angle.
[21] 'double' in the sense that it includes angle and energy changes simultaneously.

delayed neutron precursors are accounted for in N_d groups, and the neutrons introduced by the i^{th} group are emitted with probability density function $\chi_{d,i}$ for their the energy. The DNPs are grouped by how long they take to decay, with a corresponding decay constant λ_i. The concentration or number density of DNPs in each group is C_i. There are usually six (sometimes eight) DNP groups considered. The fraction of prompt neutrons is related to the fractions in the delayed groups by

$$\beta(\mathbf{r}, E) = \sum_{i=1}^{N_d} \beta_i(\mathbf{r}, E)$$

The neutron transport equation is stated above in integro-differential form, and despite looking complex, is only counting the neutrons entering and leaving an arbitrary volume, V, enclosed by a surface, S, that are characterised by a specific energy, E, and are travelling in a specific direction, $\hat{\mathbf{\Omega}}$. This equation has the terms

$$(1) + (2) + (3) = (4) + (5) + (6)$$

(1) The rate change of neutrons contained in V.

(2) The net change of neutrons streaming across S.

(3) The loss of neutrons at this specific E and $\hat{\mathbf{\Omega}}$ from V as a result of all collision reactions. For example, a neutron scattering and only changing direction and/or energy moves to a different E or $\hat{\mathbf{\Omega}}$.

(4) This is the *inscattering* term which represents neutrons that come from a different E' and $\hat{\mathbf{\Omega}}'$ scattering into this E and $\hat{\mathbf{\Omega}}$. This term is an integral because it accounts for the neutrons scattering in from all other angles and energies.

(5) The emission of prompt neutrons, depending on the scalar flux of neutrons at a different energy E' inducing fissions that release neutrons in the energy in question E.

(6) The emission of delayed neutrons from each group.

The DNP concentrations C_i need to be calculated using N_d transport equations of the form

$$\frac{\partial}{\partial t} C_i(\mathbf{r}, t) + \underbrace{\nabla \cdot \mathbf{U} C_i(\mathbf{r}, t) - \nabla \cdot \Gamma_i \nabla C_i(\mathbf{r}, t)}_{\text{convective and diffusive transport}} = \int_0^\infty \beta_i(\mathbf{r}, E) \nu(E) \Sigma_f(\mathbf{r}, E, t) \phi(\mathbf{r}, E, t) dE - \lambda_i C_i(\mathbf{r}, t)$$

where the first term on the right hand side is similar to (5), in that it is the rate of production of precursors by fission that will lead to the delayed emission of neutrons. The second term is the rate of precursor decay. The need for the convective and diffusive transport terms is specific to MSRs because the DNPs are mobile, while most neutronics calculations are based on solid fuels held in either fuel assemblies or in TRISO particles. $\mathbf{U}$ is local flow velocity vector of the salt and Γ_i is the appropriate diffusivity of C_i, taking molecular diffusion and turbulent transport into account (although this information may not be readily available in simplified flow models).

This mobility of the fuel means that the neutronics is strongly dependent on the local fluid density, with reduced reactivity in regions of higher temperature (hence correspondingly lower density). Doppler broadening also depends on local temperature, and results in a decrease in the reactivity for most reactors, although this usually has a smaller influence than density changes. Despite

their contribution to overall neutron balance being relatively small, the motion of DNPs can lead to problems with reactor control, such as the way that flow rate changes can cause reactivity changes for the reasons discussed in Section 2.1.

The neutron transport equation has 7 independent variables (3 for $\mathbf{r}$, E, 2 for $\hat{\mathbf{\Omega}}$, t) plus N_d auxiliary C_i equations, and while it is the conceptually most simple description of the processes, it cannot be readily solved. It requires approximations to be made and numerical methods applied; these have sophisticated underpinnings and steps, which can be complex to implement. The need for convective DNP transport also requires the flow solution to be coupled to the neutronics. Section 3.4 discusses the various calculation methods for neutronics and the coupling methods that are available.

3 Methodologies

This section describes the methods and tools that are available to model single-phase flow and heat transfer in geometries and flow conditions relevant to molten salt reactors, as well as giving an overview of the methods available for modelling neutronics. This scope does not cover the details of modelling dissolved gas retention and transport, species transport and inventory tracking, or solidification, although some description of how these topics can be coupled to thermal hydraulics is discussed in Section 4.2.

3.1 Convection Heat Transfer Correlations

Heat transfer by convection in molten salts is not fundamentally different to that in other fluids (as discussed in the reviews described in Section 3.1.1 below). Salts have a higher Prandtl number than gases or water, and lower Reynolds number turbulent flows are expected, but neither of these features is intrinsically difficult to model. Internal flow heat transfer correlations that are valid for Pr values relevant to molten salts are well established. The recommended heat transfer correlation for fully developed turbulent flow[1], applicable to constant wall heat flux and constant wall temperature conditions, is the Gnielinski correlation:

$$Nu = \frac{(f/8)(Re - 1000)Pr}{1 + 12.7(f/8)^{1/2}(Pr^{2/3} - 1)}$$

which has a validity of $2300 \leq Re \leq 5 \times 10^6$ and $0.5 \leq Pr \leq 2000$. This is a correlation for a *smooth* circular pipe, where the friction factor is evaluated using

$$f = \frac{4}{(1.58 \ln(Re) - 3.28)^2}$$

It also possible to include the effect of surface roughness, which tends to increase heat transfer, directly through f by using a correlation such as that of Haaland:

$$f = \frac{4}{\left[3.4735 - 1.5635 \ln\left(\left(\frac{2\epsilon}{D}\right)^{1.11} + \frac{63.635}{Re}\right)\right]^2}$$

which has a validity of $4000 \leq Re \leq 10^8$ and $2\epsilon/D \leq 0.1$. This approach is only an approximation for the effect on Nu (Incropera *et al.*, 2011). Correlations specifically designed for fully rough[2]

[1] This means both hydrodynamically and thermally fully developed. References such as Kakaç *et al.* (1987) and Rohsenow *et al.* (1998) contain the correlations for Nu and f shown here, and also describe methods and correlations for assessing Nusselt numbers in specific developing flows, such as entrance regions.

[2] Roughness Reynolds number, $Re_\epsilon = \epsilon u_\tau/\nu$, using the roughness height ϵ, is used to characterise a surface as being either hydrodynamically smooth, $Re_\epsilon < 5$, transitional, $5 \leq Re_\epsilon \leq 70$, or fully rough $Re_\epsilon > 70$.

channels are documented in Kakaç *et al.* (1987, Chapter 4), which also provides the means to modify any smooth pipe Nusselt number correlation, Nu_s, for the effects of transition roughness by using the ratio of rough to smooth friction factor:

$$\frac{Nu}{Nu_s} = \left(\frac{f}{f_s}\right)^n \quad \text{where} \begin{cases} n = 0.68Pr^{0.215} & \text{if } 1 < Pr < 6 \\ n \approx 1 & \text{if } Pr > 6 \end{cases}$$

This holds for $f/f_s \leq 4$; for larger friction factor ratios than approximately 4, there is no further increase in Nu. The relationship for n indicates that convection for fluids with $Pr > 1$ is more affected by surface roughness than, for example, gases, where $Pr \approx 0.7$.

The frequently applied Dittus-Boelter equation is not recommended for flows where $Re < 10^4$ and is also less accurate than the Gnielinski correlation at higher Reynolds numbers (Kakaç *et al.*, 1987, Chapter 4). Tube bundle heat transfer correlations for cross flow and axial flow have similar validity ranges for $Pr > 1000$, and are also not inherently limited by the properties of salt (Kakaç *et al.*, 1987, Chapters 6 and 7).

Lower Re flows and a reliance on natural circulation in some situations does mean that there will be a requirement to assess whether a correlation suitable for natural or mixed convection is needed. Free convection is well documented, but mixed convection less so (see Volume 3). Jackson *et al.* (1989) provide a thorough review from an experimental and theoretical point of view for 'moderate Pr fluids' (not liquid metals) in vertical tubes. It is worthwhile restating the review's summary:

> *In laminar mixed convection, heat transfer is enhanced in heated upward flow and impaired in heated downward flow. The problem is amenable to calculation, although transition to turbulent flow may occur earlier than for forced convection or free convection alone.*
> *Turbulent mixed convection, heat transfer to moderate Prandtl number fluids is dictated by changes in turbulent diffusion. In heated upward flow heat transfer is impaired with modest buoyancy and enhanced with high buoyancy. It is not possible to correlate with precision heat transfer in the region of impairment using local parameters. In contrast heat transfer levels in heated downflow increase monotonically with increasing buoyancy and have been correlated successfully in terms of local variables.*

The expected magnitude of these effects should be assessed wherever buoyancy is expected, and it should be specifically noted that heated upwards flow[3] can be complex and hard to predict with simple methods in some conditions.

Although there are not significant conceptual differences to other fluids, and the same modelling and correlations can be used in most circumstances as a first approximation, there are nuances and differences in emphasis that are important to consider for convection in MSR applications.

Property uncertainty: while the same correlations may be used as other fluids, their accuracy is tied to that of the fluid properties used to evaluate them. k, μ, c_P and ρ are all required to determine a Heat Transfer Coefficient (HTC), and so uncertainty in properties (either caused by lack of data or changes in composition) will propagate to the heat transfer prediction. The

[3] otherwise called 'buoyancy assisted flow', which also occurs in downwards flows that are cooled.

methods that can be used to assess the effect and significance of uncertainties in material properties when applied in a system code or in a CFD calculation are discussed in Volume 4.

Property variation: the properties of salts depend on temperature, and the effect of this on convection will be discussed in Section 3.1.2.

Heat generating fluids: the presence of heat sources in fuel salts alters their convection behaviour, and is discussed in Section 3.1.3

Simultaneous radiative heat transfer: where salts are semi-transparent there is heat transfer between fluid and walls simultaneously with convection. This will be discussed in Section 3.1.4.

Uncertainties and complexities in the use of correlations that arise from these effects will also need to be compared to the inherent uncertainty in any correlation and the situation to which it is applied. For example, the assumptions of fully developed flows and constant wall heat flux (or temperature) are rarely truly representative in realistic situations.

3.1.1 Experimental Studies and Correlation Reviews

Accompanying the resurgence of interest in MSRs, a number of reviews have been conducted into the available experimental data and assessments made of the applicability of heat transfer correlations:

Ambrosek *et al.* (2009) re-evaluate previous convection experiments, including those from ORNL related to the MSRE, in the light of improved knowledge of salt material properties. This supports the conclusion that convection behaviour in salts is not intrinsically different to other fluids, however, the high temperatures involved mean that attention needs to be paid to heat transfer fundamentals and scaling analysis in designing and interpreting experiments. The combination of convection and radiation will need to be understood, and the need for high-quality property data is essential, preferably with an estimate of its uncertainty. Britsch *et al.* (2019) also includes a review of historical experiments that supports these conclusions in its description of creating a contemporary convection loop experiment.

Holcomb and Cetiner (2010) and Yoder (2014) include a summary of historical heat transfer experiments from ORNL and the applicability of conventional correlations for internal forced convection is assessed. This demonstrates that there is not much heat transfer data available, and that the difficulty of performing the experiments, as well as the age of some of the data (mid 1950s) makes the potential uncertainties relatively large. Conventional heat transfer correlations are shown to be applicable for laminar and turbulent flow, as long as suitable material properties are used. The potential for the formation of high thermal resistance layers is also noted in conditions where there is inadequate corrosion control, which can distort results. The form of the correlations used is discussed in Section 3.1.2 below.

Wu *et al.* (2012) report experiments for turbulent and transition Reynolds numbers for HITEC and $LiNO_3$, which are compared to data from the same historical experiments as above, and to similar convection correlations that also account for temperature varying properties. Similar conclusions to that of Yoder (2014) are reached, where the correlations compare relatively well to the data, noting that it contains scatter and a typical agreement of approximately $\pm 20\,\%$ or better is seen.

Yoder *et al.* (2018) report experimental results for natural convection from a vertical cylinder in

a larger cylindrical space and demonstrate that the natural convection correlations for this configuration developed for other fluids can be successfully applied. The flows are predominantly laminar, and there are more uncertainties for turbulent results (generated by high Ra conditions). It is also noted that there is a need to correct the assessment of convective heat transfer for simultaneous radiation.

Zhang *et al.* (2020) compare correlations of the kind discussed in this volume, the same experimental data as discussed above (with attention paid to modifying historical results with improved knowledge of material properties) and the results of CFD models using coolant and fuel salts. The authors are able to find an overall good agreement between the three approaches, but note that uncertainties of up to $\pm 20\,\%$ are seen.

3.1.2 Temperature Variation in Properties

Heat transfer correlations for internal flows are typically derived with the assumption of constant fluid properties over the cross-section of a channel at a particular location, and the properties are usually evaluated at the bulk temperature (as they are in the Gnielinski correlation above). Bulk temperature is the mass flux weighted average temperature of the fluid, see Volume 2, Section 2.1.2. However, this assumption of property uniformity does not hold when the material properties depend strongly on temperature, particularly viscosity. In cases where there is significant heat transfer at a wall, the viscosity in the near-wall region can be substantially different, leading to changing velocity gradients, and a change in convection behaviour. This is the case for salts, where, because of their relatively high Pr, there can be significant temperature differences across the momentum boundary layer.

Kakaç *et al.* (1987, Chapter 18) provides the most detailed description of the effects of temperature on convection correlations (although Kays *et al.* (2005) and Incropera *et al.* (2011) also have some useful guidance), and suggests that for liquids[4] the following corrections can be applied

$$\frac{Nu}{Nu_{CP}} = \left(\frac{\mu_b}{\mu_w}\right)^n$$
$$\frac{f}{f_{CP}} = \left(\frac{\mu_b}{\mu_w}\right)^m$$

The ratio of viscosity evaluated at the bulk (b) and wall (w) temperatures is used to correct the Nusselt number evaluated assuming constant properties (CP). Various values to choose for n and m are reviewed in Kakaç *et al.* (1987), and recommended values for turbulent flow that can be applied to the Gnielinski correlation are

$$\frac{\mu_b}{\mu_w} > 1, \quad n = 0.11 \quad \text{for heating liquids}$$
$$\frac{\mu_b}{\mu_w} < 1, \quad n = 0.25 \quad \text{for cooling liquids}$$

which is valid for $10^4 < Re < 5 \times 10^6$, $2 < Pr < 140$ (Re and Pr evaluated at the bulk temperature) and $0.08 < \mu_w/\mu_b < 40$. As an example, for FLiBe at 850 K bulk and 950 K wall temperatures, the viscosity ratio is 1.59 and ratio of ratio $Nu/Nu_{CP} = 1.053$ using $n = 0.11$, meaning that heat

[4] The behaviour for gases is different – viscosity increases with temperature, and density and conductivity also change significantly. For liquids, viscosity tends to decrease with increasing temperature, and varies more than other properties.

transfer is expected to be increased by approximately 5 % due to the variation of properties.

An alternative correlation accounting for property variation in smooth pipes, that does not use the viscosity ratio approach, and is valid for liquids and gases is that of Sleicher and Rouse (1975)

$$\begin{aligned} Nu_b &= 5 + 0.015 Re_f^a Pr_w^b \\ a &= 0.88 - 0.24/(4 + Pr_w) \\ b &= 1/3 + 0.5 e^{-0.6 Pr_w} \end{aligned}$$

valid for $10^4 < Re < 10^6$ and $0.1 < Pr < 10^5$. It also a good example of the need for care and clarity in which temperature is used to evaluate properties: Nu_b, Re_f and Pr_w use the bulk, film and wall temperatures respectively in the same correlation. It is notable that turbulent correlations with validity between transition Reynolds numbers and $Re = 10^4$ are unusual – the Gnielinski correlation was created to specifically extend to lower values.

For laminar flows the Sieder-Tate correlation can be used, which includes a term where $n = 0.14$

$$Nu = 1.86 \left(RePr \frac{D}{L} \right)^{1/3} \left(\frac{\mu_b}{\mu_w} \right)^{0.14}$$

and there are some features of this correlation that raise points relevant to the reviews mentioned in Section 3.1.1 above:

- This correlation contains the Graetz number term, $Gz = RePrD/L$, making it dependent on downstream distance, so is necessarily only applicable to flows that are still developing (which in laminar conditions can be over a long distance).
- The correlation is derived for constant temperature boundary conditions – for laminar flows, the difference between constant temperature and constant heat flux boundaries matters; for turbulent flows, often the same correlation can be used by both.
- The value of Nu that this correlates is the mean Nusselt number over the entire channel length, L – it does not give the local value varying as a function of L/D. This also introduces some dependency on the upstream and inlet conditions to the channel, and the correlation has limits on its applicability, making it not accurate for very short and very long channels.
- The values of Nu, Re and Pr relate to material properties at the bulk temperature.

When the correlations are reviewed in the contemporary references it is often the case that the descriptions are incomplete with regard to these points, and the guidance is somewhat ambiguous. The original references or thorough assessments such as in Kakaç *et al.* (1987) should be consulted.

The experiment and analysis by Cooke and Cox (1973) of forced convection heat transfer using a proposed MSBR fuel salt, $LiF{-}BeF_2{-}ThF_4{-}UF_4$, is a good example. They show that the laminar Sieder-Tate correlation above, and its fully developed turbulent equivalent (also applying $n = 0.14$) agree relatively well with the data when correctly compared (Figure 3.1). They report that the correlations lie about 13 % above the experimental data in the turbulent region, and also propose slightly modified coefficients to the relations that they use that bring the agreement to within approximately 6 %. In this reference, the need for accurate properties is emphasised, which is true in all instances,

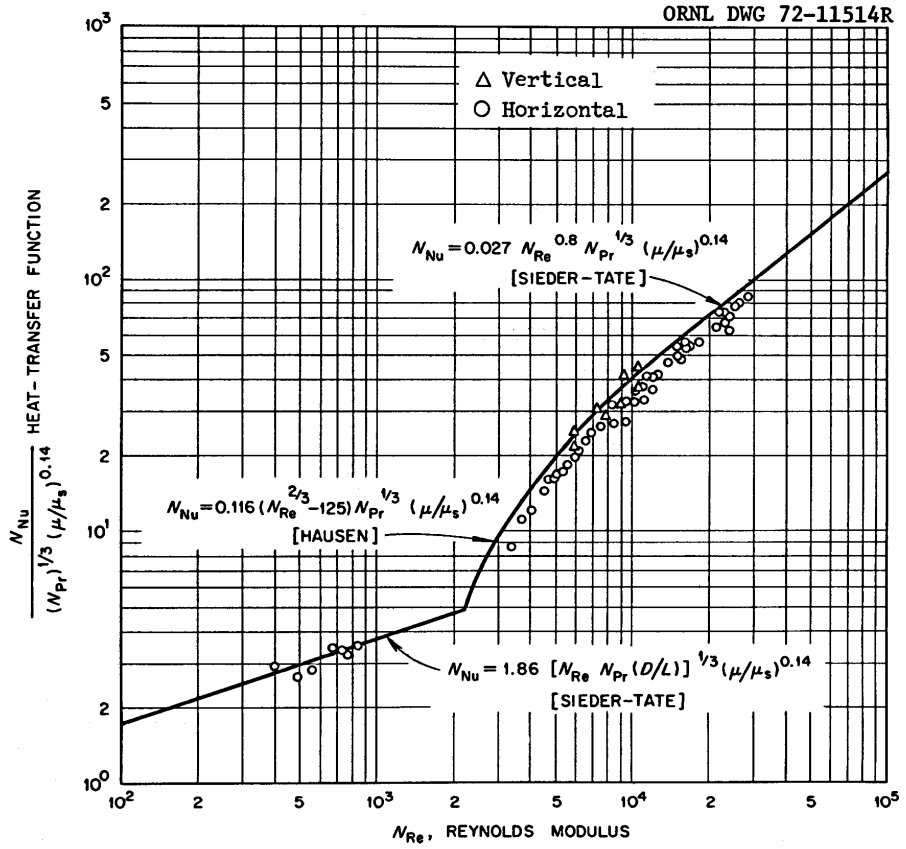

Figure 3.1: Forced convection data compared to correlations accounting for property variation across the laminar, transisiton and turbulent flow regime, from Cooke and Cox (1973). μ_s is the viscosity at the surface temperature and μ is at the bulk temperature.

but this also shows that salts do not behave in a different way to other fluids for forced convection heat transfer.

The concluding remarks in Kakaç *et al.* (1987, Chapter 18) discuss how more detailed analytical assessment is not tractable, requiring numerical methods, and that experiments are hard to perform because large wall-to-fluid temperature differences are needed. It is also the case that (minor) improvements in accuracy are possible for turbulent flows by considering the specific shape of a non-circular channel (rather than a simple circular channel equivalent hydraulic diameter).

This suggests that CFD assessment of the geometry, flow and heat transfer regime and materials specific to a problem at hand would be a valuable way of gaining insight and developing correlations. This requires that the chosen CFD turbulence modelling approach is able to represent the interaction between property changes and turbulence (as well as the effects of buoyancy and heat generation, as discussed below).

An example of determining the effective heat transfer and friction factor from CFD is given in Study B: Fuel Assembly CFD and UQ for a Molten Salt Reactor.

3.1.2.1 Natural Convection

Natural convection (free convection and buoyancy driven flow in enclosures) inherently takes density differences into account, although sometimes only as the Boussinesq approximation, but in many cases correlations do not account for other property changes. Kakaç *et al.* (1987, Chapter 18) again provides a detailed assessment, and Yoder *et al.* (2018) reviews similar correlations. Corrections that involve the ratio μ_∞/μ_w are applied and the need to incorporate a temperature varying value of β is noted, where it appears in the Grashof and Rayleigh numbers. The experiments and numerical modelling of Cuckovic-Dzodzo *et al.* (1999) for laminar recirculation in cavities for high Pr fluids shows that accounting for property variation is necessary to correctly represent the flow patterns and heat transfer.

In some cases, improved natural convection correlations are achieved by modifying the temperature used to evaluate properties that parameterise them. Reference temperatures of the form

$$T_r = T_w - x(T_w + T_\infty)$$

with values of $0.25 \leq x \leq 0.5$ may give the best result; $x = 0.5$ gives the familiar film temperature that is typically used for natural convection.

One of the conclusions that can be reached by reviewing the limited experimental data, and the careful analysis that accompanied it in historical references, is that it may serve its most useful purpose as guidance on interpreting, parameterising and generalising high quality CFD results into correlations, rather than as a source of correlations itself.

3.1.3 Fluids With Internal Heat Generation

Heat generation within a fluid means that the temperature distribution implicit in the heat transfer correlations, derived from idealised constant wall heat flux or constant wall temperature boundary conditions, is not applicable. This is particularly the case for laminar flow, where the shape of the temperature profile in a channel has a substantial effect. Typically turbulent correlations are less sensitive to the details of a channel cross-section geometry (and so they can usually be successfully parameterised by a hydraulic diameter). However, if the volumetric heat source (q_{vol}, in $\mathrm{W/m^3}$) is sufficient, it will change the temperature distribution in turbulent flows too, increasing temperatures particularly in the slow moving region near to a wall. For a given wall heat flux into a channel from the wall (heating the fluid), the presence of heat generation in the fluid will increase the wall-to-bulk temperature difference, and reduce the apparent HTC. For wall heat flux out of a channel (cooling the fluid), the opposite is true, wall-to-bulk temperature difference is reduced, indicating a higher apparent HTC.

Heat transfer from flows with internal generation was successfully analysed for hydrodynamically fully developed[5] flows in the pre-MSRE era (Poppendiek and Palmer, 1952, Poppendiek and Palmer, 1955 and Siegel and Sparrow, 1959). Subsequent experimental studies showed that the predictions made by the analysis agreed well with experiments for simple pipe flow configurations. For example, Kinney and Sparrow (1966) show experimental wall-to-bulk temperature difference

[5] i.e. the velocity field was developed in a long adiabatic section with no heat source, but the temperature field does not need to be fully developed.

results for turbulent flows of a fluid with Pr = 3 to 4 that agree with the analysis. In this case, it was demonstrated that, as predicted, when a pipe is adiabatic and there is a volumetric heat source in the fluid, the wall temperature is actually higher than the bulk (or centreline) temperature. Michiyoshi *et al.* (1968) shows experimental data for temperature profiles across a channel for turbulent flows, which compares well with the analysis of Siegel and Sparrow (1959). For laminar flows in vertical pipes, they demonstrate that buoyancy effects near to the wall would need to be taken into account in the analysis. The validation was largely intended to test the applicability of Reynolds analogy in heat generating fluids – the hypothesis that momentum and thermal diffusivity are similar in moderate to high Pr fluids was used as an assumption in the derivation of the predictions, and confirmed by the experiments.

More recent analysis using a similar approach (Di Marcello *et al.*, 2010) was also able to predict the same temperature profiles, and then express a relationship (Fiorina *et al.*, 2014) between the turbulent Nusselt number for fluids with internal heat sources, $Nu_{q_{vol}}$, and without, Nu (i.e. a conventional pipe flow correlation). This is a function of heat source, q_{vol}, wall heat flux, q (signed as inwards or outward; inwards is positive), pipe diameter, Re and Pr:

$$\frac{Nu_{q_{vol}}}{Nu} = \frac{1}{1 + \frac{q_{vol} D}{q} \frac{1.656}{Pr^{0.4} Re^{0.5}}}$$

Therefore, there is a large difference in apparent Nusselt number expected for large values of D, low values of Pr or Re, or large ratios of q_{vol}/q. This expression is not necessarily convenient to implement in a conventional system code, because it contains q, the pipe wall heat transfer, which is usually the quantity that a Nusselt number correlation is being used to evaluate in the code. Therefore, there would be a need to iterate to find the suitable value, and a code would need to be written to expect this. To implement and test functionality for wall heat transfer with heat generating fluids in a calculation, the 1950s references above are recommended as a starting point, because of the detail and clarity of their descriptions.

The analysis that is discussed in the references above for turbulent flow is for axisymmetric, fully developed flow in a pipe, assuming constant fluid properties, uniform heat source, and not considering buoyancy effects, so the ability to apply it to realistic conditions has some limits. In these analytical approaches, the success of the prediction is dependent on knowing, as an input, an accurate distribution of velocity and eddy diffusivity across the channel. This is available for simple configurations like fully developed flow in smooth circular pipes, but is not known in general. However, the conclusion that, with an appropriate description of turbulence, the presence of internal generation is readily predicted supports the application of CFD to these conditions. CFD using the material properties, geometry and heat transfer conditions for a specific situation would therefore be more insightful, both as an analysis method in itself, and to generate inputs and correlations for system code models. The references discussed here would be valuable for the interpretation of the results, and to help define the appropriate parametrisations to extract transferable correlations.

The situation of a heat generating fluid in a closed vertical cylinder (i.e. no net flow through a channel) is studied in detail in Study B.

3.1.4 Combined Convection and Radiation

Thermal radiation exchange between a scattering[6], absorbing and emitting flow and a wall has been a relatively well studied topic from the 1960s (Einstein, 1963) onwards, because it has applications in combustion, high-speed aerodynamics (where hypersonic shockwaves can radiate significantly) and in nuclear rocket propulsion.

The main consideration is a fluid's absorption coefficient, κ, and the consequent optical thickness $\tau = \kappa L$ of the fluid in a channel of dimension L (which would be the radius for a circular channel). For the condition of a hot channel wall heating an internal flow, there is an increase in apparent total heat transfer and Nusselt number caused by the participating fluid. The enhancement to heat transfer is optimal at intermediate optical thicknesses:

- When optical thickness is small ($\tau \ll 1$, optically 'thin'), the fluid does not absorb energy, so radiation does not contribute to cooling the wall[7].
- At intermediate optical thicknesses the maximum radiation interaction occurs with absorption occurring across the channel width.
- When optical thickness is large ($\tau \gg 1$, optically 'thick'') then the radiation emitted by the surface is absorbed in a thin layer near to the surface and partially re-radiated back towards the wall, shielding the central regions of a channel from the direct radiation.

The mathematical formulation of coupled convection and radiation equations is relatively, complex, even for simple geometries, and, like for heat generating fluids, is generally presented for hydrodynamically developed flows with constant properties (meaning that the velocity and turbulent dissipation is needed as an input). The main references for this topic are Kakaç *et al.* (1987, Chapter 19), Modest (2013, Chapter 22) and Howell *et al.* (2016, Chapter 13), and they each present the concepts in detail and review the studies in the wider literature.

Two important non-dimensional parameters emerge in the analysis of combined radiation and convection:

The **conduction-to-radiation** parameter, also known as Stark number:

$$N_{CR} = \frac{k\kappa}{4n^2\sigma T^3}$$

where a smaller value of N_{CR} means that situation is more influenced by radiation. Despite having 'conduction' in its name, this parameter occurs in the non-dimensionalised equations for radiation combined with both conduction and convection. Lower values have the effect of increasing the size of the thermal boundary layer, in a similar way to lower Pr. Convection dominated conditions occur with larger values of N_{CR}.

The **convection-to-radiation** parameter, usually called Boltzmann number:

$$Bo = \frac{\rho \overline{U} c_p}{n^2\sigma T^3}$$

[6] In the rest of this discussion, it is assumed that scattering is not significant (as is the case in salts), but the concepts and references readily encompass it.

[7] This is for the case where all of the walls bounding a channel are assumed to be at a uniform temperature, in the case of a difference in wall temperatures over a cross-section, what is not absorbed by one section of wall travels across the channel and there is radiative heat transfer with other surfaces.

Similarly, smaller *Bo* means more radiation influence, and convection dominates at larger *Bo*.

These parameters do not directly give the quantitative ratio of thermal radiation heat flux to that from other the heat transfer mechanism, but they are used to qualitatively indicate and compare their relative magnitudes. The actual heat flux ratio depends on the absolute temperature, wall to bulk temperature difference, and optical thickness, and is non-negligible in channel flows (typically increasing convective fluxes by approximately 5 to 20 %, depending on the flow conditions). It is also noted by Modest (2013) that *'no thermally fully developed conditions can exist for forced convection in a flow combined with appreciable thermal radiation'* because of the non-linearity of radiation with temperature. It is also the case that treating channel flows as 1D can lead to inaccuracies because axial radiation can be significant, especially where channels are converging or diverging, changing the angle of (hence of emission from) the walls relative to the channel centreline.

The analysis described in the references above (and also available in a concise form in Chawla and Chan, 1980 and Yener and Özişik, 1986) is able to predict temperature profiles and heat transfer, and was generally carried out by numerical solution even in the earliest references. It has not, however, been formulated in a way that can be easily incorporated into a heat transfer correlation in a system code. Large simplifications can be achieved in such calculations by ignoring scattering, variation of properties with temperature and wavelength (spectral dependence), but it can lead to inaccurate or unrealistic results (Howell *et al.*, 2016, Chapter 13). Even with these simplifications, the effect of radiation on convection depends on geometry, material properties, flow rate and temperature, and so creating universal correlations would be challenging. The same points also apply to predicting natural convection or boundary layer flows involving a participating fluid.

More recently there have been studies conducted by Chaleff *et al.* (2016), Derdeyn *et al.* (2018) and Coyle *et al.* (2020) that are specifically related to MSR salts, and in-particular considering the variation of absorption for realistic salts with wavelength.

Given these points, the best approach for gaining insight is likely to come from combining realistic geometries, flows and material properties with radiation modelling that is already available in CFD codes, as discussed in Section 3.3. The creation of a convection heat transfer correlation that incorporates radiation to a participating fluid using CFD is demonstrated in Study B.

3.2 Flow and Convection with CFD

The topics discussed in Section 3.1 above indicate that CFD is likely to be able to address each of the effects individually. Therefore, there is little reason to believe that, when combined, the physical effects that are most pronounced in MSRs would be expected to lead to a significant reduction in accuracy compared to that which would be expected from CFD analysis generally. The modelling of turbulence, in combination with unsteadiness and buoyancy, is still likely to be the most challenging aspect. However, the presence of thermal radiation and heat sources in near-wall layers should motivate the generation of CFD grade validation data, and resolved turbulence simulations (Large Eddy Simulation (LES) or Direct Numerical Simulation (DNS)) to assess the performance of Reynolds-Averaged Navier-Stokes (RANS) models.

The discussion here builds on the CFD guidance in Volumes 1, 2 and 3, and the contrast with the more extensive considerations needed for low Pr fluids as described in Volume 5 is also instructive. Therefore, only the specific topics of wall heat transfer for moderate Pr fluids and the modelling of pebble beds with CFD are discussed in this volume.

Study B demonstrates an example of applying CFD to a molten salt which simultaneously exhibits internal heat sources, strong property variation with temperature, buoyant turbulent flow, property uncertainties and participating thermal radiation.

3.2.1 Near-Wall Modelling

When modelling wall heat transfer with molten salts, three high level questions arise that motivate the rest of the decisions:

1. What is the effect of the moderately high Pr of the fluid?
2. Does the thermal boundary layer need to be resolved?
3. Can wall functions for heat transfer be used, or does the momentum boundary layer need to be resolved?

The answer to the first question is, to a first approximation, that the Prandtl numbers encountered are not extreme, and their effect is relatively localised for turbulent flows. Once the distance from a wall is large enough that turbulent diffusivity is dominant, then the low contribution of molecular contribution makes little difference. The effect is mainly focussed on the laminar sublayer ($y^+ < 5$) and buffer layer ($5 < y^+ < 30$). The boundary layer profiles of Kader (1981), shown in Figure 2.1, more than cover the expected Pr range for salts (Kader compares the profiles to experimental data with Pr of 5.5, 14.3 and 95). However, they also show that in the viscous sublayer

$$T^+ = Pry^+$$

where

$$T^+ = \frac{(T - T_w)}{T_\tau} \quad \text{and} \quad T_\tau = \frac{q_w}{\rho c_p u_\tau}$$

T_τ is the 'friction temperature' and uses the friction velocity u_τ. This means that, even when the momentum boundary layer mesh is resolved such that $y^+ \approx 1$, then more cells would be needed to resolve the thermal boundary layer for $Pr > 1$. This is the second question, and in general, the answer is 'no' – where the momentum boundary layer is well resolved, there is no analogous need in general to create a finer mesh that achieves $T^+ \approx 1$. Because the flow is laminar, and slow moving at the wall, the heat transfer occurs by molecular conduction. This approach to near-wall solution, with a resolved momentum layer, should be able to locally accommodate heat generation in the fluid, participating thermal radiation, and temperature dependent properties without additional modelling considerations, and should be the preferred option where computational resources permit.

There will be some case-specific reasons to test the dependence of the results on first cell T^+, however. In situations where with high Pr, high heat flux, and strongly temperature dependent properties, it may be necessary to check whether a better resolution of the temperature gradient changes the results. Another reason might be to assess the onset and development of salt freezing

at a surface – for this application Cartland Glover *et al.* (2019) resolved meshes to $T^+ \approx 1$.

This leads to the third question – does the momentum boundary layer always need to be resolved, or can wall function approaches still be used for heat transfer? The first thing to note is that wall functions are generally developed with the assumption of fully developed flows (or equilibrium boundary layers), and with the assumption of constant material properties. The latter of these two points may itself be sufficient to make the answer 'no', conventional wall functions are not sufficiently accurate for modelling molten salts where there is a large change in viscosity because of local temperature variation. However, it is not the case that the higher Pr inherently means that a wall function approach cannot be used.

Near to a wall, in the laminar sublayer, higher Pr fluids have a higher thermal resistance associated with lower conductivity. Thermal boundary layer expressions have 'P functions' that account for this, and these are used to create wall function models for heat transfer. A common P function is that derived by Jayatilleke (1966) from experimental results of fluids with moderately high Pr fluids and wall roughness. Malin (1987) reviews a range of P functions and concludes that, other than for very high values of Pr ($\gg 100$), then the Jayatilleke P function is suitable. Such models require a turbulent Prandtl number, Pr_t, but this has been studied quite extensively, as summarised by Kays (1994). The temperature profiles of Kader (1981) are also used as a basis for wall functions.

Recently Šarić and Basara (2018) developed a wall model for higher Pr fluids taking into account the variation of Pr_t near to a wall. It demonstrated improved performance over the Jayatilleke P function models for $Pr \approx 20$ where the first cell was in the buffer layer, although it was implemented in the context of the k-ζ-f RANS model, which is based on the elliptic relaxation concept (see Volume 3, Section 2.2.4.3), and is not widely available in CFD codes; the approach is also not necessarily adaptable to more common models, such as k-ω SST.

In the context of MSRs, Fiorina (2019) shows that wall functions for fluids with internal generation need to be adapted. Heat generation in the fluid causes an underestimation of temperature differences to a wall when using thermal wall functions, and a modified implementation based on the Jayatilleke P function shows good agreement with the analysis and experimental data discussed in Section 3.1.3. Participating thermal radiation with high optical thickness, causing significant energy transfer in the near-wall layer would be expected to have a similar effect.

The discussion above was mainly based on the assumption of smooth pipes. Where roughness becomes significant, it disrupts the laminar sublayer. For higher Pr fluids, the effect of this on heat transfer is more pronounced, because it allows turbulent diffusivity to reach the wall and removes the high resistance layer (and exposes the wall to turbulent shear stress, increasing friction factor). This effect of roughness is able to be accommodated in wall model boundary conditions in CFD codes – the effect of the disruption of the laminar layer is to shift the 'law of the wall' velocity profile downwards. Even in fully rough[8] conditions where there is no laminar sublayer, the effect of higher Pr is still present to an extent as the final conduction resistance to the wall (Kays *et al.*, 2005, Chapter 12). For a fully rough wall, some form of wall modelling will inevitably be present, so attempting to use a near-wall resolution suited to smooth surface boundary layer that would give $y^+ \approx 1$ will not provide the same kind of improved accuracy. Wall modelling, and especially

[8] See footnote 2 on page 41.

the implementation of roughness and heat transfer are details that are CFD code specific, and the documentation for the approach taken in the particular code being applied should be reviewed.

3.2.2 Pebble Beds

Pebble beds represent an application that is well suited to a porous medium representation within a CFD code. They have received significant modelling attention in the past (Stainsby *et al.*, 2010, IAEA, 2013), and the correlations used in system code representations and validation data can be readily applied in developing CFD models.

It has recently become possible to combine CFD grade experimental data (Nguyen *et al.*, 2018) and resolved turbulence (DNS and LES, Yildiz *et al.*, 2020) to provide insight into the details of the flows in pebble beds. This is able to be compared to the more conventional correlations for drag (such as the well-known Ergun equation) and pebble-fluid heat transfer to create and validate porous models of the whole core of pebble bed reactors (Novak *et al.*, 2019).

The references noted here are a starting point that cover (and provide further references to) all of the pertinent aspects of modelling pebble beds with CFD. Since this is a rapidly evolving area of capability development, the details are not repeated here. Examples of coupling these methods to neutronics solvers for the prediction of nuclear heat sources are also discussed briefly in Section 3.4.3.

3.3 Radiative Heat Transfer with CFD

Modelling radiative heat transfer with CFD is introduced in Volume 2, but it does not discuss participating media. Most CFD codes include participating radiation modelling capabilities and couple the energy transfer processes in the fluid[9]. The main choices of approach are the P_1, Discrete Ordinates (DO) and Monte Carlo (MC) models, all of which can incorporate scattering, absorption and emission from a fluid. Two main considerations will guide the choice and cost of a model to use to represent radiation:

- What is the optical thickness of the radiation paths in the model?
- Can the fluid be approximated as being gray?

Both of these considerations also relate to the state of knowledge of the material and surface properties – a costly model is unlikely to be worthwhile if there is poor knowledge of the inputs. However, a lack of knowledge about optical properties of a material should not be used as a reason to exclude radiation modelling – at high temperatures it can have a significant effect on heat transfer in some geometries, and an analysis that does not assess this contribution is likely to be challenged. In some cases it can be simpler and faster to include radiation modelling, compared to the effort of justifying omitting it. In other cases an unambiguously conservative approximation, whose effect on an operational or safety margin is acceptable, can be made by omitting radiation in an assessment.

[9] The energy coupling from the fluid temperature to the thermal radiation field is included, but as pointed out by Howell *et al.* (2016), radiation and turbulence are coupled. The local temperature fluctuations caused by turbulence are amplified by the T^4 dependence, which increases the emission compared to using only the mean temperature. This effect is included in specialised combustion models, where large temperature variations occur, but not in the general purpose models described in this section.

In general, non-gray behaviour (spectral dependence) is modelled using a 'banded' approach, where a representative absorption coefficient is applied across a particular wavelength band, and the bands are chosen by the user. Adding more bands adds to the cost of the simulation in the P_1 and DO models, because a set of RTEs are solved for each band. For MC, the computational cost is associated with tracking particle (photon) paths, and each band will be tracked independently. Section 3.3.1 below provides a review of the available guidance on choosing inputs for a banded approach.

The DO and MC methods are able to model any optical thickness, and should be considered as being able to provide a reference/comparison calculation for simpler methods. However, this is only the case when they are sufficiently well resolved. For DO, the unit sphere is split into segments, and higher angular discretisations lead to more cost (solving more transport equations), but without sufficient resolution, significant artefacts and inaccuracy can occur, as described by Murthy and Mathur (1998) (for the method as implemented in Fluent). MC is a ray-tracing approach, and using more rays adds to computational costs, but increases accuracy.

The P_1 method is usually recommended (for example by ANSYS, 2020) for optical thicknesses of $\tau \geq 1$, and would be expected to be significantly computationally cheaper than either DO or MC. In some geometries, using P_1 for $\tau < 1$ may be able to provide sufficiently accurate results, but not in others (Modest, 2013, Chapter 16), and this should be checked against a more accurate solution. It is likely to be the case that using P_1 will give a more accurate answer than omitting radiation altogether, and it is not expected to add significantly to solution costs.

When optical thicknesses are high ($\tau > 3$), a diffusion based approach (the Rosseland model) may be appropriate, although unless there are significant heat sources in the fluid, the difference that will be made to convective heat transfer is likely to be small in nearly opaque conditions. Diffusion approaches are usually limited to the gray assumption.

The MC, DO, P_1 and diffusion approximation methods that are applied to radiative heat transfer are conceptually the same as those used for neutron transport, discussed in Section 3.4. P_1 method is the P_N method, with $N = 1$ (related to the number of terms in the spherical harmonic expansion that are used); DO is also known as the S_N method, where N is related to the number of discrete angular directions considered.

3.3.1 Determining Banded Gray Absorption Coefficients

Extensive literature is not available describing rigorously transforming the absorption spectrum for a semi-transparent fluid, plus additional absorption from specific constituents or contaminants, into banded mean absorption coefficients, suitable for inclusion in a CFD model. There is a lack of guidance in both how to choose the number of bands, their wavelength ranges, and how to average the value of absorption.

Most of the available literature (such as Modest, 2013) on modelling spectral (non-gray) participating medium radiation transport concentrates on the propagation of radiation in molecular gases, which has an application in combustion, spectroscopy and atmospheric propagation. For example, the HITRAN database (Gordon *et al.*, 2017) is very detailed, resolving each absorption line – millions to hundreds of millions of lines for common molecular gases such as H_2O. This data can

be assimilated into coarser banded representations, or treated using other sophisticated spectral methods.

The gray approximation is commonly applied in commercial CFD codes, and none of the modern spectral methods are available[10] – only the weighted-sum-of-gray-gases method, plus some models for the effects of particles or soot. For molten salts which have an effectively continuous (rather than multiple discrete banded) absorption spectra in the wavelength interval of interest, and limited experimental knowledge, these sophisticated spectral approaches are not a 'good fit', so a simpler approach is required. It should also be noted that, because their intended application is radiation transfer in gases, some expressions for participating media omit refractive index, with the (sometimes implicit) assumption that it is approximately 1. This is not the case for molten salts.

Much of the radiative heat transfer analysis for participating media is aimed at predicting the heat transfer between an absorbing, emitting and scattering gas and a bounding surface, not for making local radiation propagation assessments. It is in this context that the concept of a 'mean beam length', L_m is introduced, which allows the emissivity of an isothermal participating medium of a particular geometry to be related to the absorption coefficient using

$$\epsilon = 1 - e^{-\kappa L_m}.$$

Fiveland and Jamaluddin (1991) rearranges this

$$\kappa = -\frac{\ln(1-\epsilon)}{L_m},$$

to produce absorption coefficients for the spectral banded DO model that is available in common CFD codes. However, the reference does not provide guidance on the source of the emissivity data, or what value of L_m to apply. Similarly an example of this method being applied to produce absorption spectra for molten salt (for a solar application) is shown in Tetreault-Friend *et al.* (2017), where the use of a fixed length is appropriate because of the simplicity of the geometry (a uniform layer of material). Furthermore, in ANSYS Fluent, the weighted-sum-of-gray-gases model requires a user specified value of L_m or, it will use a default value

$$L_m = 3.6\frac{V}{A},$$

based on the total volume, V, and surface area, A, of the model domain. While these approaches may be suitable for uniform layers of material, or for a furnace or combustor (which is typically a relatively simple, open domain, with a hot flame region and cooler walls) this is not suitable for general purpose nuclear reactor components, where the range of length scales varies from tube-spacing in heat exchangers to a large portion of the reactor diameter in an open plenum. Therefore, it is necessary to have local, composition (and temperature[11]) dependent properties that are independent of an implicit or assumed geometry, and where an absorption spectrum can be split into arbitrary wavelength bands, each of which can have very low or very high absorption, or anywhere between. Adapting Equation 11.60 from Modest (2013, Chapter 11.8), the local average

[10] From Chapter 3.3 of Chhabra (2017), written by Michael Modest: *... as of 2015 none of the better known CFD packages includes a credible non-gray spectral model.*

[11] This flexibility is available in Fluent, for example, where the absorption coefficients in each band can be given a temperature dependence via a User Defined Function.

absorption is given simply as

$$\bar{\kappa} = \frac{1}{\lambda_2 - \lambda_1} \int_{\lambda_1}^{\lambda_2} \kappa_\lambda d\lambda$$

In Modest (2013, Chapter 20.4) the stepwise-gray (or box) model also suggests that this is the appropriate approach.

This is an area of evolving research, and other methods have been suggested. Modest (2013, Chapter 11.11) describes the *Planck mean absorption coefficient* as being a useful quantity in evaluating the RTE

$$\kappa_P = \frac{\int_0^\infty I_{b\lambda} \kappa_\lambda d\lambda}{\int_0^\infty I_{b\lambda} d\lambda}$$

Noting that this is evaluated across the whole wavelength range. (Howell *et al.*, 2016, Chapter 12) describes that applying this as a single value across the whole spectrum can be inaccurate in some circumstances, and that other whole spectrum mean definitions are available, but that a banded approach offers improvements (Patch, 1967). Coyle *et al.* (2020), following the PhD thesis of Chaleff (2016), apply what is described as the 'Planck mean', but on a wavelength band basis

$$\bar{\kappa} = \frac{\int_{\lambda_1}^{\lambda_2} I_{b\lambda} \kappa_\lambda d\lambda}{\int_{\lambda_1}^{\lambda_2} I_{b\lambda} d\lambda}$$

This is not an equation that is evident in, for example, Modest (2013) or Howell *et al.* (2016), and it is notable that this approach is not taken in the similar journal paper by Chaleff *et al.* (2016), where a simple band midpoint is used. It is also not clear whether it is consistent with the definition of the banded gray model that it is applied to in Star-CCM+. In the spectral banded DO method defined by Fiveland and Jamaluddin (1991), and also stated in the Fluent Theory Guide (ANSYS, 2020) and in Modest (2013, Chapter 1.4), the blackbody radiative intensity emission over a band is

$$\int_{\lambda_1}^{\lambda_2} I_{b\lambda} d\lambda = (F(n\lambda_2 T) - F(n\lambda_1 T)) \frac{n^2 \sigma T^4}{\pi}, \quad F(n\lambda T) = \frac{\int_0^\lambda E_{b\lambda} d\lambda}{\int_0^\infty E_{b\lambda} d\lambda},$$

noting the limits of 0 and ∞ in the denominator. It is therefore possible that this banded 'Planck mean' approach is applying double weighting of the spectral variation, and more justification would be needed to suggest its use. There are methods discussed by Patch (1967) related to banded approximations that make use of *'group* [band] *Planck mean absorption coefficients'*. They have some similarity, but there is significant additional complexity in their subsequent application that suggests that their definition is specifically incorporated within those methods. The complexity also makes it challenging to readily compare it for consistency with the CFD spectral banded DO implementation of Fiveland and Jamaluddin (1991).

A simple local average is currently recommended.

3.4 Neutronics

Existing neutronics solvers are mature software tools, and an overview of the common methods and codes is described below. They have assumptions, neutronic data, numerical models and implementations based around the heterogeneity of solid fuels. These are likely to perform well with reactors that have similar layouts to the MSRE with graphite moderation, but an evaluation of the suitability of the neutronic data and the modelling assumptions in them may be necessary for fast spectrum MSRs without core internals, such as the MSFR. Similarly, for simulations of LWRs, neutronic coupling to thermal hydraulic models is relatively loose because of their static fuel, but liquid fuel density changes and the motion of DNP make tighter coupling necessary.

Therefore, a number of implementations of varying complexity have considered the impact that the motion of fluids and the influence of temperature have on the reactor physics of molten salt reactors. These measures vary from the modelling of the neutron flux based on one-dimensional representation of the fluid motion, to the coupling of fluid dynamics and neutronics solvers (using similar coupling methods to those introduced in Volume 2, Section 3.1), to the development of dedicated solvers which solve both the Navier-Stokes equations and neutron transport in one code.

The methods used in the solution of the neutron transport equation are described below, ranked in an approximate order of their accuracy from higher fidelity steady solution methods to lower fidelity methods that can model the transient behaviour of reactors. There is a clear division in accuracy between high-fidelity probabilistic (random selection of events of known probability) and deterministic (no randomness) methods.

3.4.1 Probabilistic Methods

The tools that use the probabilistic approach are generally solved using Monte Carlo methods to numerically solve the neutron transport equation. The Monte Carlo approach involves the random selection of a range of probable events defined by the neutron cross sections, the mass of fuel, the presence of absorbers, moderators and reflectors and the temperature of each material in the reactor. These methods generally apply the continuous neutron cross sections. They can provide highly accurate solutions in ‘criticality searches’ when the behaviour of a large number (or population) of neutrons is solved to find the k_{eff} of a particular reactor configuration. Accurate solutions are expected to have a 3σ (where σ is the standard deviation of k_{eff} obtained by the Monte Carlo solver) or $99.7\,\%$ confidence interval of around $10\,\mathrm{pcm}$. The unit pcm is percent mille or 10^{-5}, and is frequently encountered in reactor physics.

The Monte Carlo solvers enable the user to approximate and homogenise the macroscopic cross sections into a number of discrete energy groups that can best approximate the neutronic behaviour of the neutron spectrum of the reactor modelled. For example as few as two energy groups can be applied to some neutronics models that can be used to characterise the behaviour of an LWR, because the fast neutrons are quickly moderated to the thermal spectrum (CEA, 2015). In the case of reactor burn-up or for the modelling of fast spectrum reactors, more energy groups (hundreds) are required in order to approximate the capture of neutrons in the resonance region. In fast reactors, neutrons are not moderated by the coolant so they take much longer to reach the thermal or lower energy end of the neutron spectrum, hence more energy groups are required.

The results obtained by the Monte Carlo solvers can also be used as reference or benchmark solutions for lower fidelity deterministic methods. Common solvers include MCNP, MONK, Serpent, OpenMC, Shift and the KENO and TRITON packages from the SCALE[12] code system.

3.4.2 Deterministic Methods

Deterministic transport solvers involve the solution of the neutron transport equation discretised in the spatial domain, and may also involve the discretisation of the angular domain depending on the complexity of the model (increasing its accuracy and cost). The deterministic approach can be further sub-divided into:

- Lattice-physics codes, which can condense and homogenise neutron cross sections.
- Angularly discretised methods, diffusion approaches and point kinetics codes that need to use homogenised neutron cross sections as inputs.

3.4.2.1 Lattice Codes

Lattice physics codes are usually two-dimensional finely discretised (meshed) representations of sections of a reactor, resolving the contribution from individual components and materials of a fuel assembly or fuel pins. The solution methods either use the method of characteristics or collision probabilities to discretise the neutron transport equation.

The Method of Characteristics (MOC) solves the 'characteristic form' of the neutron transport equation (derived and expressed differently, but equivalent to the equation in Section 2.6.2, as described by Demazière, 2020) by following straight neutron paths across a domain. Solvers include MPACT, OpenMOC, APOLLO2, CASMO5, WIMS/CACTUSOT, SCALE/NEWT and DRAGON.

The collision probabilities method involves the spatial and angular discretisation of the 'integral form' of the neutron transport equation. The method uses ray-tracing to evaluate the collision probabilities to allow the discretised transport equation to be solved. Solvers include HELIOS2 and WIMS/PRIZE.

3.4.2.2 Angular Discretisation Methods

In tools that apply the spherical harmonics or discrete ordinates methods, the spatial variables are discretised on a mesh, while the angular variables are discretised by an approximation:

- In the case of spherical harmonics or the P_N method, angular variables are resolved as a series of spherical functions that describe the variation of the parameter on the surface of a sphere, where in this case N is the order of the expansion.
- In the case of the discrete ordinates (S_N) method, angular variables are resolved at discrete intervals with a discrete set of vectors for the direction of the neutron flux.

Solvers which can apply the P_N or S_N methods include FETCH2, SCALE/DENOVO, WIMS/TWOTRAN, Griffin and GeN-Foam (as the simplified SP_3 method).

[12] www.ornl.gov/scale/overview

3.4.2.3 Diffusion Approximation

If scattering and sources of neutrons can be approximated as isotropic (no angular effects), then the simplest tool used for modelling the spatial variation of neutron flux is the diffusion approximation (using Fick's law). The neutron flux is modelled using a continuum transport equation that is similar to those used for fluid mechanics.

Nodal diffusion neutron transport is a finite difference method that has been commonly implemented in solvers including DIF3D, DYN3D, Griffin[13], SIMULATE5, PARCS, WIMS/SNAP. The nodes represent the fuel assemblies of a solid fuelled reactor and therefore, they are typically arranged in the same shape as the cross-section of the assemblies forming the reactor core, with either hexagonal prism or hexahedral nodes. Each fuel assembly is modelled with a number of nodes axially, to be able to determine the power distribution in the vertical direction. Finite element and finite volume versions of the diffusion transport equation have also been implemented.

3.4.2.4 Point Kinetics

The simplest approach is the application of point kinetics, where the reactor is reduced to a point or a series of points, and an ordinary differential equation approximates the change in the averaged neutron density in the reactor with time. This assumes that there is a constant shape of neutron flux distribution.

Point kinetics solvers are typically implemented in or coupled to all system codes (see Section 3.5). Examples of point kinetics solvers applied to molten salt reactors include RELAP, SPECTRA, TRANSFORM, MELCOR, LiCore.

3.4.3 Transient and Coupled Analysis

Neutronics and thermal hydraulics calculations are coupled routinely (to the extent that it is common to see the code pairs stated as a single name, such as TRACE/PARCS or ATHLET/DYN3D), and the fidelity used for each tool will depend on the problem at hand and what the most suitable approximations are. Both diffusion approximation and point kinetics methods are capable of modelling the transient behaviour of nuclear reactors over a period of minutes, to hours and days with reasonably low computational costs. They are also suited to design iterations where a large number of conditions need to be assessed repeatedly, and are suited to being coupled to thermal hydraulics codes.

In relation to MSRs, some recent examples of applying higher fidelity methods than system codes and point kinetics include:

- Coupling DYN3D to CFD (Cartland Glover *et al.*, 2019).
- The GeN-Foam solver implemented in OpenFOAM, which solves the neutron diffusion or SP_3 equations within the finite volume CFD solver framework (Fiorina *et al.*, 2017).
- The MPACT code coupled to CTF as part of VERA (Volume 1, Section 4.4.2) to model the MSRE (Graham *et al.*, 2021).

[13] Tools often contain multiple solution methods within a common framework for nuclear data processing, as an example Griffin also contains S_N solutions capabilities. WIMS and SCALE are similar – their different modules for each solution method are noted.

- The Pronghorn porous medium CFD code was coupled to the Griffin neutronics code to assess a gas cooled pebble bed benchmark (Novak *et al.*, 2021) and an MSFR benchmark (Abou-Jaoude *et al.*, 2021).
- OpenMC coupled to Nek5000 (solving LES CFD) was recently demonstrated (Merzari *et al.*, 2021), representing the resolution of the smallest length scales in a large pebble bed geometry.

3.5 System Analysis

Molten salt reactors of any type need system analysis for the same reasons as other reactors, such as for the prediction of long duration transients including the behaviour of active control and protection systems or passive cooling. Křepel *et al.* (2014) noted three requirements for system codes that are peculiar to modelling MSRs (although some designs do not require all of them):

- The transport of DNPs.
- Heat generation in fluids from fission.
- Graphite moderator structures that can be hotter than the fuel (heated by irradiation and cooled by the salt).

The last of these means that there is likely to be a greater need for more detailed and three-dimensional predictions of solid temperatures, and so different and more sophisticated 'heat structures' may be needed compared to those used in typical system code analysis (Volume 2, Section 3.2). This can also be extended to consider the need for sufficiently good representations of the core internal structures, vessel and external structures that will play a role in passive heat removal conditions.

To enable the prediction of solid and fluid temperatures, as well as flow rates, a number of aspects of a system code's capabilities that are particularly relevant to MSRs need to be considered:

- The low Reynolds number flows that may be encountered will require laminar representations of flow losses and heat transfer correlations, which depend more on specific channel geometries than turbulent flow correlations (which can usually be used with a universal hydraulic diameter). In addition, flows with Reynolds numbers in the region of laminar-turbulent transition can be challenging to model, and can lead to oscillatory numerical behaviour.
- Modelling of natural circulation flows, which requires particular attention to be paid to hydrostatic components of pressure variation. This may require different numerical solution approaches, particularly with laminar flows, because the driving forces and pressure drops can both be very small.
- In addition, the modelling of flow conditions that are affected by buoyancy (such as heat transfer and influencing laminar-turbulent transition) requires convective heat transfer modelling able to identify the appropriate flow conditions and apply correlations that can represent mixed convection (Volume 3, Section 2.2.1).
- Convection correlations that include entrance or development effects and account for temperature varying viscosity (which will depend on the local heat transfer) may be required to be sufficiently accurate.

- The modelling of radiative heat transfer between surfaces (such as in an external reactor vessel cooling configuration) and between surfaces and adjacent semi-transparent fluids.
- If species transport needs to be modelled (for DNPs, for example), then the action of physical turbulent mixing may need to be included and the presence of numerical diffusion/dispersion (caused by low-order numerics and coarse nodalisation) needs to be controlled.

The availability and maturity of these functions and attributes depends on the tool and its previous applications. For example, system codes developed for two-phase accident predictions for LWRs will not necessarily have focussed on implementing and validating modelling of these phenomena. The available and widely applied system code tools introduced in Volume 1, Section 4.4 are therefore less mature for their applicability to MSRs. Molten salt reactor designs are, however, amenable to the same modelling approaches as other technologies, with some modification, as demonstrated by a selection of recent examples, where either existing tools have been adapted, or new tools written, for MSR applications:

TRACE has been used to model the MSRE (Xun, 2016), and also the AHTR (Wang *et al.*, 2015). The latter required salt models to be implemented in TRACE (Richard *et al.*, 2014). More generally the suitability of the US NRC's tools for modelling MSRs (and other non-LWR technologies) is reviewed in US NRC (2020a).

RELAP was extended by Shi *et al.* (2016) to add DNP transport to the point kinetics model, and a model of the MSRE was built, and validation comparisons made. A model of the MSBR design was also built and used to demonstrate a number of flow and reactivity transients.

MELCOR was conventionally an LWR severe accident code, but is being developed so that it can represent non-LWR reactors. This includes modelling reactor normal operating conditions to use as initial conditions and inputs to the modelling of MSR transients and accidents. This capability has been demonstrated using MSRE flow-reactivity transient experiment data (Beeny *et al.*, 2022). It forms part of the US NRC's intended route for the evaluation of source terms and accident consequences (US NRC, 2020b).

TRANSFORM is an open source modelling tool developed by ORNL intended to allow energy system models to be rapidly developed using a library of connected components, and its models are potentially less geometrically detailed than other system codes (more akin to process simulation models). A model of the MSDR has been demonstrated using it (Greenwood *et al.*, 2020).

SAM is a system code designed specifically for single-phase advanced reactors, and is being used by Kairos Power as their system analysis code (Blandford *et al.*, 2020) for their pebble bed core FHR. An MSRE model has also recently been created and compared to flow-reactivity transients (pump coast-down and startup, as well as natural circulation, Hua *et al.*, 2022). Some of the issues related to numerical diffusion and low order numerics described above are discussed in the context of SAM by Hu (2017).

SPECTRA is an established system code that has been applied to a wide range of reactor types, and is under development to add additional functionality needed for MSRs. As well as DNP transport, modelling of the behaviour of fission products including dissolved gaseous species and noble metals is included and compared to MSRE data (Roelofs and Stempniewicz, 2021). The same MSRE flow-reactivity transients as were modelling in SAM have been

demonstrated and the two codes compared as a recent benchmarking exercise (Hua *et al.*, 2022).

Flownex is a commercial system code applied in a number of industries, with functionality suitable for MSRs. It has been applied to the design of the IMSR[14] and to FHR flows (Andreades *et al.*, 2016). It has also been used in comparisons for gas cooled pebble beds (Novak *et al.*, 2021).

TREND is a new code written to support TMSR development, and demonstrate comparisons with the MSRE and also the CIET test facility (Yu *et al.*, 2021).

LiCore is in the early stages of development to support the assessment of the MSFR under the SAMOSAFER programme (Laureau *et al.*, 2021).

The reliance on the MSRE as a starting point for many modelling developments is apparent. This is partly because it is the only real reactor that can be used as a benchmark, but also because of the extensive design and test documentation available from that project.

3.6 Thermal Hydraulic Experiments and Validation

This section discusses flow and heat transfer experiments relevant to MSRs that have been (or are being) conducted, and what kind of data can be expected to be available from experimental methods to help with model validation. Guidance on the different types of test (such as distinguishing Separate Effect Tests (SETs) from Integral Effect Tests (IETs)), to validation and to scaling is given in Volume 1, Sections 4.6 and 4.3.2 and in Volume 4. The availability and accuracy of thermophysical properties is highly relevant, but these experiments are not discussed here – Section 2.3 and the references mentioned provide that context.

Two types of experimental approach are discussed: those using simulant fluids, and those using molten salts.

3.6.1 Simulant Fluid Experiments

The MSRE programme used a full-size mockup to study flow distribution and heat transfer. This is described in detail by Kedl (1970), and was modelled in SAM (Leandro *et al.*, 2019) as a stage in building an MSRE system code model. The mockup used water, or water with additives to increase viscosity to provide a better Reynolds number match.

The ability to use low temperature water, or another easier to handle simulant fluid, is common practice for some types of experimental investigation, and compared to high temperature salts, allows for faster development, cost reductions and high-fidelity measurements to be made. It can also enable access for optical techniques to provide spatially resolved, ‘CFD grade’ validation data. An example of this is the use of a fluid with a refractive index matched to a transparent acrylic, so that Particle Image Velocimetry (PIV) can ‘see through’ the solid objects in pebble beds (Nguyen *et al.*, 2018) and rod bundles (Nguyen *et al.*, 2020) to resolve the flow fields in the spaces between them. Using alternative fluids, which have different material properties to the prototypical application, requires a scaling analysis to be performed to match the non-dimensional number characteristics

[14] flownex.com/industries/nuclear-smr

between the test and real reactor as well as possible, and to quantify scaling distortions. Compared to the two-phase flow and heat transfer requirements of LWR tests, however, matching the behaviour for single-phase flows is more straightforward.

Heat transfer experiments with alternative fluids have additional complications in attempting to represent the dependence of Nu on surface heat flux via the temperature dependence of viscosity on temperature. Laboratory experiments may not be able to work with the high heat fluxes necessary to create sufficient temperature differences, or the extent of the temperature difference necessary for the property variation may distort the applicability of the simulant fluid. Mixtures of several fluids will be needed to match the required temperature-viscosity relationship, as well as other thermophysical properties and the refractive index.

It has been found that the heat transfer oil Dowtherm A can be used as a simulant for FLiBe, as discussed by Andreades *et al.* (2016) and Liu *et al.* (2018). The properties of water, Dowtherm A and FLiBe are compared in Figure 3.2. Three example properties relevant to thermal hydraulic performance are shown, and each fluid is plotted over its own temperature range from T_L to T_H, normalised to $T' = (T - T_L)/(T_H - T_L)$. This shows that, over the range chosen, the Prandtl numbers of Dowtherm A and FLiBe are very well matched, and while that of water is lower, it does decline in a similar ratio with increasing temperature. The values of β and ρc_p for water and FLiBe are comparable.

Dowtherm A was applied in the Compact Integral Effects Test (CIET) facility to study natural-circulation driven decay heat removal in FHRs (Zweibaum *et al.*, 2016), and scaling analysis can be used to design facilities with reduced size and power where the Re, Gr and Pr numbers can be matched simultaneously to a reactor (Zweibaum *et al.*, 2020). Blandford *et al.* (2020) describes how both water and oil based systems are being developed to test the flow and heat transfer performance of the Kairos Power FHR design, prior to the construction of a molten salt based (non nuclear) larger 'Engineering Test Unit'. This ETU has objectives more focussed around proving the ability to build equipment at prototypical scale and conditions, and the integrated process of operating the nuclear Structures, Systems and Components (SSCs) (including pumping salts and handling fuel for example). It is not intended for investigating and demonstrating more fundamental thermal hydraulic phenomena and validating models, which is more suited to scaled SET and IET test facilities.

3.6.2 Molten Salt Experiments

The MSRE project documentation is a source of a large range of information, including thermal hydraulic test data (as noted in Section 3.5), but it is not a source of sufficiently well resolved results to be used as CFD grade validation data.

A number of contemporary molten salt flow and heat transfer facilities are being developed. While they are less able to provide detailed flow and precise heat transfer validation data[15], they have an important role to play in allowing organisations to *'to acquire some technical experience on the handling and processing of molten salts.'* (Pioro, 2016, Chapter 7) – providing a technology

[15] Temperature measurements are complicated by heat losses from test fixtures at high temperature – the details of insulation and external convective and radiative heat transfer can be significant. The accuracy of material property data at elevated temperatures may also not be sufficient.

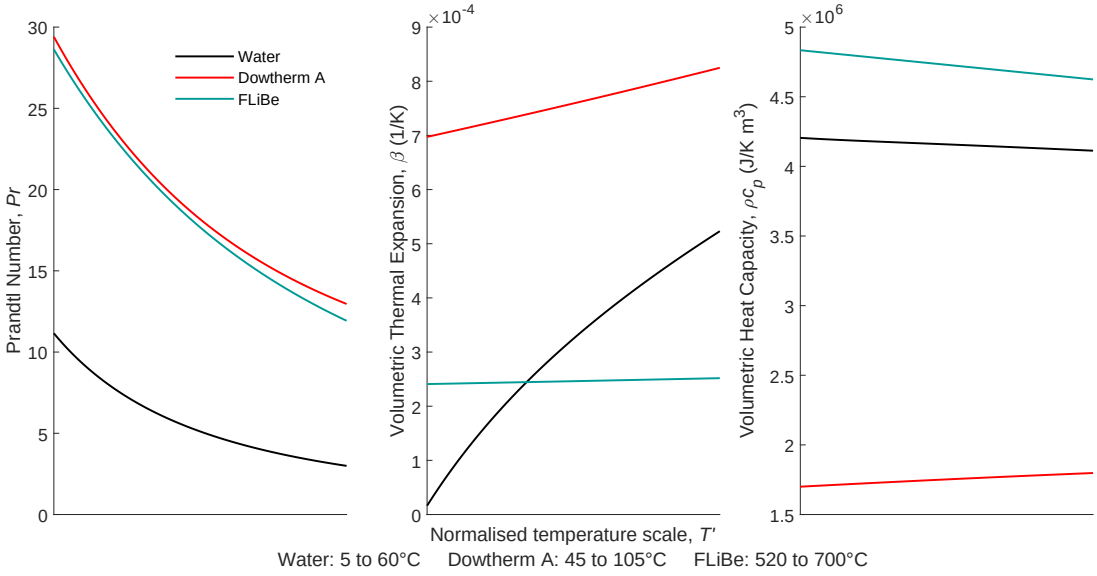

Figure 3.2: Comparison of some properties of water, Dowtherm A and FLiBe. Data sources: FLiBe: Romatoski and Hu (2017) Water: IAPWS (Wagner *et al.*, 2000); Dowtherm A Dow (2021).

development route for valves, pumps, heaters, insulation and materials. A substantial part of the challenge of obtaining valuable data is using instrumentation appropriate for the high temperature salt environment; this is reviewed by Holcomb *et al.* (2018).

There are several experimental facilities associated with the SAMOFAR and SAMOSAFER projects:

FFFER: Forced Fluoride Flow for Experimental Research. A recirculating loop with gas injection and a bubble separator, testing the efficiency of gas removal from flowing salt.

SWATH: Salt at WAll: Thermal ExcHanges. A channel geometry to study heat transfer. Laminar and turbulent flows can be created and solidification at walls can be studied.

DYNASTY: DYnamics of NAtural circulation for molten SalT internallY heated. A high aspect ratio loop geometry with heated pipe walls to replicate some of the features of a salt with internal heat generation undergoing natural circulation.

Rubiolo *et al.* (2017) describes FFFER and SWATH. Both SWATH and DYNASTY use water experiments for development and flow validation purposes as a precursor to salt operation.

DYNASTY has similarities to other molten salt loops, such as those described by Srivastava *et al.* (2016), Srivastava *et al.* (2017), and the data available is generally limited to integral parameters such as flow rates and individual temperature measurements at a given location. While these are suitable for the purpose of assessing natural convection stability as well as overall circulation and heat transfer (useful for assessing and validating system code models, and also the situation for water based experiments with similar geometries, Wilson *et al.*, 2022), it does not provide spatially resolved data.

Salt loop geometries with spatially resolved temperature fields are beginning to be developed. Arora *et al.* (2021) describe how 'optical fiber distributed temperature sensors' (combined with point measurements by thermocouples) are able to measure the temperature distribution of FLiNaK under forced convection conditions over the cross-section of a channel and along its length. Britsch

et al. (2019) describe a FLiBe loop operating under natural circulation, with laminar flow that uses similar distributed fiber measurements.

Local salt velocity or flow rate measurements are difficult to make, but bulk flow rate measurements can be made using indirect methods (for example tracking the progress of a temperature perturbation) or external sensors (such as a transit time ultrasonic flow meter).

Freezing within salt experiments, whether desired or inadvertent is a significant factor. Britsch *et al.* (2019) describes how frozen salt layers formed in cooler sections, affecting heat transfer. Some experiments are specifically aimed at the assessment and development of 'freeze valves' and the validation of modelling predictions of them (Jiang *et al.*, 2020) – Chisholm *et al.* (2020) provides a review of the design and operational experience of these components from the MSRE.

4 Future Developments

Most of the modelling methods for thermal hydraulics (and coupled neutronics) phenomena that are necessary for the prediction of single-phase flow and heat transfer in MSRs are relatively mature and available for industrial application. The areas of future development that will broaden these methods to be able to perform a wider range of assessments with more fidelity and accuracy (or less uncertainty) are:

- The prediction of material properties using atomistic simulations.
- Broadening the range of coupled multiphysics that interact with thermal hydraulics to include chemistry and fuel performance.

These topics are discussed below to conclude this volume.

4.1 Property Derivation from Atomistic Models

Where material properties are unavailable and are hard to measure, it may be possible to determine them using atomistic simulations – broadly termed Molecular Dynamics (MD). While this section is aimed at molten salt properties, it is also applicable to nuclear fuel performance and other disciplines involving material science and physical chemistry. The descriptions here are intended for thermal hydraulics engineers who may wish to access MD derived quantities. The intention is to introduce the relevant vocabulary, provide an understanding of the physics that can be modelled, and what models of various scales and costs can be expected to achieve. It is not expected that these simulations will be performed in an industrial setting in the near future – specialists normally found within academic or research organisations are required. However, the modelling discipline is active, broadly practised and mature, with long standing international collaborative organisations[1], so the necessary skills should be obtainable.

In most engineering thermal hydraulics simulations, the atomistic nature of matter does not need to be considered and the continuum mechanics approximation is valid. ‘Constitutive equations’ mathematically express the role of the material properties, which are themselves a mathematical expression of the net effect of the very small scale physical interatomic (or intermolecular) forces. It is unusual in fluid mechanics to need to consider a fluid in a non-continuum manner directly[2], but of knowledge microscopic behaviour can be used to provide macroscopic information.

MD solves Newton’s equations of motion on a per-atom basis, where the forces (or potential energies) between them are described by ‘interatomic potentials’ that describe the attractive and repulsive interaction between atoms as a function of their distance. For molecules, bonds can be

[1] Such as CECAM, www.cecam.org.
[2] Nano-scale liquid geometries and rarefied gas dynamics, such as high speed re-entry flows, are two examples.

treated like flexible springs or rigid links that hold the atoms together, and individual atoms in one molecule 'feel' the effect of many other atoms in other adjacent molecules. Net charge, polarisation and electric fields, and the associated longer range forces between atoms produced can also be included.

In 'classical' MD simulations, the functional forms and coefficients of the potentials are empirical, with values for coefficients chosen to best replicate the properties of materials. Forces are generally assumed to apply only between pairs of atoms (so excluding simultaneous multi-atom interactions).

The interatomic potentials can also be described using quantum mechanics[3]. One method to implement this is known as Density Functional Theory (DFT), which models the simultaneously interacting electronic structure of many atoms in their condensed state (liquid or solid). *Ab initio*[4] calculations merge DFT (or another quantum mechanical method) with molecular dynamics, which enables 'on-the-fly' calculation of the forces, and simulates the resulting motion of atoms (Iftimie *et al.*, 2005).

Classical MD offers a significant (orders-of-magnitude) reduction in complexity and computational effort compared to *ab initio* calculations[5], and is still able to make a substantial range of predictions, but is dependent on the applicability and accuracy of the potentials used. For simple fluids (liquid mono-atomics) and covalent molecules (from water to polymers and large biomolecules) the potentials are well described and tested, and are applicable across a large range of conditions (for example, they can model from solidification to high temperatures without modification or tuning). They can be derived or validated using many different types of data (including X-ray and neutron diffraction/scattering for example). However, where there is a substantial influence from electrons or ions in a material, such as in metals, or ionic liquids like salts, accurate and transferable classical potentials are harder to determine.

MD is a computationally expensive discipline, usually requiring access to a High Performance Computing (HPC) facility. However, there are a large number of established software packages available, which are typically open source.

- For classical MD, LAMMPS has a material properties focus, DL_POLY is a general purpose code, and GROMACS and NAMD are more focussed on biomolecules, but also able to be used for material property assessment. Classical MD can be used to determine a material's viscosity, heat capacity, thermal conductivity, density (and β), diffusion coefficient, electrical conductivity and surface tension. Methods for measuring properties from a simulation are divided into
  - equilibrium methods, where the properties are determined from statistical fluctuations in a homogeneous sample of a material, and
  - non-equilibrium (NEMD) methods, which directly apply gradients of velocity or temperature, and measure the stress or heat flux response.

  Choosing which method to use is usually a case of that which will give the most converged (lowest variance) answer with the minimum computational cost, which depends on the num-

[3] From Schrödinger's equation, and the Born-Oppenheimer approximation, which is the separation of electronic and nuclear motion, arising from the fact that nuclei are much more massive, so are considered stationary relative to the motion of the electrons.
[4] From latin, meaning literally 'from the beginning', but in scientific contexts, meaning 'from first principles'.
[5] As an approximate analogy, *ab initio* MD is to classical MD as DNS (or LES) is to RANS CFD.

ber of atoms simulated (thousands to millions) and the duration modelled (picoseconds to nanoseconds).

- For *ab initio* MD, commonly applied packages include ABINIT, CASTEP, CP2K, CPMD and VASP, and can also determine redox potentials and optical/IR spectral properties as well as being able to include chemical interactions. It is also possible to use *ab initio* simulations to derive coefficients for classical MD potentials, as discussed in the context of MSRs salts below.

4.1.1 Examples of Using MD for Molten Salts

There are a relatively large number of examples of the application of MD to the prediction of molten salt properties that can be found in the academic literature. These include storage/solar salts and MSR coolants and fuel salts. In common with the assessment of the outputs from any modelling field, caution is needed to distinguish the literature that is most rigorous and well developed (in the same way as for CFD research). In particular, the assessment given for whether a prediction requires a classical or *ab initio* approach, and for the former especially, where the input data (potentials) come from are key determinants of utility.

For example, Madden and Salanne (2016) provide an introduction to the opportunities for using MD to determine the properties of fuel bearing salts, and also indicate some of the more subtle limitations of what can be expected, for example:

- It is possible for different ionic states of the same cation[6] to be present (U^{3+} *vs* U^{4+}). These cations can be treated as a separate species, but the effect of charge transfer will need to be accommodated by part of the potential.
- The presence of covalent bonds is neglected by assuming that salts are pure halide melts in classical models. The presence of other negatively charged ions, such as oxygen may invalidate this assumption because some long-lived covalent species (such as UO_2^{2+}) will form. This would require the use of *ab initio* MD to treat correctly, which may be computationally too expensive to be practical.

Ab initio approaches have been recently used directly:

- To assess the effect on redox potential of solute ions in MSR relevant salts (Nam and Morgan, 2015).
- To predict the effect of various metal impurities in fluoride salts on the IR absorption spectrum for thermal radiation (Chaleff *et al.*, 2018).

However, for transport property derivation, they are computationally too expensive to apply widely. There is a significant body of ongoing research where classical molecular dynamics models are used to determine properties, applying a 'polarizable ion model', which are potentials obtained with the assistance of *ab initio* calculations.

The process of determining the constants for the polarizable ion model potentials is described by Heaton *et al.* (2006) and Salanne *et al.* (2012), and demonstrated in a number of studies, such as

[6] Cations are positively charged, such as U^{4+}, anions are negatively charged, such as F^-.

those of Salanne *et al.* (2009), Dewan *et al.* (2013), Gheribi *et al.* (2014) and Li *et al.* (2020). These papers report confident viscosity, specific heat capacity and density predictions, but only Gheribi *et al.* (2014) reports thermal conductivity. All references agree that conductivity is the hardest property to determine from an MD simulation.

A recent combination of polarizable ion model MD and computational thermodynamics (Section 2.4.5) is demonstrated by Smith *et al.* (2020) such that

> *. . . a comprehensive structural-thermodynamic model of the $LiF-BeF_2$* [FLiBe] *system is therefore reported that brings together the output of the experimental thermodynamic data and MD simulations.*

Again, however, the challenge of predicting thermal conductivity is highlighted.

4.2 Coupled Multiphysics for Chemistry and Fuel Performance

Multiphysics coupling of thermal hydraulics with neutronics is relatively mature, and important in MSRs. The neutronic and fuel performance of the reactor is highly influenced by the constituents of the salt, as are the redox conditions, and more coupling between chemical processes and other phenomena is expected to be of benefit to best estimate analysis.

Chemical species transport models for MSRs are divided into two categories, depending on their purpose:

Burnup/depletion: Aufiero *et al.* (2013), Betzler *et al.* (2017) and Hu *et al.* (2021) demonstrate the modelling of the evolution of fissile fuel cycles from startup to equilibrium including fast and thermal (in Betzler *et al.*, 2017) spectrum reactor models. They include online refuelling and reprocessing as well as the removal of fission products (for both nuclear reactivity and chemical reasons). These models are intended to account for the mass present in a system, and the effect that the presence of species (that transmute to other elements through nuclear reactions) have on criticality and source terms over time periods of years.

Physico-chemical transport: The behaviour of DNPs and fission products such as ^{135}Xe (with a large thermal neutron absorption cross section) affect neutronic performance, as do helium bubbles injected to enhance the transport and removal of gaseous fission products. The redox potential (Section 2.4.1) of the salt influences the solubility of gaseous and noble metals fission products and the corrosion of vessel structural materials. Methods that can account for the complex and coupled mass transfer, mass accountancy, thermodynamic and chemical reaction effects are under development. For example Walker *et al.* (2021) describe a proposed test reactor experiment for gas and noble metal experiments in a molten salt. The test arrangement is modelled using CTF (which had additional functionality developed for this purpose) to predict surface deposition of fission products and their transport in bubbles and off-gases. Walker and Ji (2021) review MSRE data on fission product transport (and also provides a source of further relevant references) and applies the same CTF modelling to interpret the noble metal transport and deposition seen in those experiments. In physico-chemical models, accounting for the number of atoms of each element present is not sufficient for all purposes – how they form compounds (speciation) can have a significant effect, but modelling this is challenging in fuel salts because of the number of elements present, and

the limited knowledge that exists for some of their physical and chemical reactivity properties (for lanthanide and actinide species in particular).

Much of this modelling is ‘standalone’; it is not common for the more detailed chemical aspects to be modelled alongside burnup. To provide a ‘digital twin’ of a reactor through its life, future analyses that are more coupled or integrated are desirable, accounting for the evolution of species and reactor performance on long timescales, in the same framework as thermal hydraulics and neutronics.

The transport of tritium is an example of this. There are existing standalone codes for tritium migration (Kim *et al.*, 2010, Ohashi *et al.*, 2008), developed with an emphasis on hydrogen production by Very High Temperature Reactors (VHTRs). The functionality of these would be useful to be included in a system level model that predicted other species transport, to make a unified tool.

Two recent examples demonstrate the beginning of a unified approach, each starting from one of the two categories of model discussed above:

- In most burnup models, the representation of thermal hydraulic conditions is very simple, and spatial resolution of the temperature field or DNP distribution is not included. Hu *et al.* (2021) demonstrates a model of the effect on the rate of fuel addition and criticality as influenced by coupled, spatially resolved thermal hydraulics, DNP transport, neutronics and fission product removal. The MSFR model demonstrated tracks mass inventories over years, so the modelling and numerical approaches used are required to be suited for long transients.
- Graham *et al.* (2021) describes how CTF, with modifications to add multispecies modelling, coupled to MPACT for neutronics, was applied as part of VERA to model DNPs, gaseous fission products and helium bubbles. The Thermochimica tool (Section 2.4.5) was also coupled to provide thermodynamic and solubility predictions for the species included. VERA, when applied previously to LWRs, is also able to model coupled thermal hydraulics, neutronics and depletion for the long term evolution of fissile material (Kochunas *et al.*, 2017).

5 References

Abou-Jaoude A, Harper S, Giudicelli G, Balestra P, Schunert S, Martin N, Lindsay A, Tano M, et al. (2021) A Workflow Leveraging MOOSE Transient Multiphysics Simulations to Evaluate the Impact of Thermophysical Property Uncertainties on Molten-Salt Reactors. *Annals of Nuclear Energy*, 163, 108546, dx.doi.org/10.1016/j.anucene.2021.108546.

Ambrosek J, Anderson M, Sridharan K, Allen T (2009) Current Status of Knowledge of the Fluoride Salt (FLiNaK) Heat Transfer. *Nuclear Technology*, 165(2), 166–173, dx.doi.org/10.13182/NT165-166.

Andreades C, Cisneros A T, Choi J K, Chong A Y K, Fratoni M, Hong S, Huddar L R, Huff K D, et al. (2016) Design Summary of the Mark-I Pebble-Bed, Fluoride Salt–Cooled, High-Temperature Reactor Commercial Power Plant. *Nuclear Technology*, 195(3), 223–238, dx.doi.org/10.13182/NT16-2.

ANSYS (2020) Fluent Theory Guide, Release 2020 R1.

Arora O, Lancaster B, Yang S R, Vaghetto R, Hassan Y (2021) Advanced Flow and Temperature Measurements in a Forced Convection Molten Salt Test Loop. *Annals of Nuclear Energy*, 159, 108269, dx.doi.org/10.1016/j.anucene.2021.108269.

Aufiero M, Cammi A, Fiorina C, Leppänen J, Luzzi L, Ricotti M (2013) An Extended Version of the SERPENT-2 Code to Investigate Fuel Burn-up and Core Material Evolution of the Molten Salt Fast Reactor. *Journal of Nuclear Materials*, 441(1-3), 473–486, dx.doi.org/10.1016/j.jnucmat.2013.06.026.

Beeny B A, Humphries L L, Wagner K C, Haskin T C, Luxat D L (2022) MELCOR Integrated Severe Accident Code for Molten Salt Reactor Applications Including Fluid-Fuel Point Reactor Kinetics Equations. In *Proceedings of 19th International Topical Meeting on Nuclear Reactor Thermal Hydraulics (NURETH-19)*.

Beneš O, Capelli E, Morelová N, Colle J Y, Tosolin A, Wiss T, Cremer B, Konings R J M (2021) Cesium and Iodine Release from Fluoride-Based Molten Salt Reactor Fuel. *Physical Chemistry Chemical Physics*, 23(15), 9512–9523, dx.doi.org/10.1039/D0CP05794K.

Beneš O, Konings R J M (2012) Molten Salt Reactor Fuel and Coolant. In *Comprehensive Nuclear Materials, Chapter 3.13*, pp. 359–389, Elsevier, dx.doi.org/10.1016/B978-0-08-056033-5.00062-8.

Besmann T M, Schorne-Pinto J (2021) Developing Practical Models of Complex Salts for Molten Salt Reactors. *Thermo*, 1(2), 168–178, dx.doi.org/10.3390/thermo1020012.

Bettis E S, Alexander L G, Watts H L (1972) Design Studies of a Molten-Salt Reactor Demonstration Plant. ORNL-TM–3832, Oak Ridge National Laboratory, dx.doi.org/10.2172/4668569.

Betzler B R, Heidet F, Feng B, Rabiti C, Sofu T, Brown N R (2019) Modeling and Simula-

tion Functional Needs for Molten Salt Reactor Licensing. *Nuclear Engineering and Design*, 355, 110308, dx.doi.org/10.1016/j.nucengdes.2019.110308.

Betzler B R, Powers J J, Worrall A (2017) Molten Salt Reactor Neutronics and Fuel Cycle Modeling and Simulation with SCALE. *Annals of Nuclear Energy*, 101, 489–503, dx.doi.org/10.1016/j.anucene.2016.11.040.

Blandford E, Brumback K, Fick L, Gerardi C, Haugh B, Hillstrom E, Johnson K, Peterson P F, et al. (2020) Kairos Power Thermal Hydraulics Research and Development. *Nuclear Engineering and Design*, 364, 110636, dx.doi.org/10.1016/j.nucengdes.2020.110636.

Britsch K, Anderson M, Brooks P, Sridharan K (2019) Natural Circulation FLiBe Loop Overview. *International Journal of Heat and Mass Transfer*, 134, 970–983, dx.doi.org/10.1016/j.ijheatmasstransfer.2018.12.180.

Brown D, Chadwick M, Capote R, Kahler A, Trkov A, Herman M, Sonzogni A, Danon Y, et al. (2018) ENDF/B-VIII.0: The 8 Th Major Release of the Nuclear Reaction Data Library with CIELO-Project Cross Sections, New Standards and Thermal Scattering Data. *Nuclear Data Sheets*, 148, 1–142, dx.doi.org/10.1016/j.nds.2018.02.001.

Bystrai G P, Desyatnik V N, Zlokazov V A (1974) Thermal Conductivity of Molten Mixtures of Uranium Tetrachloride with Sodium and Potassium Chlorides. *Soviet Atomic Energy*, 36(6), 654–655, dx.doi.org/10.1007/BF01127242.

Cantor S (1968) Physical Properties of Molten-Salt Reactor Fuel, Coolant, and Flush Salts. ORNL-TM-2316, Oak Ridge National Laboratory, dx.doi.org/10.2172/4492893.

Cantor S (1973) Density and Viscosity of Several Molten Fluoride Mixtures. ORNL-TM–4308, Oak Ridge National Laboratory, dx.doi.org/10.2172/4419855.

Cartland Glover G, Skillen A, Litskevich D, Rolfo S, Emerson D R, Merk B, Moulinec C (2019) On the Numerical Modelling of Frozen Walls in a Molten Salt Fast Reactor. *Nuclear Engineering and Design*, 355, 110290, dx.doi.org/10.1016/j.nucengdes.2019.110290.

CEA (2015) Neutronics. DEN Monograph, Editions Le Moniteur.

Cervi E, Lorenzi S, Cammi A, Luzzi L (2019) Development of a Multiphysics Model for the Study of Fuel Compressibility Effects in the Molten Salt Fast Reactor. *Chemical Engineering Science*, 193, 379–393, dx.doi.org/10.1016/j.ces.2018.09.025.

Chaleff E S (2016) The Radiative Heat Transfer Properties of Molten Salts and Their Relevance to the Design of Advanced Reactors. Ph.D. thesis, Ohio State University.

Chaleff E S, Antolin N, Windl W, Blue T (2018) Ab-Initio Calculation of Spectral Absorption Coefficients in Molten Fluoride Salts with Metal Impurities. *Nuclear Technology*, 204(1), 59–65, dx.doi.org/10.1080/00295450.2018.1464288.

Chaleff E S, Blue T, Sabharwall P (2016) Radiation Heat Transfer in the Molten Salt FLiNaK. *Nuclear Technology*, 196(1), 53–60, dx.doi.org/10.13182/NT16-52.

Chase M W (1998) NIST-JANAF Thermochemical Tables. Number Monograph No. 9 in Journal of Physical and Chemical Reference Data, fourth edition, National Institute of Standards and Technology.

References

Chawla T C, Chan S H (1980) Combined Radiation Convection in Thermally Developing Poiseuille Flow with Scattering. *Journal of Heat Transfer*, 102(2), 297–302, dx.doi.org/10.1115/1.3244277.

Chhabra R P (editor) (2017) CRC Handbook of Thermal Engineering. Second edition, Taylor & Francis, CRC Press.

Chisholm B M, Krahn S L, Sowder A G (2020) A Unique Molten Salt Reactor Feature – The Freeze Valve System: Design, Operating Experience, and Reliability. *Nuclear Engineering and Design*, 368, 110803, dx.doi.org/10.1016/j.nucengdes.2020.110803.

Cooke J W (1973) Development of the Variable-Gap Technique for Measuring the Thermal Conductivity of Fluoride Salt Mixtures. ORNL-4831, Oak Ridge National Laboratory, dx.doi.org/10.2172/4556565.

Cooke J W, Cox B (1973) Forced-Convection Heat-Transfer Measurements with a Molten Fluoride Salt Mixture Flowing in a Smooth Tube. ORNL-TM–4079, Oak Ridge National Laboratory, dx.doi.org/10.2172/4486196.

Coyle C, Baglietto E, Forsberg C (2020) Advancing Radiative Heat Transfer Modeling in High-Temperature Liquid Salts. *Nuclear Science and Engineering*, dx.doi.org/10.1080/00295639.2020.1723993.

Cuckovic-Dzodzo D M, Dzodzo M B, Pavlovic M D (1999) Laminar Natural Convection in a Fully Partitioned Enclosure Containing Fluid with Nonlinear Thermophysical Properties. *International Journal of Heat and Fluid Flow*, 20(6), 614–623, dx.doi.org/10.1016/S0142-727X(99)00053-3.

Delpech S, Cabet C, Slim C, Picard G S (2010) Molten Fluorides for Nuclear Applications. *Materials Today*, 13(12), 34–41, dx.doi.org/10.1016/S1369-7021(10)70222-4.

Demazière C (2020) Modelling of Nuclear Reactor Multi-Physics. Elsevier, dx.doi.org/10.1016/C2017-0-01631-2.

Derdeyn W, Dbai M A, Scarlat R O, Trujillo M (2018) FLiBe Radiative Heat Transfer. *Transactions of the American Nuclear Society*, 118.

Desyatnik V N, Katyshev S F, Raspopin S P, Chervinskii Y F (1975) Density, Surface Tension, and Viscosity of Uranium Trichloride-Sodium Chloride Melts. *Soviet Atomic Energy*, 39(1), 649–651, dx.doi.org/10.1007/BF01121527.

Dewan L C, Simon C, Madden P A, Hobbs L W, Salanne M (2013) Molecular Dynamics Simulation of the Thermodynamic and Transport Properties of the Molten Salt Fast Reactor Fuel LiF–ThF_4. *Journal of Nuclear Materials*, 434(1-3), 322–327, dx.doi.org/10.1016/j.jnucmat.2012.12.006.

Di Marcello V, Cammi A, Luzzi L (2010) A Generalized Approach to Heat Transfer in Pipe Flow with Internal Heat Generation. *Chemical Engineering Science*, 65(3), 1301–1310, dx.doi.org/10.1016/j.ces.2009.10.004.

Di Ronco A, Cammi A, Lorenzi S (2019) Preliminary Analysis and Design of the Heat Exchangers for the Molten Salt Fast Reactor. *Nuclear Engineering and Technology*, dx.doi.org/10.1016/j.net.2019.07.013.

References

Diamond D J, Brown N R, Denning R, Bajorek S (2018) Phenomena Important in Modeling and Simulation of Molten Salt Reactors. BNL-114869-2018-IR, Brookhaven National Laboratory.

Dow (2021) DOWTHERM™ A Technical Data Sheet. Dow Chemical Company.

Duderstadt J J, Hamilton L J (1976) Nuclear Reactor Analysis. Wiley.

Einstein T (1963) Radiant Heat Transfer to Absorbing Gases Enclosed in a Circular Pipe with Conduction, Gas Flow, and Internal Heat Generation. NASA TR R-156, National Aeronautics and Space Administration.

Engel J R, Haubenreich P N, Houtzeel A (1970) Spray, Mist, Bubbles, and Foam in the Molten Salt Reactor Experiment. ORNL-TM-3027, Oak Ridge National Laboratory, dx.doi.org/10.2172/4086308.

EPRI (2015) Program on Technology Innovation: Technology Assessment of a Molten Salt Reactor Design: The Liquid-Fluoride Thorium Reactor (LFTR). 3002005460, Electric Power Research Institute.

Fiorina C (2019) Impact of the Volume Heat Source on the RANS-Based CFD Analysis of Molten Salt Reactors. *Annals of Nuclear Energy*, 134, 376–382, dx.doi.org/10.1016/j.anucene.2019.06.024.

Fiorina C, Cammi A, Luzzi L, Mikityuk K, Ninokata H, Ricotti M E (2014) Thermal-Hydraulics of Internally Heated Molten Salts and Application to the Molten Salt Fast Reactor. *Journal of Physics: Conference Series*, 501, 012030, dx.doi.org/10.1088/1742-6596/501/1/012030.

Fiorina C, Hursin M, Pautz A (2017) Extension of the GeN-Foam Neutronic Solver to SP3 Analysis and Application to the CROCUS Experimental Reactor. *Annals of Nuclear Energy*, 101, 419–428, dx.doi.org/10.1016/j.anucene.2016.11.042.

Fiveland W A, Jamaluddin A S (1991) Three-Dimensional Spectral Radiative Heat Transfer Solutions by the Discrete-Ordinates Method. *Journal of Thermophysics and Heat Transfer*, 5(3), 335–339, dx.doi.org/10.2514/3.268.

Forsberg C, Hu L W, Peterson P, Sridharan K (2015) Fluoride-Salt-Cooled High-Temperature Reactor (FHR) for Power and Process Heat. DOE/NEUP–11-3272, U.S. DoE Nuclear Energy University Program.

Forsberg C, Zheng G T, Ballinger R G, Lam S T (2019) Fusion Blankets and Fluoride-Salt-Cooled High-Temperature Reactors with Flibe Salt Coolant: Common Challenges, Tritium Control, and Opportunities for Synergistic Development Strategies Between Fission, Fusion, and Solar Salt Technologies. *Nuclear Technology*, pp. 1–24, dx.doi.org/10.1080/00295450.2019.1691400.

Forsberg C W, Lam S, Carpenter D M, Whyte D G, Scarlat R, Contescu C, Wei L, Stempien J, et al. (2017) Tritium Control and Capture in Salt-Cooled Fission and Fusion Reactors: Status, Challenges, and Path Forward. *Nuclear Technology*, 197(2), 119–139, dx.doi.org/10.13182/NT16-101.

Fredrickson G L, Cao G, Gakhar R, Yoo T S (2018) Molten Salt Reactor Salt Processing – Technology Status. INL/EXT–18-51033-Rev0, Idaho National Laboratory, dx.doi.org/10.2172/1484689.

References

Gat U (1986) The Ultimate Safe (U.S.) Reactor. In *Fourth International Conference on Emerging Nuclear Energy Systems*.

Gheribi A E, Corradini D, Dewan L, Chartrand P, Simon C, Madden P A, Salanne M (2014) Prediction of the Thermophysical Properties of Molten Salt Fast Reactor Fuel from First-Principles. *Molecular Physics*, 112(9-10), 1305–1312, dx.doi.org/10.1080/00268976.2014.897396.

Gordon I, Rothman L, Hill C, Kochanov R, Tan Y, Bernath P, Birk M, Boudon V, et al. (2017) The HITRAN2016 Molecular Spectroscopic Database. *Journal of Quantitative Spectroscopy and Radiative Transfer*, 203, 3–69, dx.doi.org/10.1016/j.jqsrt.2017.06.038.

Graham A M, Taylor Z, Collins B S, Salko R K, Poschmann M (2021) Multiphysics Coupling Methods for Molten Salt Reactor Modeling and Simulation in VERA. *Nuclear Science and Engineering*, 195(10), 1065–1086, dx.doi.org/10.1080/00295639.2021.1901000.

Greenwood M S, Betzler B R, Qualls A L, Yoo J, Rabiti C (2020) Demonstration of the Advanced Dynamic System Modeling Tool TRANSFORM in a Molten Salt Reactor Application via a Model of the Molten Salt Demonstration Reactor. *Nuclear Technology*, 206(3), 478–504, dx.doi.org/10.1080/00295450.2019.1627124.

Grimes W R (1970) Molten-Salt Reactor Chemistry. *Nuclear Applications and Technology*, 8(2), 137–155, dx.doi.org/10.13182/NT70-A28621.

Haubenreich P N, Engel J R (1970) Experience with the Molten-Salt Reactor Experiment. *Nuclear Applications and Technology*, 8(2), 118–136, dx.doi.org/10.13182/NT8-2-118.

Heaton R J, Brookes R, Madden P A, Salanne M, Simon C, Turq P (2006) A First-Principles Description of Liquid BeF_2 and Its Mixtures with LiF: 1. Potential Development and Pure BeF_2. *The Journal of Physical Chemistry B*, 110(23), 11454–11460, dx.doi.org/10.1021/jp061000+.

Heijna M, de Groot S, Vreeling J (2017) Comparison of Irradiation Behaviour of HTR Graphite Grades. *Journal of Nuclear Materials*, 492, 148–156, dx.doi.org/10.1016/j.jnucmat.2017.05.012.

Holcomb D E, Cetiner S M (2010) An Overview of Liquid Fluoride Salt Heat Transport Systems. ORNL/TM-2010/156, 990239, Oak Ridge National Laboratory.

Holcomb D E, Flanagan G F, Patton B W, Gehin J C, Howard R L, Harrison T J (2011) Fast Spectrum Molten Salt Reactor Options. ORNL/TM-2011/105, Oak Ridge National Laboratory, dx.doi.org/10.2172/1018987.

Holcomb D E, Kisner R A, Cetiner S M (2018) Instrumentation Framework for Molten Salt Reactors. ORNL/TM–2018/868, Oak Ridge National Laboratory, dx.doi.org/10.2172/1462848.

Howell J R, Mengüç M P, Siegel R (2016) Thermal Radiation Heat Transfer. Sixth edition, CRC Press.

Hu R (2017) A Fully-Implicit High-Order System Thermal-Hydraulics Model for Advanced Non-LWR Safety Analyses. *Annals of Nuclear Energy*, 101, 174–181, dx.doi.org/10.1016/j.anucene.2016.11.004.

Hu T, Cao L, Yang S, Fratoni M, Wu H (2021) Analysis of the Thermal Feedback Effect and Nuclides Flow Effect on the Fuel-cycle Characteristics of Molten Salt Reactors. *International Journal of Energy Research*, 45(8), 11677–11688, dx.doi.org/10.1002/er.5490.

References

Hua T, Fei T, Feng B, Hu R, Stempniewicz M, Roelofs F (2022) Benchmarking MSRE Transient Tests Using SPECTRA and SAM. In *Proceedings of 19th International Topical Meeting on Nuclear Reactor Thermal Hydraulics (NURETH-19)*.

IAEA (2013) Evaluation of High Temperature Gas Cooled Reactor Performance: Benchmark Analysis Related to the PBMR-400, PBMM, GT-MHR, HTR-10 and the ASTRA Critical Facility. IAEA-TECDOC-1694, International Atomic Energy Agency.

Iftimie R, Minary P, Tuckerman M E (2005) Ab Initio Molecular Dynamics: Concepts, Recent Developments, and Future Trends. *Proceedings of the National Academy of Sciences*, 102(19), 6654–6659, dx.doi.org/10.1073/pnas.0500193102.

Ignatiev V, Feynberg O, Gnidoi I, Merzlyakov A, Surenkov A, Uglov V, Zagnitko A, Subbotin V, et al. (2014) Molten Salt Actinide Recycler and Transforming System without and with Th–U Support: Fuel Cycle Flexibility and Key Material Properties. *Annals of Nuclear Energy*, 64, 408–420, dx.doi.org/10.1016/j.anucene.2013.09.004.

Incropera F P, DeWitt D P, Bergman T L, Lavine A S (2011) Fundamentals of Heat and Mass Transfer. Seventh edition, John Wiley & Sons.

IUPAC (1991) Gases in Molten Salts. Solubility Data Series Volume 45/46, International Union of Pure and Applied Chemistry.

Jackson J D, Cotton M A, Axcell B P (1989) Studies of Mixed Convection in Vertical Tubes. *International Journal of Heat and Fluid Flow*, 10(1), 2–15, dx.doi.org/10.1016/0142-727X(89)90049-0.

Janz G J (1988) Thermodynamic and Transport Properties for Molton Salts: Correlation Equatations for Critically Evaluated Density, Surface Tension, Electrical Conductance, and Viscosity Data. *Journal of Physical and Chemical Reference Data*, 17(Suppliment 2).

Janz G J, Allen C B, Bansal N P, Murphy R M, Tomkins R P T (1979) Physical Properties Data Compilations Relevant to Energy Storage. II. Molten Salts: Data on Single and Multi-Component Salt Systems. NSRDS-NBS 61 Part II, U.S. Department of Commerce National Bureau of Standards.

Janz G J, Allen C B, Downey J R, Tomkins R P T (1978) Physical Properties Data Compilations Relevant to Energy Storage. I. Molten Salts: Eutectic Data. NSRDS-NBS-61-PT-1, U.S. Department of Commerce National Bureau of Standards.

Jayatilleke C L V (1966) The Influence of Prandtl Number and Surface Roughness on the Resistance of the Laminar Sub-Layer to Momentum and Heat Transfer. Ph.D. thesis, Imperial College.

Jerden J (2019) Molten Salt Thermophysical Properties Database Development: 2019 Update. ANL/CFCT-19/6, Argonne National Laboratory, dx.doi.org/10.2172/1559846.

Jiang X Y, Lu H J, Chen Y S, Fu Y, Wang N X (2020) Numerical and Experimental Investigation of a New Conceptual Fluoride Salt Freeze Valve for Thorium-Based Molten Salt Reactor. *Nuclear Science and Techniques*, 31(2), 16, dx.doi.org/10.1007/s41365-020-0729-5.

Jin Y, Cheng J, An X, Su T, Zhang P, Li Z (2016) Accurate Viscosity Measurement of Ni-

trates/Nitrites Salts for Concentrated Solar Power. *Solar Energy*, 137, 385–392, dx.doi.org/10.1016/j.solener.2016.08.037.

Kader B A (1981) Temperature and Concentration Profiles in Fully Turbulent Boundary Layers. *International Journal of Heat and Mass Transfer*, 24(9), 1541–1544, dx.doi.org/10.1016/0017-9310(81)90220-9.

Kakaç S, Shah R K, Aung W (1987) Handbook of Single-Phase Convective Heat Transfer. Wiley.

Kattner U R (1997) The Thermodynamic Modeling of Multicomponent Phase Equilibria. *JOM*, 49(12), 14–19, dx.doi.org/10.1007/s11837-997-0024-5.

Katyshev S F, Chervinskii Y F, Desyatnik V N (1982) Density and Viscosity of Fused Mixtures of Uranium Chlorides and Potassium Chloride. *Soviet Atomic Energy*, 53(2), 565–566, dx.doi.org/10.1007/BF01122100.

Kays W M (1994) Turbulent Prandtl Number—Where Are We? *Journal of Heat Transfer*, 116(2), 284–295, dx.doi.org/10.1115/1.2911398.

Kays W M, Crawford M E, Weigand B (2005) Convective Heat and Mass Transfer. Fourth edition, McGraw-Hill.

Kedl R J (1970) Fluid Dynamic Studies of the Molten-Salt Reactor Experiment (MSRE) Core. ORNL-TM–3229, Oak Ridge National Laboratory, dx.doi.org/10.2172/4080377.

Khokhlov V, Ignatiev V, Afonichkin V (2009) Evaluating Physical Properties of Molten Salt Reactor Fluoride Mixtures. *Journal of Fluorine Chemistry*, 130(1), 30–37, dx.doi.org/10.1016/j.jfluchem.2008.07.018.

Kim E S, Oh C H, Patterson M (2010) Development of Tritium Permeation Analysis Code (TPAC). INL/CON-10-27602, Idaho National Laboratory.

Kinney R B, Sparrow E M (1966) Turbulent Pipe Flow of an Internally Heat Generating Fluid. *Journal of Heat Transfer*, 88(3), 314–321, dx.doi.org/10.1115/1.3691551.

Kochunas B, Collins B, Stimpson S, Salko R, Jabaay D, Graham A, Liu Y, Kim K S, et al. (2017) VERA Core Simulator Methodology for Pressurized Water Reactor Cycle Depletion. *Nuclear Science and Engineering*, 185(1), 217–231, dx.doi.org/10.13182/NSE16-39.

Křepel J, Hombourger B, Fiorina C, Mikityuk K, Rohde U, Kliem S, Pautz A (2014) Fuel Cycle Advantages and Dynamics Features of Liquid Fueled MSR. *Annals of Nuclear Energy*, 64, 380–397, dx.doi.org/10.1016/j.anucene.2013.08.007.

Laureau A, Rosier E, Merle E, Beils S, Bruneau O, Blanchon J, Gathmann R, Heuer D, et al. (2021) The LiCore Power Plant Simulator of the Molten Salt Fast Reactor. *EPJ Web of Conferences. PHYSOR2020 – International Conference on Physics of Reactors: Transition to a Scalable Nuclear Future*, 247, 06030, dx.doi.org/10.1051/epjconf/202124706030.

Leandro A M, Heidet F, Hu R, Brown N R (2019) Thermal Hydraulic Model of the Molten Salt Reactor Experiment with the NEAMS System Analysis Module. *Annals of Nuclear Energy*, 126, 59–67, dx.doi.org/10.1016/j.anucene.2018.10.060.

References

LeBlanc D (2010) Molten Salt Reactors: A New Beginning for an Old Idea. *Nuclear Engineering and Design*, 240(6), 1644–1656, dx.doi.org/10.1016/j.nucengdes.2009.12.033.

Li B, Dai S, Jiang D e (2020) Molecular Dynamics Simulations of Structural and Transport Properties of Molten NaCl-UCl_3 Using the Polarizable-Ion Model. *Journal of Molecular Liquids*, 299, 112184, dx.doi.org/10.1016/j.molliq.2019.112184.

Li H H (1980) The Infrared Absorption Coefficient of Alkali Halides. *International Journal of Thermophysics*, 1(1), 97–134, dx.doi.org/10.1007/BF00506275.

Lin H C, Zhang S, Diamond D, Bajorek S, Christensen R, Guo Y, Yoder G, Shi S, et al. (2019) Phenomena Identification and Ranking Table Study for Thermal Hydraulics for Advanced High Temperature Reactor. *Annals of Nuclear Energy*, 124, 257–269, dx.doi.org/10.1016/j.anucene.2018.08.038.

Liu L, Zhang D, Li L, Yang Y, Wang C, Qiu S, Su G (2018) Experimental Investigation of Flow and Convective Heat Transfer on a High-Prandtl-Number Fluid through the Nuclear Reactor Pebble Bed Core. *Applied Thermal Engineering*, 145, 48–57, dx.doi.org/10.1016/j.applthermaleng.2018.09.017.

MacPherson H G (1985) The Molten Salt Reactor Adventure. *Nuclear Science and Engineering*, 90(4), 374–380, dx.doi.org/10.13182/NSE90-374.

Madden P A, Salanne M (2016) Thorium Molten Salts: Theory and Practice. In **Revol J P, Bourquin M, Kadi Y, Lillestol E, de Mestral J C, Samec K** (editors) *Thorium Energy for the World*, pp. 111–116, Springer International Publishing, dx.doi.org/10.1007/978-3-319-26542-1_15.

Malin M (1987) On the Calculation of Heat Transfer Rates in Fully Turbulent Wall Flows. *Applied Mathematical Modelling*, 11(4), 281–284, dx.doi.org/10.1016/0307-904X(87)90143-0.

Mamiya M (1965) The Near-Infrared Absorption Spectra of Lanthanide Chlorides Dissolved in Molten LiCl–NaCl–KCl Eutectic. *Bulletin of the Chemical Society of Japan*, 38(2), 178–183, dx.doi.org/10.1246/bcsj.38.178.

McMurray J, Besmann T, Ard J, Utlak S, Lefebvre R (2019) Status of the Molten Salt Thermodynamic Database, MSTDB. ORNL/SPR-2019/1208, Oak Ridge National Laboratory.

McMurray J, Johnson K, Agca C, Betzler B, Kropaczek D, Besmann T, Andersson D, Ezell N D (2021) Roadmap for Thermal Property Measurements of Molten Salt Reactor Systems. ORNL/SPR-2020/1865, Oak Ridge National Laboratory, dx.doi.org/10.2172/1778081.

Merzari E, Yuan H, Min M, Shaver D, Rahaman R, Shriwise P, Romano P, Talamo A, et al. (2021) Cardinal: A Lower Length-Scale Multiphysics Simulator for Pebble-Bed Reactors. *Nuclear Technology*, pp. 1–23, dx.doi.org/10.1080/00295450.2020.1824471.

Michiyoshi I, Kikuchi Y, Furukawa O (1968) Heat Transfer in a Fluid with Internal Heat Generation Flowing through a Vertical Tube. *Journal of Nuclear Science and Technology*, 5(11), 590–595, dx.doi.org/10.1080/18811248.1968.9732518.

Modest M F (2013) Radiative Heat Transfer. Third edition, Academic Press.

Moltex (2018) An Introduction to the Moltex Energy Technology Portfolio. Moltex Energy.

Murthy J Y, Mathur S R (1998) Finite Volume Method for Radiative Heat Transfer Using Unstructured Meshes. *Journal of Thermophysics and Heat Transfer*, 12(3), 313–321, dx.doi.org/10.2514/2.6363.

Myers P D, Yogi Goswami D, Stefanakos E (2015) Molten Salt Spectroscopy for Quantification of Radiative Absorption in Novel Metal Chloride-Enhanced Thermal Storage Media. *Journal of Solar Energy Engineering*, 137(4), 041002, dx.doi.org/10.1115/1.4029934.

Nam H O, Morgan D (2015) Redox Condition in Molten Salts and Solute Behavior: A First-Principles Molecular Dynamics Study. *Journal of Nuclear Materials*, 465, 224–235, dx.doi.org/10.1016/j.jnucmat.2015.05.028.

Nguyen T, Kappes E, King S, Hassan Y, Ugaz V (2018) Time-Resolved PIV Measurements in a Low-Aspect Ratio Facility of Randomly Packed Spheres and Flow Analysis Using Modal Decomposition. *Experiments in Fluids*, 59(8), 127, dx.doi.org/10.1007/s00348-018-2583-3.

Nguyen T, Vaghetto R, Hassan Y (2020) Experimental Investigation of Turbulent Wake Flows in a Helically Wrapped Rod Bundle in Presence of Localized Blockages. *Physics of Fluids*, 32(7), 075113, dx.doi.org/10.1063/5.0008589.

Novak A, Peterson J, Zou L, Andrš D, Slaybaugh R, Martineau R (2019) Validation of Pronghorn Friction-Dominated Porous Media Thermal-Hydraulics Model with the SANA Experiments. *Nuclear Engineering and Design*, 350, 182–194, dx.doi.org/10.1016/j.nucengdes.2019.04.037.

Novak A J, Carlsen R W, Schunert S, Balestra P, Reger D, Slaybaugh R N, Martineau R C (2021) Pronghorn: A Multidimensional Coarse-Mesh Application for Advanced Reactor Thermal Hydraulics. *Nuclear Technology*, 207(7), 1015–1046, dx.doi.org/10.1080/00295450.2020.1825307.

Ohashi H, Sakaba N, Nishihara T, Tachibana Y, Kunitomi K (2008) Analysis of Tritium Behavior in Very High Temperature Gas-Cooled Reactor Coupled with Thermochemical Iodine-Sulfur Process for Hydrogen Production. *Journal of Nuclear Science and Technology*, 45(11), 1215–1227, dx.doi.org/10.1080/18811248.2008.9711909.

Ottewitte E H (1992) Cursory First Look at the Molten Chloride Fast Reactor as an Alternative to the Conventional BATR Concept. Idaho National Engineering Laboratory.

Palmer K F, Williams D (1974) Optical Properties of Water in the near Infrared. *Journal of the Optical Society of America*, 64(8), 1107, dx.doi.org/10.1364/JOSA.64.001107.

Patch R W (1967) Approximation for Radiant Energy Transport in Nongray, Nonscattering Gases. NASA-TN-D-4001, National Aeronautics and Space Administration.

Pelton A D (2019) Phase Diagrams and Thermodynamic Modeling of Solutions. Elsevier, dx.doi.org/10.1016/C2013-0-19504-9.

Pioro I L (editor) (2016) Handbook of Generation IV Nuclear Reactors. Number Number 103 in Woodhead Publishing Series in Energy, Woodhead.

Plompen A J M, Cabellos O, De Saint Jean C, Fleming M, Algora A, Angelone M, Archier P, Bauge E, et al. (2020) The Joint Evaluated Fission and Fusion Nuclear Data Library, JEFF-3.3. *The European Physical Journal A*, 56(7), 181, dx.doi.org/10.1140/epja/s10050-020-00141-9.

References

Poppendiek H F, Palmer L D (1952) Forced Convection Heat Transfer in Pipes with Volume Heat Sources within the Fluids. ORNL-1395, Oak Ridge National Laboratory, dx.doi.org/10.2172/4394843.

Poppendiek H F, Palmer L D (1955) Application of Temperature Solutions for Forced Convection Systems with Volume Heat Sources to General Convection Problems. ORNL-1933, Oak Ridge National Laboratory, dx.doi.org/10.2172/4373390.

Qualls A L, Betzler B R, Brown N R, Carbajo J J, Greenwood M S, Hale R, Harrison T J, Powers J J, et al. (2017) Preconceptual Design of a Fluoride High Temperature Salt-Cooled Engineering Demonstration Reactor: Motivation and Overview. *Annals of Nuclear Energy*, 107, 144–155, dx.doi.org/10.1016/j.anucene.2016.11.021.

Rahnema F, Diamond D, Serghiuta D, Burke P (2019) Phenomena, Gaps, and Issues for Neutronics Modeling and Simulation of FHRs. *Annals of Nuclear Energy*, 123, 172–179, dx.doi.org/10.1016/j.anucene.2018.08.035.

Ricci J E (1958) Guide to the Phase Diagrams of the Fluoride Systems. ORNL-2396, Oak Ridge National Laboratory, dx.doi.org/10.2172/4286439.

Richard J, Wang D, Yoder G, Carbajo J, Williams D, Forget B, Forsberg C (2014) Implementation of Liquid Salt Working Fluids into TRACE. In *Proceedings of ICAPP 2014*.

Roelofs F, Stempniewicz M (2021) Molten Salt Modelling Capabilities in SPECTRA and Application to MSRE and Mk1-PB-FHR. *Nuclear Engineering and Design*, 381, 111360, dx.doi.org/10.1016/j.nucengdes.2021.111360.

Rogers G F C, Mayhew Y (1992) Engineering Thermodynamics: Work and Heat Transfer. Fourth edition, Prentice Hall.

Rohsenow W M, Hartnett J P, Cho Y I (1998) Handbook of Heat Transfer. Third edition, McGraw-Hill.

Romatoski R, Hu L (2017) Fluoride Salt Coolant Properties for Nuclear Reactor Applications: A Review. *Annals of Nuclear Energy*, 109, 635–647, dx.doi.org/10.1016/j.anucene.2017.05.036.

Rosenthal M W (2009) An Account of Oak Ridge National Laboratory's Thirteen Research Reactors. ORNL/TM-2009/181, Oak Ridge National Laboratory, dx.doi.org/10.2172/970897.

Rosenthal M W, P N Haubenreich, Briggs R B (1972) Development Status of Molten-Salt Breeder Reactors. ORNL–4812, Oak Ridge National Laboratory, dx.doi.org/10.2172/4622532.

Rouch H, Geoffroy O, Rubiolo P, Laureau A, Brovchenko M, Heuer D, Merle-Lucotte E (2014) Preliminary Thermal–Hydraulic Core Design of the Molten Salt Fast Reactor (MSFR). *Annals of Nuclear Energy*, 64, 449–456, dx.doi.org/10.1016/j.anucene.2013.09.012.

Rubiolo P R, Retamales M T, Ghetta V, Giraud J (2017) High Temperature Thermal Hydraulics Modeling of a Molten Salt: Application to a Molten Salt Fast Reactor (MSFR). *ESAIM: Proceedings and Surveys. LMLFN 2015 – Low Velocity Flows – Application to Low Mach and Low Froude regimes*, 58, 98–117, dx.doi.org/10.1051/proc/201758098.

Salanne M, Rotenberg B, Jahn S, Vuilleumier R, Simon C, Madden P A (2012) Including Many-

Body Effects in Models for Ionic Liquids. *Theoretical Chemistry Accounts*, 131(3), 1143, dx.doi.org/10.1007/s00214-012-1143-9.

Salanne M, Simon C, Turq P, Madden P A (2009) Heat-Transport Properties of Molten Fluorides: Determination from First-Principles. *Journal of Fluorine Chemistry*, 130(1), 38–44, dx.doi.org/10.1016/j.jfluchem.2008.07.013.

Sangster J, Pelton A D (1987) Phase Diagrams and Thermodynamic Properties of the 70 Binary Alkali Halide Systems Having Common Ions. *Journal of Physical and Chemical Reference Data*, 16(3), 509–561, dx.doi.org/10.1063/1.555803.

Šarić S, Basara B (2018) A Near-Wall Model for Heat Transfer at High Prandtl Numbers. In *Proceedings of Tenth International Conference on Computational Fluid Dynamics (ICCFD10)*.

Saunders N, Miodownik A P (1998) CALPHAD (Calculation of Phase Diagrams): A Comprehensive Guide. Pergamon.

Schacherl B, Eloirdi R, Konings R J M, Beneš O (2021) Thermodynamic Assessment of the NaF-KF-UF4 System. *Thermo*, 1(2), 232–250, dx.doi.org/10.3390/thermo1020016.

Senatore G, Tosi M, Woodruff T (1984) A Simple Formula for the Fundamental Optical Absorption of Alkali Halide Melts. *Solid State Communications*, 52(2), 173–176, dx.doi.org/10.1016/0038-1098(84)90621-5.

Serp J, Allibert M, Beneš O, Delpech S, Feynberg O, Ghetta V, Heuer D, Holcomb D, et al. (2014) The Molten Salt Reactor (MSR) in Generation IV: Overview and Perspectives. *Progress in Nuclear Energy*, 77, 308–319, dx.doi.org/10.1016/j.pnucene.2014.02.014.

Serrano-López R, Fradera J, Cuesta-López S (2013) Molten Salts Database for Energy Applications. *Chemical Engineering and Processing: Process Intensification*, 73, 87–102, dx.doi.org/10.1016/j.cep.2013.07.008.

Shi C, Cheng M, Liu G (2016) Development and Application of a System Analysis Code for Liquid Fueled Molten Salt Reactors Based on RELAP5 Code. *Nuclear Engineering and Design*, 305, 378–388, dx.doi.org/10.1016/j.nucengdes.2016.05.034.

Siegel R, Sparrow E M (1959) Turbulent Flow in a Circular Tube With Arbitrary Internal Heat Sources and Wall Heat Transfer. *Journal of Heat Transfer*, 81(4), 280–287, dx.doi.org/10.1115/1.4008203.

Sleicher C, Rouse M (1975) A Convenient Correlation for Heat Transfer to Constant and Variable Property Fluids in Turbulent Pipe Flow. *International Journal of Heat and Mass Transfer*, 18(5), 677–683, dx.doi.org/10.1016/0017-9310(75)90279-3.

Smith A, Capelli E, Konings R, Gheribi A (2020) A New Approach for Coupled Modelling of the Structural and Thermo-Physical Properties of Molten Salts. Case of a Polymeric Liquid LiF-BeF2. *Journal of Molecular Liquids*, 299, 112165, dx.doi.org/10.1016/j.molliq.2019.112165.

Sohal M S, Ebner M A, Sabharwall P, Sharpe P (2013) Engineering Database of Liquid Salt Thermophysical and Thermochemical Properties. INL/EXT-10-18297 Rev.1, Idaho National Laboratory, dx.doi.org/10.2172/980801.

Srivastava A, Kudariyawar J Y, Borgohain A, Jana S, Maheshwari N, Vijayan P (2016) Experimental and Theoretical Studies on the Natural Circulation Behavior of Molten Salt Loop. *Applied Thermal Engineering*, 98, 513–521, dx.doi.org/10.1016/j.applthermaleng.2015.12.065.

Srivastava A K, Chouhan R, Borgohain A, Jana S S, Maheshwari N K, Pilkhwal D S, Rama Rao A, Hareendhran K N, et al. (2017) An Experimental and Numerical Study to Support Development of Molten Salt Breeder Reactor. *Journal of Nuclear Engineering and Radiation Science*, 3(3), 031007, dx.doi.org/10.1115/1.4036027.

Stainsby R, Worsley M, Grief A, Dawson F, Davies M, Coddington P, Baker J, Dennier A (2010) Development of Local Heat Transfer Models for Safety Assessment of High Temperature Gas-Cooled Reactor Cores—Part I: Pebble Bed Reactors. *Journal of Engineering for Gas Turbines and Power*, 132(1), 012906, dx.doi.org/10.1115/1.3126775.

Taube M (1978) Fast Reactors Using Molten Chloride Salts as Fuel. EIR-332, Swiss Federal Institute for Reactor Research (EIR/PSI).

Taube M, Heer W (1980) Reactor with Very Low Fission Product Inventory. EIR-411, Swiss Federal Institute for Reactor Research (EIR/PSI).

Tetreault-Friend M, Gray L A, Berdibek S, McKrell T, Slocum A H (2017) Optical Properties of High Temperature Molten Salt Mixtures for Volumetrically Absorbing Solar Thermal Receiver Applications. *Solar Energy*, 153, 238–248, dx.doi.org/10.1016/j.solener.2017.05.054.

Thoma R E (1959) Phase Diagrams of Nuclear Reactor Materials. ORNL-2548, Oak Ridge National Laboratory, dx.doi.org/10.2172/4234144.

UKAEA (1974) An Assessment of a 2500 MWe Molten Chloride Salt Fast Reactor. AEEW - R956, United Kingdom Atomic Energy Authority.

US NRC (2020a) NRC Non-Light Water Reactor (Non-LWR) Vision and Strategy, Volume 1 – Computer Code Suite for Non-LWR Design Basis Event Analysis. Revision 1, U.S. Nuclear Regulatory Commission.

US NRC (2020b) NRC Non-Light Water Reactor (Non-LWR) Vision and Strategy, Volume 3 – Computer Code Development Plans for Severe Accident Progression, Source Term, and Consequence Analysis. Revision 1, U.S. Nuclear Regulatory Commission.

Wagner W, Cooper J R, Dittmann A, Kijima J, Kretzschmar H J, Kruse A, Mareš R, Oguchi K, et al. (2000) The IAPWS Industrial Formulation 1997 for the Thermodynamic Properties of Water and Steam. *Journal of Engineering for Gas Turbines and Power*, 122(1), 150–184, dx.doi.org/10.1115/1.483186.

Walker S A, Abou-Jaoude A, Taylor Z, Salko R K, Ji W (2021) Coupled Thermal-Hydraulic Analysis and Species Mass Transport in a Versatile Experimental Salt Irradiation Loop (VESIL) Using CTF. *Journal of Nuclear Engineering*, 2(3), 309–317, dx.doi.org/10.3390/jne2030025.

Walker S A, Ji W (2021) Species Transport Analysis of Noble Metal Fission Product Transport, Deposition, and Extraction in the Molten Salt Reactor Experiment. *Annals of Nuclear Energy*, 158, 108250, dx.doi.org/10.1016/j.anucene.2021.108250.

Wang D, Yoder G L, Pointer D W, Holcomb D E (2015) Thermal Hydraulics Analysis of the

Advanced High Temperature Reactor. *Nuclear Engineering and Design*, 294, 73–85, dx.doi.org/10.1016/j.nucengdes.2015.08.017.

Weaver C F, Thoma R E, Insley H, Friedman H A (1961) Phase Equilibria in Molten Salt Breeder Reactor Fuels. I. The System LiF- BeF_2-UF_4-ThF_4. ORNL-2896, Oak Ridge National Laboratory, dx.doi.org/10.2172/4081840.

Wieliczka D M, Weng S, Querry M R (1989) Wedge Shaped Cell for Highly Absorbent Liquids: Infrared Optical Constants of Water. *Applied Optics*, 28(9), 1714, dx.doi.org/10.1364/AO.28.001714.

Williams D (2006a) Assessment of Candidate Molten Salt Coolants for the Advanced High Temperature Reactor (AHTR). ORNL/TM-2006/12, Oak Ridge National Laboratory, dx.doi.org/10.2172/885975.

Williams D F (2006b) Assessment of Candidate Molten Salt Coolants for the NGNP/NHI Heat-Transfer Loop. ORNL/TM-2006/69, Oak Ridge National Laboratory, dx.doi.org/10.2172/1360677.

Williams D F, Clarno K T (2008) Evaluation of Salt Coolants for Reactor Applications. *Nuclear Technology*, 163(3), 330–343, dx.doi.org/10.13182/NT08-A3992.

Wilson D, Craft T, Iacovides H (2022) Unsteady LES and RANS Computations of Natural Convection Cooling Loops. In *Proceedings of 19th International Topical Meeting on Nuclear Reactor Thermal Hydraulics (NURETH-19)*.

Wu Y T, Chen C, Liu B, Ma C F (2012) Investigation on Forced Convective Heat Transfer of Molten Salts in Circular Tubes. *International Communications in Heat and Mass Transfer*, 39(10), 1550–1555, dx.doi.org/10.1016/j.icheatmasstransfer.2012.09.002.

Xu H (2017) Status and Perspective of TMSR in China. In *GIF Molten Salt Reactor Workshop*.

Xun H (2016) Validation of the TRACE Code for the System Dynamic Simulations of the Molten Salt Reactor Experiment and the Preliminary Study on the Dual Fluid Molten Salt Reactor. Ph.D. thesis, Technical University of Munich.

Yener Y, Özişik M N (1986) Simultaneous Radiation and Forced Convection in Thermally Developing Turbulent Flow through a Parallel-Plate Channel. *Journal of Heat Transfer*, 108(4), 985–988, dx.doi.org/10.1115/1.3247051.

Yildiz M A, Botha G, Yuan H, Merzari E, Kurwitz R C, Hassan Y A (2020) Direct Numerical Simulation of the Flow Through a Randomly Packed Pebble Bed. *Journal of Fluids Engineering*, 142(4), 041405, dx.doi.org/10.1115/1.4045439.

Yoder G L (2014) Examination of Liquid Fluoride Salt Heat Transfer. In *Proceedings of ICAPP 2014*.

Yoder G L, Heatherly D, Caja M (2018) Natural Convection Heat Transfer Experiments in Fluoride Salt. *Journal of Heat Transfer*, 140(4), 042501, dx.doi.org/10.1115/1.4038132.

Yu W, Ruan J, He L, Kendrick J, Zou Y, Xu H (2021) Development of TREND Dynamics Code for Molten Salt Reactors. *Nuclear Engineering and Technology*, 53(2), 455–465, dx.doi.org/10.1016/j.net.2020.07.030.

References

Zhang J, Forsberg C W, Simpson M F, Guo S, Lam S T, Scarlat R O, Carotti F, Chan K J, et al. (2018) Redox Potential Control in Molten Salt Systems for Corrosion Mitigation. *Corrosion Science*, 144, 44–53, dx.doi.org/10.1016/j.corsci.2018.08.035.

Zhang S, Sun X, Dominguez-Ontiveros E E (2020) Numerical Study on Convective Heat Transfer and Friction Characteristics of Molten Salts in Circular Tubes. *Annals of Nuclear Energy*, 142, 107375, dx.doi.org/10.1016/j.anucene.2020.107375.

Zheng G, Sridharan K (2018) Corrosion of Structural Alloys in High-Temperature Molten Fluoride Salts for Applications in Molten Salt Reactors. *JOM*, 70(8), 1535–1541, dx.doi.org/10.1007/s11837-018-2981-2.

Zhimin D, Yang Z, Kun C (2016) Thorium Molten Salt Reactors (TMSR) Development in China. In *IAEA Technical Meeting on the Status of Molten Salt Reactor Technology*.

Zweibaum N, Blandford E, Gerardi C, Peterson P (2020) Scaling Methodology for Integral Effects Tests in Support of Fluoride Salt–Cooled High-Temperature Reactor Technology. *Nuclear Science and Engineering*, 194(8-9), 793–811, dx.doi.org/10.1080/00295639.2019.1710976.

Zweibaum N, Guo Z, Kendrick J C, Peterson P F (2016) Design of the Compact Integral Effects Test Facility and Validation of Best-Estimate Models for Fluoride Salt–Cooled High-Temperature Reactors. *Nuclear Technology*, 196(3), 641–660, dx.doi.org/10.13182/NT16-15.

6 Nomenclature

Latin Symbols

A	Area, m^2
At	Atwood number ($At = (\rho_1 - \rho_2)/(\rho_1 + \rho_2)$)
Bi	Biot number ($Bi = hL/k_s$)
c_p, c_v	Specific heat at constant pressure or volume, $J\,kg^{-1}\,K^{-1}$
d or D	Diameter ($D_h = 4A_{cs}/p_{cs}$ for hydraulic diameter), m
f	Darcy-Weisbach friction factor
Fo	Fourier number ($Fo = \alpha_s t/L^2$)
Gr	Grashof number ($Gr = gL^3\Delta\rho/\nu^2\rho = gL^3\beta\Delta T/\nu^2$, using the Boussinesq approximation $\Delta\rho/\rho \approx -\beta\Delta T$, where ΔT is often taken as $T_w - T_{s,\infty}$)
g	Acceleration due to gravity, $m\,s^{-2}$
h	Specific enthalpy, $J\,kg^{-1}$, Heat Transfer Coefficient (HTC), $W\,m^{-2}\,K^{-1}$ or height, m
I	Radiative intensity, $W\,m^{-2}\,sr^{-1}$ or $W\,m^{-2}\,sr^{-1}\,\mu m^{-1}$ for a spectral density, where sr (steradian) is solid angle
J	Radiosity, $W\,m^{-2}$
k	Thermal conductivity, $W\,m^{-1}\,K^{-1}$
L	Length or wall thickness, m
M	Molar mass of a species, $kg\,kmol^{-1}$
Ma	Mach number ($Ma = U/a$, where a is the speed of sound)
n	Refractive index
Nu	Nusselt Number ($Nu = hL/k_f$)
p	Perimeter, m
P	Pressure (P_s = static pressure, P_T = total pressure), $N\,m^{-2}$ or Pa
Pe	Péclet number ($Pe = RePr$)
Pr	Prandtl number ($Pr = c_p\mu/k_f$)
q	Heat flux (rate of heat transfer per unit area, $q = Q/A$), $W\,m^{-2}$
Q	Rate of heat transfer, W
r	Radius, m
R	Gas constant (for a particular gas, $R = \tilde{R}/M$), $J\,kg^{-1}\,K^{-1}$
$\tilde{R}$	Universal gas constant, $8314.5\,J\,kmol^{-1}\,K^{-1}$
R_{th}	Thermal resistance, $K\,W^{-1}$
Ra	Rayleigh number ($Ra = GrPr$)
Re	Reynolds number ($Re = \rho UL/\mu$, or for an internal flow $Re = WD_h/A_{cs}\mu$)
Ri	Richardson number ($Ri = Gr/Re^2$)
Sr	Strouhal number ($Sr = fL/U$, where f is frequency)

St	Stanton number ($St = Nu/RePr$)
t	Time, s
T	Temperature (T_s = static temperature, T_T = total temperature), K
u_τ	Wall friction velocity ($u_\tau = \sqrt{\overline{\tau_w}/\rho}$), $\mathrm{m\,s^{-1}}$
U	Velocity, $\mathrm{m\,s^{-1}}$ or thermal transmittance, $\mathrm{W\,m^{-2}\,K^{-1}}$
v	Specific volume, $\mathrm{m^3\,kg^{-1}}$
V	Volume, $\mathrm{m^3}$
W	Mass flow rate, $\mathrm{kg\,s^{-1}}$
y	Wall distance, m
y^+	Non-dimensional wall distance ($y^+ = y u_\tau/\nu$)

Greek Symbols

α	Thermal diffusivity ($\alpha = k/\rho c_p$), $\mathrm{m^2\,s^{-1}}$
β	Volumetric thermal expansion coefficient ($\beta = -(1/\rho)(\partial\rho/\partial T)$), $\mathrm{K^{-1}}$
γ	Ratio of specific heats ($\gamma = c_p/c_v$)
ϵ	Emissivity or surface roughness height, m
κ	Absorption coefficient, $\mathrm{m^{-1}}$
λ	Wavelength, m
μ	Viscosity, $\mathrm{kg\,m^{-1}\,s^{-1}}$
ν	Kinematic viscosity and momentum diffusivity ($\nu = \mu/\rho$), $\mathrm{m^2\,s^{-1}}$
ρ	Density, $\mathrm{kg\,m^{-3}}$
σ	Stefan Boltzmann constant, $5.67 \times 10^{-8}\,\mathrm{W\,m^{-2}\,K^{-4}}$
τ	Shear stress, $\mathrm{N\,m^{-2}}$
ϕ	Porosity or void fraction

Subscripts and Modifications

b	Bulk (mass-averaged) quantity
cs	Cross-sectional quantity
f	Quantity relating to a fluid
i	Quantity relating to a particular species
T	Total (stagnation) quantity
t	Turbulent quantity
s	Static quantity or quantity relating to a solid
w	Quantity relating to a wall or surface
∞	Quantity far from a wall or in free-stream
$\overline{\square}$	Average quantity
$\tilde{\square}$	Molar quantity
$\square'$	Varying quantity

7 Abbreviations

AGR	Advanced Gas-cooled Reactor
AHTR	Advanced High Temperature Reactor
ANL	Argonne National Laboratory
ARE	Aircraft Reactor Experiment
ARIS	Advanced Reactor Information System
CALPHAD	CALculation of PHAse Diagrams
CFD	Computational Fluid Dynamics
CHT	Conjugate Heat Transfer
CIET	Compact Integral Effects Test
CSP	Concentrating Solar Power
DFT	Density Functional Theory
DHR	Decay Heat Removal
DNP	Delayed Neutron Precursor
DNS	Direct Numerical Simulation
DO	Discrete Ordinates
DRACS	Direct Reactor Auxiliary Cooling System
DYNASTY	DYnamics of NAtural circulation for molten SalT internallY heated
ENDF	Evaluated Nuclear Data File
FFFER	Forced Fluoride Flow for Experimental Research
FHR	Fluoride-Salt-Cooled High-Temperature Reactor
GEM	Gibbs Energy Minimisation
Gen IV	Generation IV
HPC	High Performance Computing
HTC	Heat Transfer Coefficient
HTGR	High Temperature Gas-cooled Reactor
IAEA	International Atomic Energy Agency
IET	Integral Effect Test
IMSR	Integral Molten Salt Reactor
IR	Infrared
JEFF	Joint Evaluated Fission and Fusion
JRC	European Commission Joint Research Centre
LES	Large Eddy Simulation
LFTR	Liquid-Fluoride Thorium Reactor
LMFR	Liquid Metal-cooled Fast Reactor
LWR	Light Water Reactor
MA	Minor Actinide
MC	Monte Carlo
MCFR	Molten Chloride Fast Reactor
MD	Molecular Dynamics
MOC	Method of Characteristics

Abbreviations

MOSART	MOlten Salt Actinide Recycler and Transforming
MSBR	Molten Salt Breeder Reactor
MSDR	Molten Salt Demonstration Reactor
MSFR	Molten Salt Fast Reactor
MSR	Molten Salt Reactor
MSRE	Molten Salt Reactor Experiment
NEA	Nuclear Energy Agency
OECD	Organisation for Economic Co-operation and Development
ORNL	Oak Ridge National Laboratory
OSTI	Office of Scientific and Technical Information
PIRT	Phenomena Identification and Ranking Table
PIV	Particle Image Velocimetry
PSI	Paul Scherrer Institute
RANS	Reynolds-Averaged Navier-Stokes
RCCS	Reactor Cavity Cooling System
RTE	Radiative Transfer Equation
RVACS	Reactor Vessel Auxiliary Cooling System
SA	Sensitivity Analysis
SAMOFAR	Safety Assessment of the Molten Salt Fast Reactor
SAMOSAFER	Severe Accident Modeling and Safety Assessment for Fluid-fuel Energy Reactors
SET	Separate Effect Test
SFR	Sodium-cooled Fast Reactor
SSC	Structure, System and Component
SSR–W	Stable Salt Reactor – Wasteburner
SWATH	Salt at WAll: Thermal ExcHanges
TMSR	Thorium Molten Salt Reactor
TRISO	TRIstructural-ISOtropic
UQ	Uncertainty Quantification
US DOE	United States Department of Energy
US NRC	United States Nuclear Regulatory Commission
UV	Ultraviolet
VERA	Virtual Environment for Reactor Applications
VHTR	Very High Temperature Reactor


Volume 6